NASA CONTRACTOR REPORT

NASA CR-2

NASA CR-2109

METEOR RESEARCH PROGRAM

by A. F. Cook, M. R. Flannery, H. Levy II,
R. E. McCrosky, Z. Sekanina, C.-Y. Shao,
R. B. Southworth, and J. T. Williams

Prepared by
SMITHSONIAN ASTROPHYSICAL OBSERVATORY
Cambridge, Mass. 02138
for Langley Research Center

NATIONAL AERONAUTICS AND SPACE ADMINISTRATION • WASHINGTON, D. C. • SEPTEMBER 1972

1. Report No.	2. Government Accession No.	3. R
NASA CR-2109		

4. Title and Subtitle	5. Report Date
METEOR RESEARCH PROGRAM	September 1972
	6. Performing Organization Code
7. Author(s): A. F. Cook, M. R. Flannery, H. Levy II, R. E. McCrosky, Z. Sekanina, C. -Y. Shao, R. B. Southworth, and J. T. Williams	8. Performing Organization Report No.
	10. Work Unit No.
9. Performing Organization Name and Address Smithsonian Astrophysical Observatory Cambridge, Massachusetts 02138	11. Contract or Grant No. NSR 09-015-033
	13. Type of Report and Period Covered Contractor Report
12. Sponsoring Agency Name and Address National Aeronautics and Space Administration Washington, D.C. 20546	14. Sponsoring Agency Code

15. Supplementary Notes

16. Abstract

Statistics from a synoptic year sample of 20,000 radar meteor observations using an eight station radar network are presented. The synoptic year sample constitutes the largest, most accurate, and most complete body of radar meteor data in existence. Since it is such a large sample, results of individual meteors from the synoptic year sample such as orbital parameters, heights, ionization, etc., are listed on magnetic tape. Results of 29 simultaneous meteor observations are presented. Simultaneous meteor observations are observations of the same meteor using radar in conjunction with an image orthicon optical system. The simultaneous observations have been used to calibrate masses of radar meteors. Results indicate that masses of radar meteors have been underestimated by about an order of magnitude.

17. Key Words (Suggested by Author(s))	18. Distribution Statement
meteor; radar observation; simultaneous observation; image orthicon; ionization; orbital parameters; meteor masses; analysis procedures; fragmentation; luminosity; recombination; diffusion	Unclassified - Unlimited

19. Security Classif. (of this report)	20. Security Classif. (of this page)	21. No. of Pages	22. Price*
Unclassified	Unclassified	170	$3.00

*For sale by the National Technical Information Service, Springfield, Virginia 22151

TABLE OF CONTENTS

TABLE OF CONTENTS (Cont.)

TABLE OF CONTENTS (Cont.)

TABLE OF CONTENTS (Cont.)

METEOR RESEARCH PROGRAM

FINAL REPORT

1. EXECUTIVE SUMMARY

The smallest bodies in the solar system – the meteoroids – are bodies whose study is important, at one extreme, for practical engineering of artificial satellites and, at the other extreme, for clarification of the birth of the solar system.

At present, observations of the meteor process in the earth's atmosphere provide probably the best of the very few sources of data to determine the nature of these small bodies and their interrelationships in the solar system. These facts have motivated the Smithsonian Astrophysical Observatory (SAO) to conduct a comprehensive program of meteor research, of which the effort reported here was a major component for several years.

To assist the reader in following the webs of our results, we provide here a framework statement of three problems together with brief comments on advances made during the course of this research. Specific topics are amplified at the end of this summary (Section 1.2) and treated in detail in the body of the report (Sections 2 to 13).

1.1 The Problems

1.1.1 Generic relationships among comets, asteroids, meteorites, and meteoroids

A paramount question in solar-system astronomy revolves around the problem of the parent bodies of meteorites. Asteroids, comets, and Apollo asteroids have been or are candidate parent bodies. In many ways, meteorites are the most special small bodies of the solar system. Our detailed knowledge of them is surpassed only, possibly, by our knowledge of the earth and the moon. Paradoxically, we have sufficient

information on their recent histories in space to exclude – or at least make unlikely – all known objects as their parent bodies.

Most meteoroids are unquestionably generated by comets, as demonstrated by the comparison of shower meteor orbits with specific comet orbits. If meteorites are also derived from comets, our knowledge of the physical structure of meteorites can assist in understanding the meteor phenomena. But if meteorites are from another source, the burden of investigating the details of the nonvolatile substance in comets rests with meteor observations. Comets are thought to be the most primordial material in the solar system and consequently have eventual importance in establishing boundary conditions on its origin. We also note here, for future reference, that carbonaceous chondrites are recognized as the most primordial type of meteorite.

Apollo asteroids are thought by some to be stray, but true, asteroids and by others to be "dead" comet nuclei. It is possible that both classes are included in the Apollo group. The known Apollos probably do not produce meteorites, although undiscovered members of the group may.

We see then that small bodies of the solar system present a complex problem in genealogy. The answers are inherently of great interest to astronomy and important in the planning of comet and asteroid missions.

While much of this problem lies outside the area of research reported here, some of our results are pertinent.

A. We have discovered in our radar meteor data some weak meteor showers that appear to be associated with Apollo asteroids (Section 1.2.3.2). Thus, at least some of these objects bear the mark of a comet.

B. A number of previously suspected meteor showers have been verified and numerous new showers detected in the radar data. Unlike photographic showers, very few of these new showers can be associated with known comets; this presents a fruitful subject for dynamical studies (Section 1.2.3.1).

C. The similarity of orbits defines a meteor stream, but the spread of orbits within a stream tells much about the ejection process and other properties of comets. The distribution of orbits in radar streams has been investigated (Section 1.2.3.1).

D. A reanalysis of optical meteor results has shown that comets are comprised of at least two distinct kinds of material and, more importantly, that for the most part, individual comets do not provide both types to their meteor stream (Section 1.2.4.2). It is probable that the two samples represent the interior core and exterior shell of the original comet. A tentative identification of the core material with carbonaceous chondrites has been made.

1.1.2 Meteor physics

Our primary reason for investigating the interaction of meteoroids with the atmosphere is to enable us to use the information in the raw data when solving the other problems herein discussed; this is to say that the physics is not an end in itself. Nevertheless, a number of physical processes and parameters were so poorly understood or recognized that a considerable fraction of our effort has been devoted to these areas.

An important case in point is the determination of meteoroid masses. Optical observation alone suggests an approximate form of the proportionality between mass and the observable luminosity and velocity. If, in addition, enough were known about the structure, composition, and ablation characteristics of the meteoroid, the optical mass proportionality could be written as a reasonably accurate equality. It follows from the discussion in Section 1.1.1 that the structure and composition of meteoroids are not known with certainty and that a prejudgment of these quantities immediately eliminates the possibility of determining the nature of cometary material. It was therefore important to obtain external information on the mass-luminosity relation. With this accomplished, we can then reverse the process and proceed with the more difficult, but far more interesting, problem of determining the nature of cometary material.

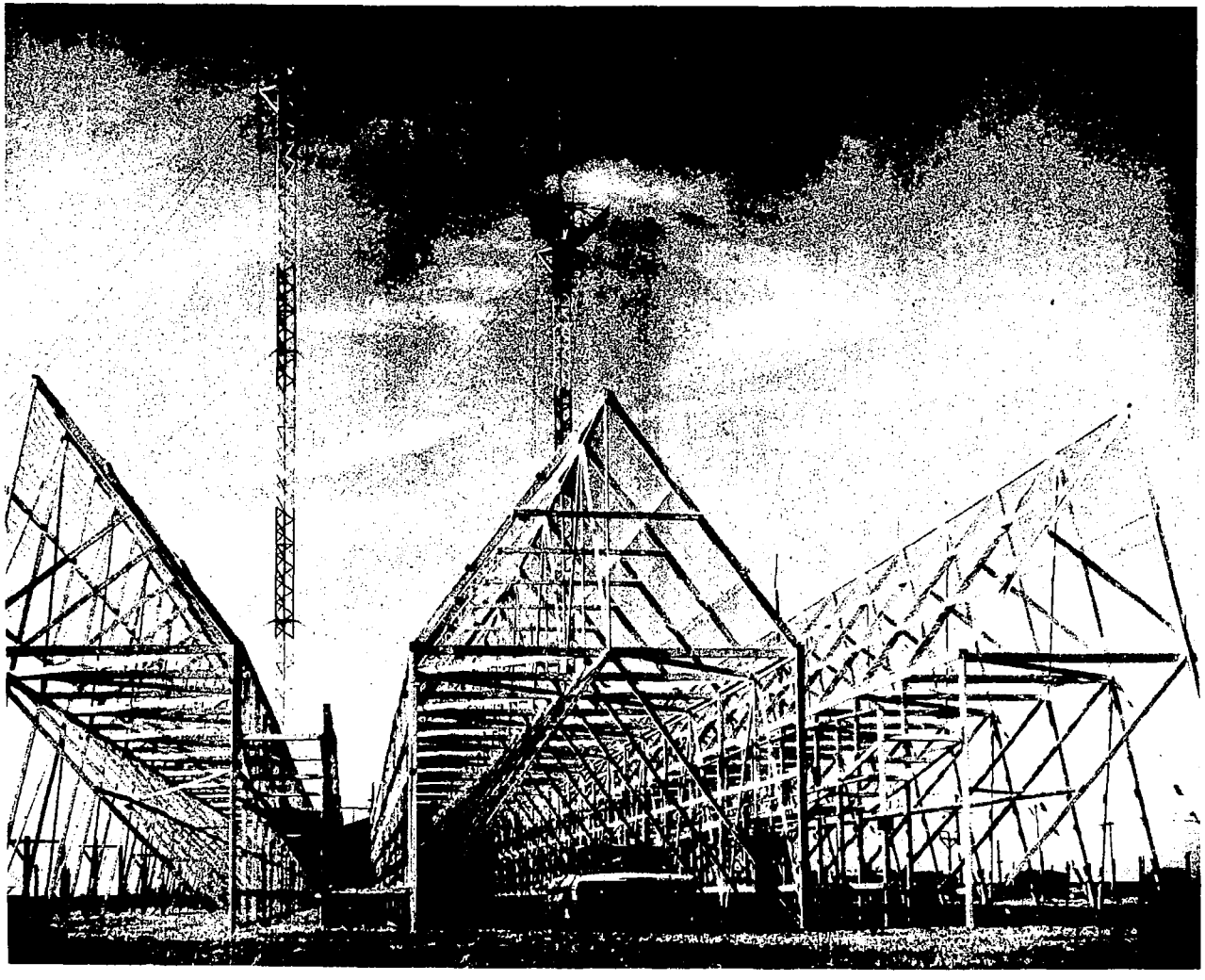

Plate 1. The double-trough transmitting and receiving antenna at Havana. The five other trough antennas were similar. In the background are the microwave towers linking this site to the seven other sites.

A similar problem occurs for radar meteors. The mass of a meteoroid is, in principle, determined by the number of electrons it produces. In this case, both the form of the relationship and the proportionality constant were in question.

Finally, radar observations have been beset by a number of real and mythical physical biases that have hampered interpretation of results. Various theories disagreed on the importance of certain biases, and it proved necessary to find the correct answers within the data themselves.

We will report very significant advances in all these areas.

A. Observations and analyses of artificial meteors launched by NASA at Wallops Island, Virginia, have provided the first firm point for the mass-luminosity relationship (Section 1.2.4.1).

B. This luminosity standard has been transferred to radar meteors by a long series of observations made of the same meteors by both radar and a fast image-orthicon system (Section 1.2.5). Some information on the dependence of ionization on meteor velocity was also obtained from the same observations. We have corrected the (old) provisional masses of radar meteors upward by more than an order of magnitude.

C. We have observed that low-altitude meteors suffer from electron-ion recombination and have identified the probable mechanism through which this recombination occurs (Section 1.2.2.1). We also conclude that our high-power radar observations are the only existing set for which this particular bias can be corrected.

D. Radar techniques are far more sensitive than optical in the detection of the onset of fragmentation in meteoroids. We have observed fragmentation in most of the radar meteors and thus confirm the important but often questioned similar result obtained optically (Section 1.2.2.2). The multiple source generated by a meteor after it has fragmented is a poor radar target for our observing techniques. Thus we realize the existence of a new selection effect but cannot yet specify its importance.

E. A radar echo can be severely attenuated if the meteor ion column has a width comparable to or larger than $1/\pi$ times the radar wavelength. It had been proposed that this critical dimension is reached very rapidly for high-altitude (and therefore high-velocity) meteors and that radars would be severely biased against such objects. Our observations show that these pessimistic views are in error (Section 1.2.2.3).

F. The quantum mechanics of collisions among meteoric and atmospheric atoms and molecules was virgin ground. We made a start on the necessary theoretical developments, for eventual benefit in meteor and other research (Section 1.2.2.4).

G. Unobserved winds in the meteor layer would introduce errors in our orbits. With a phase-coherent radar (Section 1.2.1.1), we avoid these errors (Section 1.2.2.5). Further, we can properly attribute apparent inconsistencies in atmospheric diffusion to wind.

1.1.3 Meteoroid hazard and the spatial distribution of meteoroid material

The practical problem of the meteoroid hazard to spacecraft and many other problems of meteor astronomy require for their solutions an identical set of basic data. Our radar meteor-observing program was designed to obtain meteor data for those objects too small to be detected by optical techniques and too large – and thus too infrequent – to be recorded by direct measurements made in space.

Number distributions of meteoroid masses and velocities as a function of position in the solar system are needed for a complete answer to any of the problems. Our new observations, together with the advances in analysis described in Section 1.2, provide a quantitative and qualitative increase in the information needed to define those distributions.

A. We have constructed the most sophisticated and highest power meteor radar system in existence. Complete calibration of both receivers and transmitter is among its unique features (Section 1.2.1.1).

B. The system gathered a large body of reliable and homogeneous data. During the period October 1968 to December 1969 (our so-called synoptic year of observations) (Section 1.2.1.2), nearly 20,000 meteors were observed for which the data have been reduced for velocities, decelerations, ion densities, heliocentric orbits, and atmospheric winds and diffusion rates. An equal number of earlier (less accurate) reduced meteors and a larger number of unreduced meteors are at hand, together with extensive rate data.

C. The complete analysis of these and earlier data has commenced. Provisional values of the mass-number distribution have been prepared and are currently being updated to include the new data on the mass-ionization relationship obtained through the optical and radar observations. Stream meteors have been distinguished from sporadic meteors in the earlier data (Section 1.2.3.1), and the process will be quickly extended to the synoptic year. The final spatial distributions are being determined and studied under a current NASA contract (NAS 1-11204).

1.2 Summary of Results

1.2.1 The meteor radar

1.2.1.1 The equipment. Meteor observations typically have been limited by available technology; i.e., most of what could be done within the state of the art and a reasonable budget has been done. The eight-station meteor radar system at Havana, Illinois, is the best example of that generalization. Based on principles developed at Jodrell Bank, England, all aspects of the radar system were extended in order to get the best possible radar meteor observations. The system was expanded to eight stations, rather than the necessary minimum of three, enabling documentation of all phases of the interaction of single meteoroids with the atmosphere. This proved most valuable to our understanding of the physics of these interactions. In order to be able to observe radar meteors fainter than previously observed, we used a powerful transmitter, high-gain antennas, and sensitive receivers. From observation of faint meteors, we were able to collect a large observational sample for space-distribution studies, to probe a previously unobserved range of meteor masses, and to make a meaningful comparison of our results with the zodiacal light and space observation of

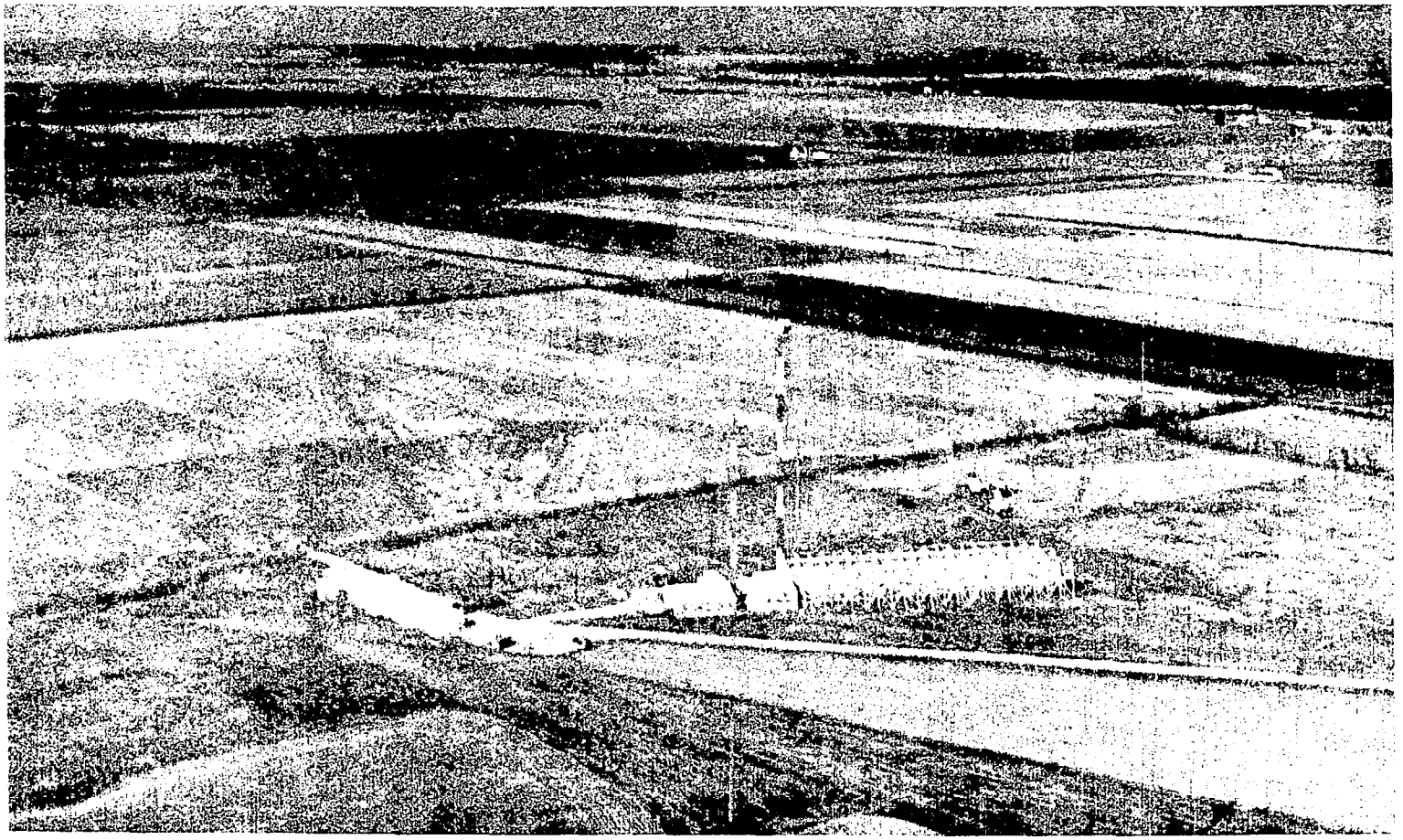

Plate 2. The transmitter site, during the antenna-gain measurements. Left of the trough antenna are the microwave towers, the receiver building, and the transmitter building. Further left is the National Bureau of Standards building. Right of the trough are the small white Prairie Network camera building and the derelict 1024-dipole antenna. Above are the NASA aircraft-tracking radar and two vans for receivers and recorders.

the meteoroid flux. For full use of the observed radar echo amplitudes, the system was carefully calibrated throughout, enabling important discoveries in meteor physics to be made. So that errors caused by atmospheric winds could be corrected, the system was adapted to measure echo phase as well as echo amplitude. Numerous other improvements in techniques were made.

Last but not least, the eight-station radar system was used to collect a large, reliable homogeneous body of data.

1.2.1.2 The basic data. Between 1963 and 1966 the Havana radar system was updated and extended from six to eight stations. New receivers to detect both the phase and the amplitude of incoming meteor echoes gave the means for accurate height determinations and corrections of errors due to winds at meteor altitudes. The antennas were improved and their gain patterns measured. Finally, with the system in its historically best condition, it was operated from October 1968 to December 1969 on a regular schedule. We have called this the synoptic year, a 1-yr period of reliable high-quality homogeneous operation, designed to yield the best (and largest) sample of meteor data in existence. One year of observation is a natural period to include the earth's entire orbit and annual variations in the atmosphere. On completion of the reductions at NASA/Langley, the synoptic-year sample contained roughly 20,000 meteors.

Overall statistics of the synoptic-year sample are given in Section 7.

The synoptic-year data will be useful for many years to come for virtually every problem in meteor physics and astronomy. Particular applications in the coming year include assessment of observing biases (also by use of simultaneous radar-optical observations) and of space-density and stream distributions in interplanetary space.

For studies of meteor streams, it will be advantageous to combine the synoptic-year data with earlier Havana observations. Over 19,000 pre-1966 meteors are completely reduced, and at least as many post-1966 meteor observations can be reduced now that the synoptic year has been completed.

Complementary to accurate observations of individual meteors are observations of meteor hourly rates (Section 9). These yield the number distribution of echo amplitudes unaffected by recording biases, which is necessary for finding the distribution of meteoroid masses.

1.2.2 Physical processes and biases in radar meteors

1.2.2.1 Recombination. We have observed electron-ion recombination in many of our meteors. When the initial space density of electrons is high, as in relatively bright low meteors, recombination rapidly reduces the electron density and thus attenuates the radar echo.

In a single meteor, the observable effects of recombination are unusually large oscillations in the early part of the Fresnel pattern and, in some cases, rates of amplitude decay that are much higher than the normal decays caused by electron diffusion. In our large sample of meteors, recombination is also observable in an apparent scarcity of comparatively bright meteors in the lower part of the observed height range, although there are numerous faint low meteors.

Dissociative recombination of ionized atmospheric molecules N_2^+ and O_2^+ is the only atomic process consistent with our observations. We infer that these molecules are ionized in the initial formation of the ionized column or that there is rapid charge exchange. Photographic meteor spectra primarily show atomic radiation, with occasional neutral molecular (N_2) bands. Consequently, observation of ionized molecules may provide an important clue to the detailed atomic and molecular processes in meteors, which are now virtually unknown.

Recombination eliminated almost all slow meteors from earlier radar surveys, so their velocity and orbit statistics suffer from severe bias. Because the Havana observations reach fainter meteors, they include numerous slow meteors. Consequently, the Havana observations are less biased than others and constitute the only set of observations that can be corrected for this bias.

Unsuspected recombination invalidates virtually all determinations of meteor ionizing efficiency derived from combined radar optical observations made before the Havana-Sidell observations, in particular, all comparisons at lower meteor velocities.

1.2.2.2 Fragmentation. We have observed fragmentation in the majority of our meteors and infer that fragmentation probably occurred unobserved in many others.

Spatial separation of the meteor fragments in flight has two effects on the radar echo: 1) separation along the trajectory damps out the later oscillations in the Fresnel patterns, and 2) separation normal to the trajectory severely attenuates the whole radar echo. We have observed 1) in a large proportion of our meteors, and we believe that 2) explains why our observed ionization curves are significantly shorter, on the average, than our meteor light curves. This is confirmed by some simultaneous radar-optical observations, where the radar echo ends several kilometers before the luminosity does.

The occurrence of fragmentation shows that most small radar meteors, like most larger photographic and visual meteors, have comparatively low strength. Thus they are not similar to meteorites, except perhaps to carbonaceous chondrites. This light and fragile structure has been plausibly associated with a cometary origin.

There must be an appreciable selection effect against radar observations of fragmenting meteors, but its real importance remains to be discovered.

1.2.2.3 Initial radius of the ionized column. The immediate spread of newly ionized electrons away from a meteoroid before they are slowed to thermal velocities is not simple to calculate, and widely differing values have been published. However, if the initial radius of the column is comparable to or larger than $1/2\pi$ times the radar wavelength, the radar echo is severely attenuated. Since the initial radius must be approximately proportional to the atmospheric mean free path, the initial-radius phenomenon sets an observational ceiling on the heights of meteors that can be observed with a radar of given wavelength.

Our observations of meteor heights show that Manning's (1958) value for the initial radius is much more nearly right than Öpik's (1958) larger value, at least for our range of observed magnitudes. The observational ceiling due to the initial radius approximately coincides with that due to electron diffusion in the atmosphere and does not conceal a large fraction of the meteoric influx.

We will be able to make reliable and undramatic corrections to our statistics for the initial radius. Nonetheless, the importance of knowing the initial radius can be seen in some Russian orbital distributions (Kascheev, Lebèdinets, and Lagutin, 1967) computed from observations using a radar similar in wavelength to ours. Believing that the initial radius was comparatively large and making the appropriate corrections to their statistics, they inferred that radar meteor orbits contain a large fraction in retrograde motion, with larger average eccentricities and inclinations than any other set of bodies in the solar system. Of course, this is contrary to every other meteor study.

1.2.2.4 Ionizing efficiency: a theoretical approach. No detailed description exists of the interaction, on the molecular scale, between a meteoroid and the atmosphere, and none can be constructed until we have much more information in at least one of two areas (probably both). The first area is the composition, density, and structure of the meteoroid, on all scales down to the atomic. The second area is the response of atoms and molecules to collisions in the energy range from a few electron volts to a few hundred. Interpretation of radar observations is much more hampered than optical observations by the general ignorance in this second area.

Large electronic computers and theoretical advances had brought the quantum-mechanical study of meteoric atoms at meteoric energies within reach by 1968. We grasped this opportunity.

The quantum-mechanical study of collision processes at meteoric energies is necessarily a long-term effort (several years) because the usual approximations are applicable only to much higher or much lower energies. It is necessary first to elaborate each possible approximate model and then to test and apply it to a long succession of more complex particles and interactions.

M. R. Flannery and H. Levy II, with the guidance of A. Dalgarno, made a vigorous beginning on the theory (Section 12), but shortage of funds prevented continuation. Their work cannot help but prove valuable for eventual advances in this area.

1.2.2.5 Atmospheric winds. Winds at meteor heights, and more particularly shears between winds at different heights, have degraded radar meteor observations that did not take proper account of them. Distortion of the ionized column by unknown winds introduced radiant errors of a few degrees and anomalies in apparent atmospheric diffusion. The consequent errors in meteor orbits exceeded all other errors, and the diffusion errors caused much misunderstanding.

Coherent phase was introduced throughout the Havana radar system in 1963 to 1966 in order to measure winds and correct for them. Thus we have been able to eliminate wind errors in our 1966 to 1970 radiants and orbits and to assess diffusion data in valid fashion. We also possess many wind observations of potential value.

1.2.3 Meteor streams and the spatial distribution of meteoric material

1.2.3.1 Meteor-stream structure. The large sample of reliable meteor orbits observed in Havana is the best material in existence for studies of the structure of stream orbits. Thus far, we have used Havana orbits observed before the synoptic year for this work. Z. Sekanina, using the D-criterion previously found valuable for stream studies, has shown that a stream-orbit distribution can be well fitted by a Maxwellian distribution of orbital elements superposed on a uniform background of nonstream orbits. The probability that observed clusters of similar orbits are not just random groupings is readily determined.

The spread in orbital elements within a stream is found to be positively correlated with the age of the stream; older streams are less compact.

The statistical model of meteor streams makes it possible to estimate the stream-to-sporadic space-density ratio of meteors. We find that the density in meteor streams is 1/2 to 2 1/2 orders of magnitude higher than that in the surrounding background; the hazards for a spaceship passing through a meteor stream would be correspondingly higher.

The largest radar stream search yet conducted has revealed 72 streams, in addition to the major optical streams. There is a strong tendency for these streams to cluster among themselves, but few are associated with known comets. There can be no doubt that these new facts will be highly important in understanding meteor evolution.

1.2.3.2 Apollo asteroid streams. Streams were discovered moving in orbits similar to those of the minor planets Icarus, Adonis, Hermes, and Apollo. The associations are statistically very significant, but practical proof requires analysis of more observations. Preliminary studies suggest that the association between a stream and Adonis is the most likely.

The logical difficulty of perturbing these asteroids from the main asteroid belt to their present orbits had already led to the hypothesis that earth-crossing asteroids were remnants of comets. Sekanina's surprising discovery of associated streams thus gives strong support to the comet-remnant hypothesis, in view of the difficulty of generating a meteor stream from a purely solid body.

1.2.3.3 Space density of meteoroids. The space-density distribution of small meteoroids has been computed from radar meteor orbits observed at Havana, with corrections applied for observational selection and for orbits that do not intersect the earth. We expect that our newly revised ionizing efficiency will refine the following results without qualitative changes. Within the limits 0.1 to 10 a.u., the space density decreases monotonically outward from the sun. The distribution in heliocentric latitude has a very broad maximum centered on the ecliptic and a deep minimum over the ecliptic poles. There is no evidence for any substantial enhancement of density in the asteroid belt.

The meteor orbital distribution is generally similar to that of short-period comets. Eccentricities and inclinations are significantly higher than for the main-belt asteroids, apparently precluding an asteroidal origin for at least the majority of meteors. An origin in short-period or long-period comets is quite consistent with observations, since perturbations by Jupiter would transform long-period meteor orbits to short-period, just as they would for comet orbits. The radial gradient of

meteor space density shows that most meteors do not survive to spiral into the sun under the Poynting-Robertson effect; doubtless they are destroyed by collisions with the small particles seen in the zodiacal light.

1.2.4 Optical observation

1.2.4.1 Luminous efficiency. The luminous efficiency of a meteor is the effective fraction of its kinetic energy used in producing observable luminosity in a specified spectral bandpass. Luminous efficiency has been measured in the laboratory, in upper atmosphere flights of artificial meteors, from photography of a very few unfragmenting natural meteors whose masses can be deduced from their aerodynamic deceleration, and recently from the photographed fall of the Lost City Meteorite.

Observations of the last few of a series of artificial meteors launched from Wallops Island were made under this NASA contract (Ayers, McCrosky, and Shao, 1970). Although these were difficult observations and of limited precision, they alone yielded realistic measures of the luminous efficiency of well-known objects in the real atmosphere. In practice, artificial-meteor observations have been the indispensable standard, used to show that other measures of luminous efficiency had taken all factors into account and could be used to deduce meteor masses from luminosity.

1.2.4.2 Discrete levels of beginning heights of meteors in streams. Ceplecha (1968) found that observed beginning heights of photographic meteors clustered to three discrete levels spaced at intervals about 5 km in height. Each level depends on meteor velocity in the same way and is higher for faster meteors. These levels correspond to differences in meteoroid density. The highest density meteors, Class A, are clustered near the lowest beginning height, and the lowest density meteors, Class C, are clustered at the highest beginning height. Class B meteors cluster to an intermediate maximum in beginning height and are intermediate in density. Class A meteors, however, exhibit more fragmentation than do those of Class C.

Cook (1970) showed that the beginning heights of meteors of a given stream cluster about one or another of the Ceplecha levels, or sometimes about levels A and C with a gap at B. No Class B stream is associated with an observed comet. Cook interprets this clustering in terms of Whipple and Stefanik's (1966) model of an icy conglomerate comet nucleus with radioactive heating and redistribution of ices: Class A meteors originate in the core of a nucleus, and Class C meteors, in the outer layers after the ices have evaporated. Some ices were redistributed to Class A meteors in the core. Class B meteors originate in the cores of comets too small to have redistributed ice.

Thus, the discrete levels of beginning height are an exceptionally promising clue to the detailed origin of meteors.

1.2.5 Simultaneous radar-optical observations

In 1967, a borrowed Navy image-orthicon system was installed at Sidell, Illinois, 188 km east of the Havana radar system, to observe some of the same meteors that were observed in Havana. This site was chosen to maximize the rate of simultaneous observations (SIMOBS) by both systems. A SEC Vidicon was also used in Sidell during September, November, and December 1970. Approximately 95 meteors were adequately observed by both the radar and the optical systems from February 1969 to December 1970. We have fully reduced the first 29 of these. We plan next to reduce 22 more from the nights of November 6-7 and December 1-2, which promise to contain the bulk of the information from the remaining observations.

Simultaneous observations were instituted to answer the pressing need to know the ionizing efficiency, so that we could determine the masses of the Havana radar meteors. The first few SIMOBS yielded a realistic approximate value for the ionizing efficiency, averaging one-tenth the previously accepted value, and an indication of the velocity dependence of ionizing efficiency.

We also expect to observe other physical effects by means of simultaneous observations. We have confirmed the great importance of recombination and fragmentation to the interpretation of radar echoes; analysis of all the simultaneous observations may bring forth other such effects.

1.3 References

Ayers, W. G., McCrosky, R. E., and Shao, C.-Y. (1970). Photographic observations of 10 artificial meteors. Smithsonian Astrophys. Obs. Spec. Rep. No. 317, 40 pp.

Ceplecha, Z. (1968). Discrete levels of meteor beginning height. Smithsonian Astrophys. Obs. Spec. Rep. No. 279, 54 pp.

Cook, A. F. (1970). Discrete levels of beginning height of meteors in streams. Smithsonian Astrophys. Obs. Spec. Rep. No. 324, 22 pp.; also in Smithsonian Contr. Astrophys., in press.

Kascheev, B. L., Lebedinets, V. N., and Lagutin, M. F. (1967). Meteoric phenomena in the earth's atmosphere. Results of Researches on International Geophysical Projects, Investigations of Meteors, no. 2, Nauka, Moscow, 260 pp.

Manning, L. A. (1958). The initial radius of meteoric ionization trails. Journ. Geophys. Res., vol. 63, pp. 181-196.

Öpik, E. J. (1958). Physics of Meteor Flight in the Atmosphere. Interscience Publ., New York, 174 pp.

Whipple, F. L., and Stefanik, R. P. (1966). On the physics and splitting of cometary nuclei. Mém. Soc. Roy. Sci. Liège, sér. 5, tome XII, pp. 32-52.

2. DESCRIPTION OF EIGHT-STATION RADAR NEAR HAVANA, ILLINOIS

Richard B. Southworth

2.1 General

The concept of a triangular array of three radar stations to determine the trajectories of radar meteors is due to T. R. Kaiser (see Hawkins, 1964, p. 44). Gill and Davies (1956) constructed such a system at Jodrell Bank, England. The Harvard Radio Meteor Project six-station system at Havana, Illinois, developed by Hawkins (1963) was a considerable enlargement and elaboration of the Jodrell Bank system. In particular, the Havana system incorporated high-gain antennas and a powerful transmitter in order to reach much fainter meteors, down to at least radar magnitude +12.

The eight-station system at Havana was the result of a further considerable enlargement and elaboration of the six-station network. The two additional stations were sited primarily for wind measures, but they also served to increase the accuracy of measurement. The most important change was the transformation to a phase-coherent system, permitting measurement of atmospheric winds, and thereby permitting correction of wind effects in the data. The conversion to phase coherence necessitated new receivers and much added equipment. Other important changes included digital-recording equipment, transmitter and receiver calibration units, and subcarriers in the microwave links between the stations.

A detailed system description is available (Deegan, Fitzpatrick, Forti, Grossi, Schaffner, and Southworth, 1970). We give only a general description here. The antenna-gain patterns are described in Section 4.

2.2 Station Locations

Figure 2-1 shows the general layout of the system, and Table 2-1 gives accurate station locations. Station 3 is the transmitting station, at the former Long Branch

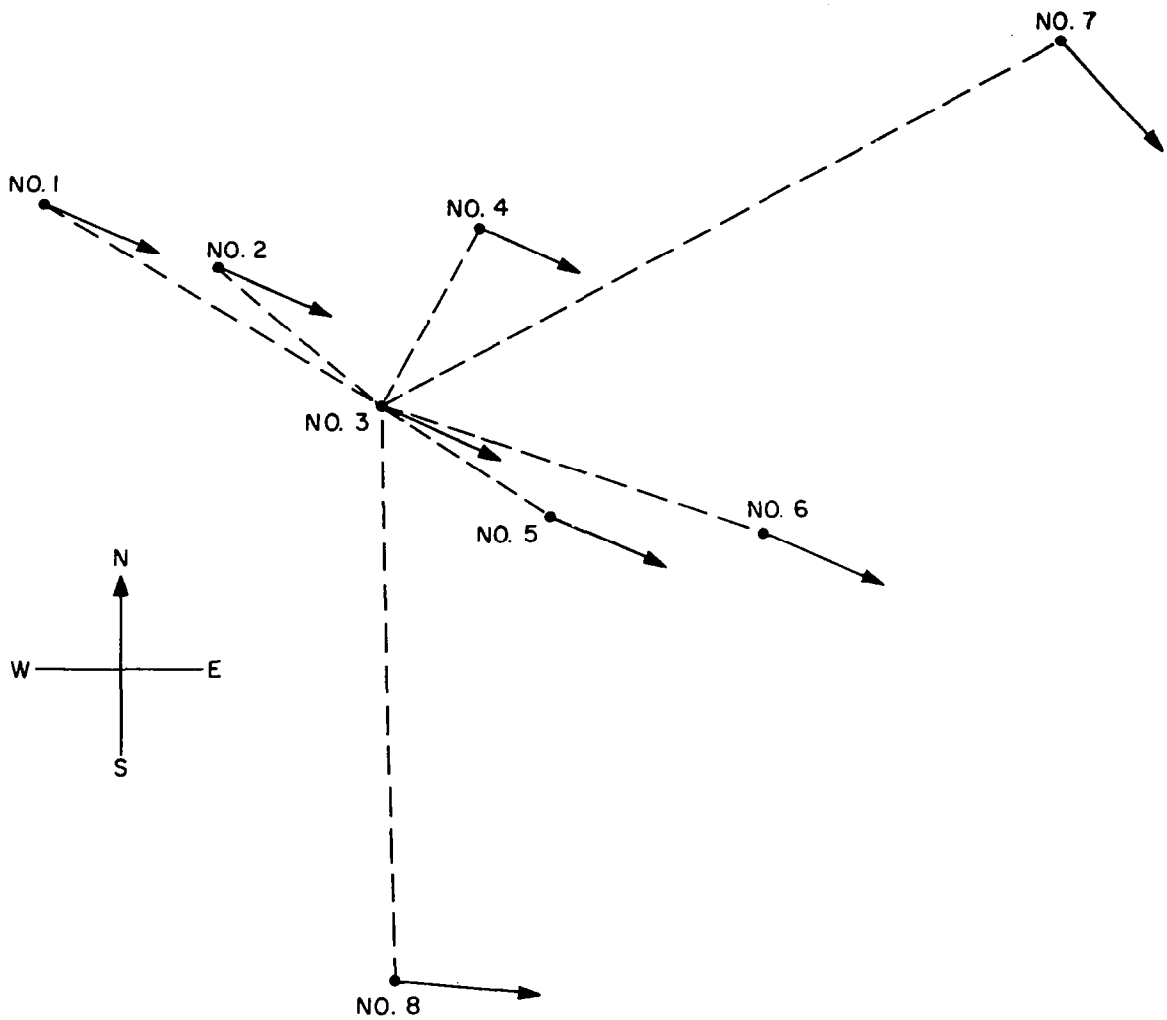

Figure 2-1. Network layout. Dashed lines represent microwave links. Arrows represent antenna axes: azimuth 113° East of North at sites 1 to 6, 139° at site 7, and 94° at site 8.

field station of the National Bureau of Standards (it now belongs to the National Oceanic and Atmospheric Administration) near Havana, Illinois. All other stations are linked to station 3 by two-way microwave equipment, and all stations including station 3 have receivers. Stations 1 to 6 have double trough-guide antennas with 22-db gain, while stations 7 and 8 have 13-element Yagi antennas with 14-db gain. Most meteors are observed at slant ranges of about 150 to 250 km, between azimuths of about 90° and 135° from station 3.

Table 2-1. Station coordinates.

Station number	Latitude	Longitude	Bearing East of North from site 3	Distance from site 3 (km)
1	40° 19'34"	90° 15'22"	300° 44'53"	23.14
2	40 17 36	90 08 08	310 08 57	12.64
3	40 13 11	90 01 19		
4	40 18 44	89 57 46	26 09 16	11.43
5	40 09 47	89 54 32	123 11 36	11.53
6	40 09 23	89 45 45	107 34 17	23.19
7	40 25 02	89 31 44	62 14 20	47.29
8	39 54 36	90 00 51	178 53 03	34.42

2.3 Principle of System Design

A meteoroid in its passage through the atmosphere leaves a column of ions and electrons; our radar detects only the electrons. A simplified picture of the scattering phenomenon can be obtained by considering that a radiowave at VHF (as in our case) incident on the column is scattered by individual free electrons, each of which oscillates as if no other were present (underdense trail condition). The "specular reflection point" (for a station or pair of stations) is the point on the trail at minimum distance from the station, or minimum sum of distances from the pair of stations. Echoes from electrons near the specular reflection point arrive in phase and are observed; echoes from points distant from the specular reflection point arrive out of phase and cancel each other.

Of the whole trail, the effective length that contributes to the scattering is the first Fresnel zone around the specular reflection point, half of which equals $\sqrt{R_0\lambda/2} \cong 1$ km when the receiver and transmitter are at the same station. (R_0 is the distance of the trail from the radar station, and λ the wavelength.) When the receiver and transmitter are not at the same station, this zone has a more complicated expression. Different pairs of stations receive scattered signals from different parts of the trail.

Upper atmospheric winds displace the effective specular reflection points and physical processes alter the amplitude of received echoes, but both effects are almost always of second order in determining the position of a trail. They are measured and used to correct the reduction.

We use the motion of the meteoroid that forms the meteor trail (the "target") to find the position of the trail. As the trail is extended past a specular reflection point, the addition of electrons that are alternately in and out of phase with the main echo from the principal Fresnel zone generates a characteristic "Fresnel" pattern in the received signal. From the spacing in time of the oscillations in this pattern and the length of the principal Fresnel zone, we find the velocity of the meteoroid (McKinley, 1961; Southworth, 1962). From that velocity and the spacing in time between the Fresnel patterns observed at different stations, we find the distances between specular reflection points. Two such distances, corresponding to noncolinear pairs of stations, determine the direction of motion of the meteoroid; additional distances may strengthen the determination.

From these data, we can further determine that the specular reflection point from the main site lies in a plane normal to the direction of motion of the meteoroid, at an observed range from the main site. The meteor trail lies on a cylinder normal to that plane. Measures of differential range from our closely spaced sites are, in general, not sufficiently accurate to fix the location of the meteor trail on the cylinder; but this location is determined by an interferometric measure at station 3 by using the two halves of the double trough guide as separate antennas for reception.

The intent of the six-station (and later the eight-station) system was to observe a large sample of radio meteors as well as possible. Kaiser pointed out that three

stations would be sufficient to establish the meteor's trajectory, but three points do not determine the ionization curve or the run of other physical parameters so completely as we need to know them. Six or eight stations would yield useful ionization curves, as well as a larger number of meteors, greater accuracy, and greater reliability. Five of the six original stations were placed approximately along a straight line, spaced to observe at intervals over most of the length of some of the longest meteor trails expected. We found that meteor trails are notably shorter than expected – a very important result that would not have been discovered with only three stations. Six observations were obtained on a single meteor trail only when the trail was oriented to have the observed points at less than maximum spacing.

2.4 System Connections

Figure 2-2 is a simplified block diagram of the eight-station electronic equipment. A frequency generator embodying a master oscillator supplied coherent phase to the transmitter and all receivers. Phase was communicated to the distant stations by a 2.5-kHz reference tone, initially via telephone lines and later via microwave links. At each distant site, a servoloop kept slave oscillators in phase.

2.5 Transmitter

The Continental PO-830 transmitter was built for the National Bureau of Standards, intended as part of the prototype for the Jicamarca radar. The operating frequency was 40.92 MHz. We operated it at 738 pulses sec^{-1}, with pulses 6 μsec long at half-power. The maximum peak power available was 4 Mw, but it was usually operated at 2 Mw. The twin transmitter outputs were connected to the double-trough antenna by TR-ATR networks, enabling the station 3 receiver to use the same antenna between transmitter pulses.

2.6 Receivers

Each distant station had a single-channel phase-sensitive receiver with three outputs, proportional, respectively, to the logarithm of received amplitude and to the linear amplitude multiplied by the sine and cosine of the phase of the signal relative

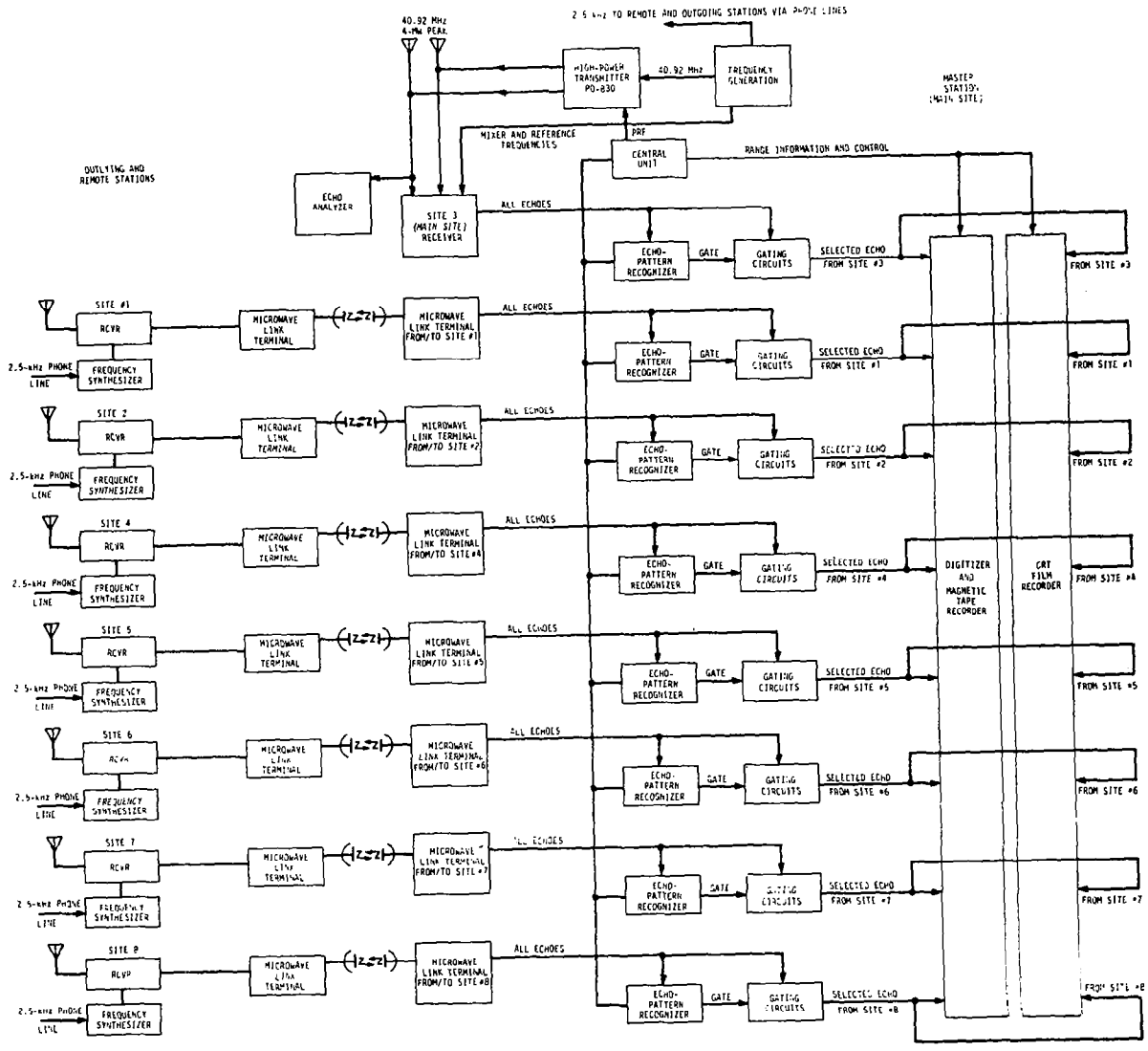

Figure 2-2. Simplified system block diagram of the radar network.

to the system phase. These outputs were multiplexed and returned to station 3 via the microwaves. Receiver noise was negligible compared to galactic noise; the bandpass was 230 kHz.

At station 3, a similar two-channel receiver with six outputs was connected to the two antenna troughs via the TR-ATR networks.

2.7 Logics

Observation of faint meteors necessitated elimination of as much noise and interference as possible; this included recording only one echo at any time when two or more echoes were present. Furthermore, we could not afford to record on tape and film when no echo was present. The meteor-recognition logics, designed by Dr. M. R. Schaffner, maintained representations of all echoes at each station as digital words in a delay line. Meteors were recognized as echoes that repeated at the pulse frequency to at least a threshold amplitude for eight (normally) pulses, or for 8 + x with x repetitions below threshold. A newly appearing meteor was eligible for recording if another was not already being recorded. Any echo enduring more than 0.75 sec was ineligible for continued recording; these included overdense meteors and airplanes. All noise and interference more than a few tens of microseconds (i.e., more than a few kilometers in range) from eligible echoes were gated out from the recording.

A separate logic for each station was located at station 3, the station 3 logic using the outputs of one channel of the receiver there. All logics communicated to a central unit, which triggered the recording equipment whenever the recording was stopped and a new meteor echo was recognized at any station (except usually not for new echoes at station 7 or 8).

2.8 Range Measurement

The slant range to the meteor was measured by the propagation time to and from the ionized column. In the six-station system, range was measured only from station 3. The ambiguity of multiples of 200 km (corresponding to the ambiguity of pulse intervals in the propagation time) was resolved by doubling every fifth transmitted pulse. However, the doubled pulse caused difficulties with the transmitter.

In the eight-station system, the ambiguity was resolved by delaying every fifth pulse after each recording was triggered, for the duration of the recording. The central logic unit communicated the pulse delays to the transmitter and sent range measures to the recording equipment (in digital form to the tape recorder). The loop propagation time was measured every five pulses for each station in turn that newly recognized an echo.

2.9 Recording

Meteors were recorded in parallel on film and magnetic tape. The 70-mm film recording was used for field inspection and for selecting records for computer analysis. Eighteen cathode-ray tubes presented analog representations of nine sets of phase data, eight sets of logarithmic amplitude data, and one set of range data at each pulse. Sine and cosine of phase from each station except station 3 were multiplexed on one tube; station 3 phases were multiplexed on two. The amplitude from the south trough channel at station 3 was not recorded on either film or tape. A digital clock illuminated by a strobe identified each record frame.

Half-inch computer-readable magnetic tape recording was used for all detailed analysis. Eighteen channels recorded essentially the same information as the film, except that the sine and cosine phase signals were recorded alternately. All quantities except range were digitized to 8-bit accuracy; the range gave the propagation time in units of 0.25 μsec and the station identification. Time was recorded at the end of each meteor record.

Additional recording equipment is described in Sections 9 and 10.

2.10 Calibrators

The transmitted pulse powers were measured with the aid of calibrated probes in the TR-ATR networks. Received power was calibrated by signal generators at each station, controlled by tones transmitted over the microwaves. Signals were inserted into the receivers through stepping attenuators that covered the dynamic range of the system. Calibrator signals were recorded in the same way as meteors and applied in the computer reductions.

2.11 References

Deegan, N. F., Fitzpatrick, R. J., Forti, G., Grossi, M. D., Schaffner, M. R., and Southworth, R. B. (1970). Study of Meteor Wind Measurement Techniques. Final Report on Contract AF 19(628)-3248. Smithsonian Astrophys. Obs., 2 vols.

Gill, J. C., and Davies, J. G. (1956). A radio echo method of meteor orbit determination. Mon. Not. Roy. Astron. Soc., vol. 116, pp. 105-113.

Hawkins, G. S. (1963). The Harvard Radio Meteor Project. Smithsonian Contr. Astrophys., vol. 7, pp. 53-62.

Hawkins, G. S. (1964). Meteors, Comets, and Meteorites. McGraw-Hill Book Co., New York, 134 pp.

McKinley, D. W. R. (1961). Meteor Science and Engineering. McGraw-Hill Book Co., New York, 309 pp.

Southworth, R. B. (1962). Theoretical Fresnel patterns of radio meteors. Harvard College Observatory Radio Meteor Project Res. Rep. No. 14, 60 pp.

3. SIMULTANEOUS OBSERVATIONS BY TELEVISION CAMERA AND RADAR

Richard E. McCrosky and J. T. Williams

In 1967, we acquired on temporary loan from the Naval Research Laboratory (NRL) an image-orthicon system to observe artificial meteors at Wallops Island. At about the same time, we initiated a study of the feasibility of obtaining simultaneous radar and optical observations (SIMOBS) of the same meteor using the Havana radar and the NRL image orthicon or some similar device. The SIMOBS program was the result of the great interest in relating the newly acquired information on the luminous efficiency of optical meteors derived from the artificial-meteor experiments to the relatively unknown ionizing efficiency. The results of the study and our experience at Wallops Island (see Meteor Research Program Semiannual Technical Report No. 4, 1968) suggested that SIMOBS were possible, although perhaps difficult.

In fact, the initial study somewhat underestimated the difficulty of the observations, partly because the television equipment could not be operated at peak sensitivity when photometry was required and partly because of a secular decrease in the sensitivity associated with aging of the image-orthicon tube. Nevertheless, the program has been most successful. Corrections of about a factor of 16 in previous estimates of the ionizing efficiency are indicated. The observations and analysis leading to this result are given in Sections 6 and 8. Here, we describe the original image-orthicon equipment, adaptations made to enhance its usefulness for meteor observations, the specialized calibration and photometric procedures developed for our purposes, and finally, some brief comments on our experience with a second observing system, the Secondary Electron Conduction (SEC) Vidicon.

Figure 3-1 shows a flow chart of the system.

3.1 Equipment and Modifications

A U.S. Navy shipboard image-orthicon system, AN/SXQ-3, was originally modified by G. T. Hicks and G. G. Barton of NRL to accept a 105-mm focal length, f/0.75

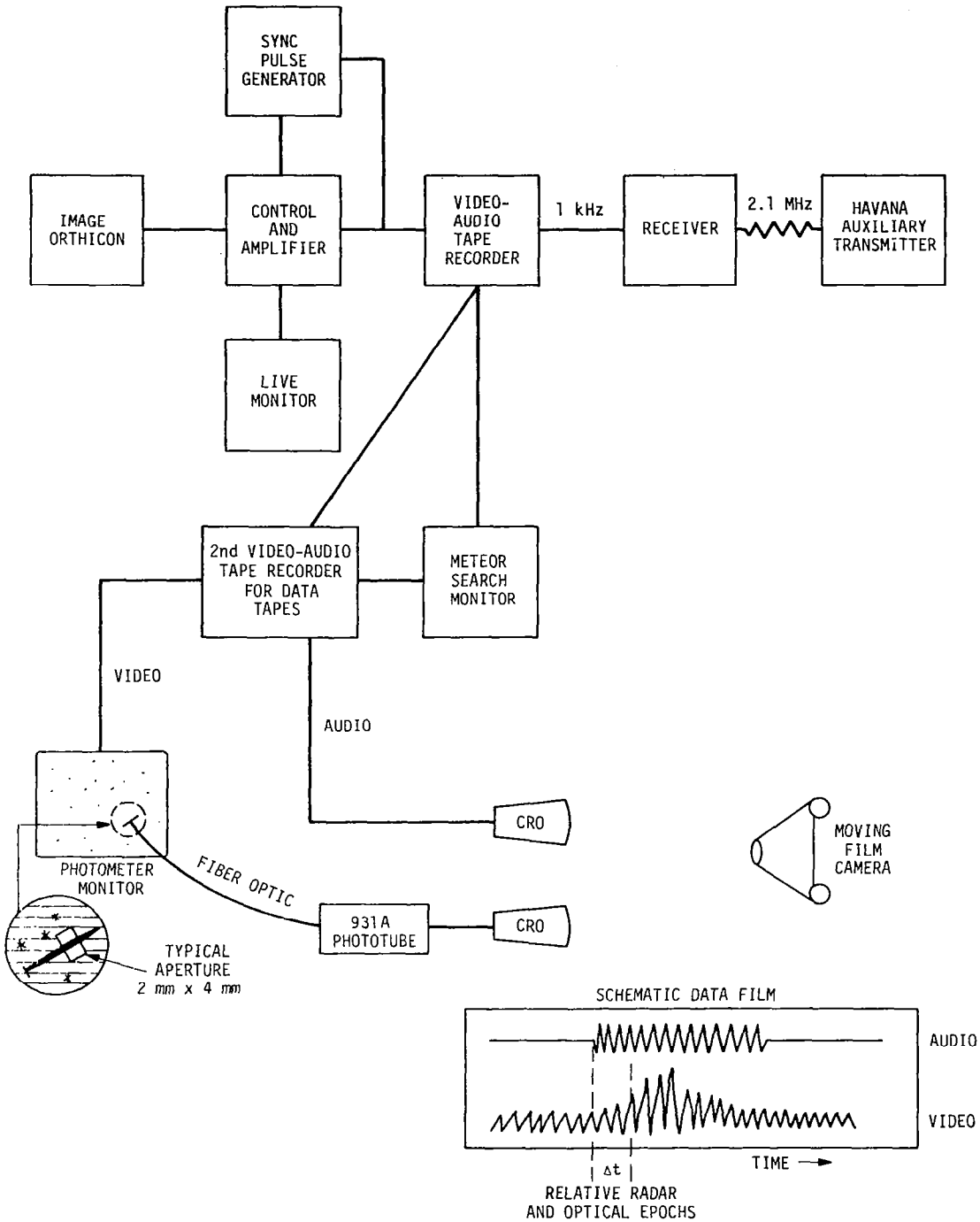

Figure 3-1. Image-orthicon observing and data-reduction system.

lens for night-sky observations. The system consists of 1) an image-orthicon camera equipped with a GE 7967 image-orthicon tube and fitted with the 12.5-cm objective, 2) a motor-driven altitude-azimuth pedestal on which the camera is mounted, 3) a camera control console with video amplifiers and a monitoring kinescope; and 4) a remote 14-inch kinescope suitable for photographic recording. The normal video format of the SXQ is 30 interlaced 875-line frames per second with separate vertical and horizontal drive signals. To facilitate magnetic tape recording of the video for our purposes, vertical and horizontal sync pulses were generated from the drive signals. We added these pulses to the video through a separate distribution amplifier. This modification made practical the use of an inexpensive helical-scan video tape recorder (Ampex VR-7500) for routine recording of observations. The recorders were slightly changed to improve the playback quality of the 875-line video by increasing the tape speed by 4%.

In order to preserve a nearly constant sensitivity independent of sky conditions, much of the automatic gain-control (AGC) circuitry was eliminated or bypassed. These modifications permitted a less frequent calibration of the sensitivity of the system.

We also modified the camera beam-current control to expand the adjustment in the very low light-level region. This enabled the image erasing beam to be carefully adjusted to erase the image-orthicon target charge slightly more slowly than the rate of deposit for images within the useful dynamic range. The resulting "image lag" not only was tolerated but in fact became a useful part of the scheme for the photometry of slower moving images.

In order to ensure consistent short-term performance and repeatable month-to-month operation of the image orthicon, a monitoring scheme was devised for the image-orthicon electronics. A 10-MHz bandpass oscilloscope sampled and displayed the video (at the horizontal rate) early in the control electronics where the video balance, horizontal shading, and relative background-signal level are set. Monitoring at this point was beneficial in minimizing across-field gain variations horizontally and in controlling the video preamplifiers (the AGC circuitry had been disabled). A second oscilloscope display at the vertical scan rate was alternated between the amplified video (after blanking) out of the control unit and the composite video/sync at the video tape

recorders. The video/sync displays, 60 fields per second, unmasked subtle changes in the target-scanning beam current, background noise level, and vertical shading. There is no specific vertical-shading control in the SXQ system; however, variations in gain across the field vertically were minimized when the beam current and gain parameters were properly adjusted for dark sky conditions.

Generally, the electronic gain of the system proved to be fairly stable. However, the beam current was subject to subtle variations over a period of 1 to 3 hr. Consequently, the beam-current adjustment became the primary control for the camera video, leaving the gain controls for the entire camera-control unit—recorder system reasonably constant for the last 18 months (July 1969 through December 1970) of simultaneous observations.

3.2 Observing Techniques

Radar meteors are observed when the meteor is at a minimum range, i.e., when the meteor is 90° from the radiant and moving with maximum angular velocity. Optical detection systems are most sensitive for meteors near the radiant when the writing speed at the focal plane is at minimum. An optical observing site was established near Sidell, Illinois (Long. 87°51.2 W, Lat. 39°56.6 N). From this site, an optical system directed at elevation 49° and azimuth 263° has a maximum probability of observing objects in the meteor region at about 90-km altitude that are also observable by the Havana radar (see Figure 3-2).

When operated in full sensitivity, the radar observes meteors at about 100 times the image-orthicon rate. This mismatch has two deleterious consequences. First, the problem of selecting those meteors that are true SIMOBS is difficult since, almost assuredly, some radar object will be under observation whenever the image orthicon records a meteor. Second, since the radar logic constrains the system to observing one meteor at a time, the radar data-recording system is quite likely to have been pre-empted by a faint, uninteresting meteor that occurred shortly before the brighter object was observed optically. Consequently, the radar receivers were attenuated at their input by 13 to 25 db when SIMOBS were being attempted. To further ease the arduous task of selecting possible SIMOBS, the audio channel of the video tape recorded a 1000-Hz signal transmitted by an auxiliary transmitter at Havana whenever the radar data system began a record of a new meteor.

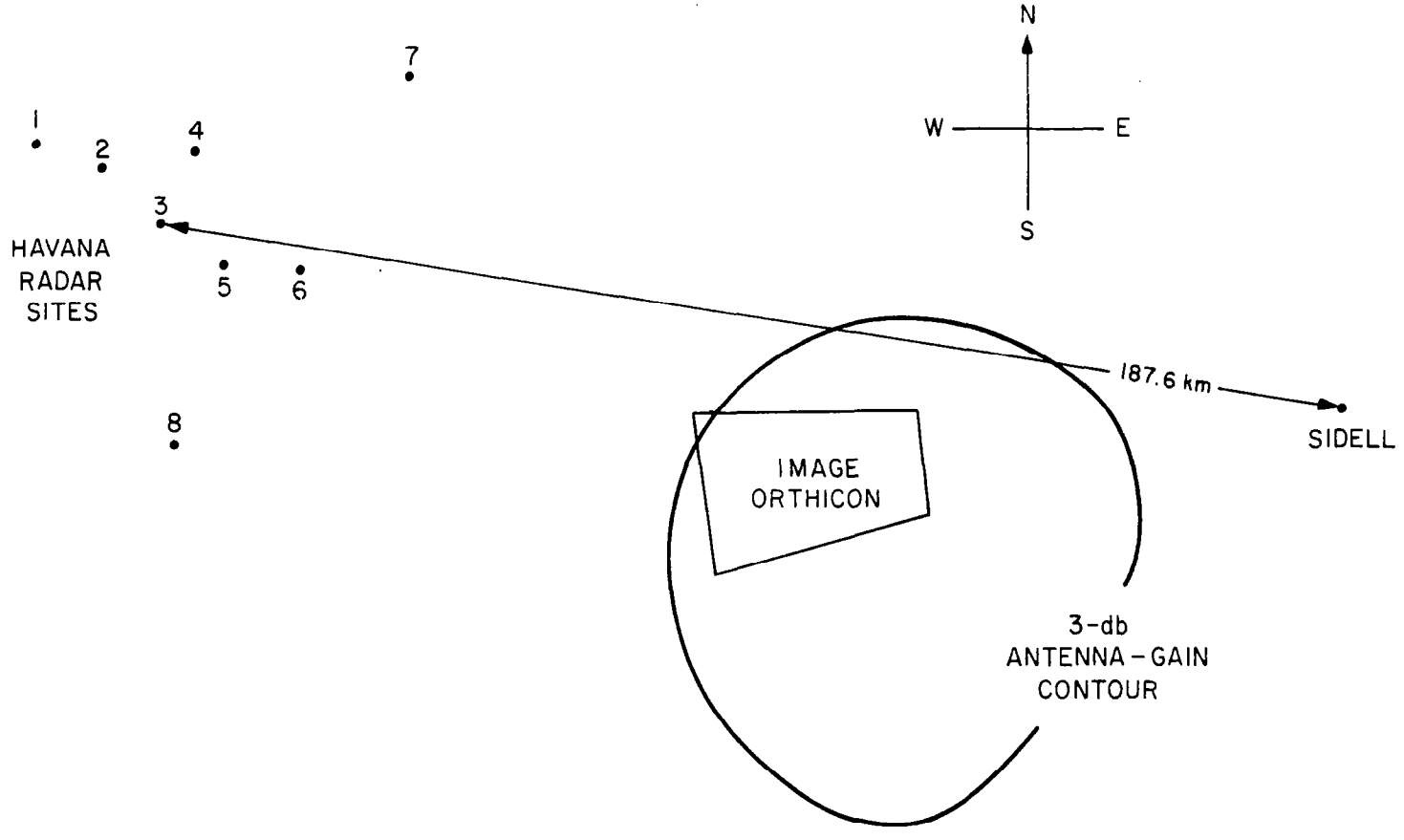

Figure 3-2. Projections of the intersections of the image-orthicon field of view and the antenna pattern with a plane 90 km above sea level. The image-orthicon field is offset from the center of the antenna pattern so that meteors moving normal to the line of sight from Havana move as nearly as possible in the line of sight from Sidell.

Observations were generally made during moonless skies and between 11 p.m. CST and morning twilight. Observing was usually curtailed when atmospheric extinction was variable or exceeded about 1 mag. Well-regulated line power and a 1-hr warmup ensured stability. The output was observed visually on a live monitor and recorded on tape. About 75% of the meteors were discovered on the live monitor, and the remaining during subsequent playbacks of the tape. Possible SIMOBS and calibration tests were copied repeatedly on data tape for future use.

3.3 Calibration

A two-step calibration procedure was followed. A pinhole light source was set up in the loft of a nearby barn. Direct current for the source was supplied from and monitored at the image-orthicon site. The source could be attenuated remotely from the site by sequential advancement of a neutral-density step wedge located between the source and the pinhole. A total of 10 steps of 0.5-mag attenuation per step were available. These calibration observations were made with the camera slewing in altitude. Slew rates of 1° to 15° sec^{-1} were used. These rates bracket the angular rates of most SIMOBS meteors, and the fundamental calibration was thus performed on a moving source comparable to a meteor.

The second calibration step was used to define an absolute scale, in terms of stellar magnitude, for the relative response determined for the artificial light source. Stars of known brightness were recorded while the image orthicon was slewed. In general, unreddened A0 stars in or near the observing field were chosen, but on some occasions stars of spectral class as early as B8 or as late as A3 (and rarely as late as A5) were used.

In summary, the first calibration step determined what in photography is called the characteristic curve, and the second supplied the zero point for this curve in terms usually employed to define meteor luminosity. This last procedure simultaneously accounted for changes in the image-orthicon system sensitivity and for variations in sky conditions.

3.4 Photometric Reductions

Photometry of meteors observed by photographic techniques presents problems not often encountered in astronomy or, indeed, in most areas of any science. The obvious (but seldom noted) fact that we can observe our objects only once immediately places stringent signal-to-noise restrictions on the data. The unexpected nature of the meteor event may introduce problems of dynamic range. Both problems are more serious in television techniques: System noise is much higher than for photographic emulsions, and the dynamic range is lower.

We considered two general techniques for our photometry. The first was to photograph the image-orthicon outputs – both meteor and calibration – and proceed in the manner familiar to us from our photographic work. There, we compare by eye the meteor and standard source images. We rejected this approach, however, because kinescope techniques are incapable of recording the fainter images.

The second approach was to deal directly with the electrical signal, generated from the video tape, which contains the maximum amount of undistorted information. However, observing the signal from each pixel on the meteor trail is not sufficient. It is necessary also to subtract the average signal of that pixel at a time before or after the meteor appears, i.e., to detect and account for that part of the signal that is due to night sky, stars, or system noise. Furthermore, an image orthicon does not read out its entire signal in a single frame. Since, as we learned, the integrated signal is a better and more useful measure than the peak signal is, the problem of interpreting the electrical signal is increased. Finally, expensive instrumentation is required to isolate the signal that forms a specific picture element.

We bypassed most of these problems by physically isolating the pixels of interest on a television monitor and generating a new electrical analog signal with a phototube observing the isolated region. It might appear that this technique suffers seriously by introducing nonlinearities of the phosphor of the monitor and indeterminate effects produced by the phosphor decay. In fact, none of the effects is important so long as our calibration data are treated by the same system of analysis as the meteor data. In a sense, we bring both the meteor and the calibration into the laboratory and observe them photoelectrically at our leisure.

In practice, all but a small aperture of the monitor screen – that part through which the meteor or calibration source will pass – is covered. The phototube records the luminosity of this area. The phototube output is registered on a chart recorder or displayed on a cathode-ray oscilloscope (CRO) and photographed. The integrated intensity of the meteor pulse above the background is taken to be proportional to the original intensity of the source or meteor for the time interval required to pass through the aperture. It is the integrated intensity, rather than the peak intensity, that is pertinent since an image orthicon, and particularly one adjusted for high sensitivity, reads out the signal much more slowly than the signal is impressed on the target. We also demonstrated that the integrated intensity divided by the time the source was in the aperture was nearly independent of the angular velocity of the source, or, in terms used in photography, this system obeys the reciprocity law. (This happy circumstance could hardly have been anticipated since the entire photometric system contains a number of nonlinear components.) Therefore, the instantaneous intensity can be determined once the angular velocity of the meteor is known. No second-order corrections are required when the meteor and calibration source are of different angular velocities.

Photometry is performed on as many independent points on the meteor trail as is necessary to define the light curve. For each point observed on the trail, a second pen of the recorder or a second CRO records the audio channel of the tape. Time correlation with the radar data is determined from the time difference between the meteor pulse and the onset of the 1000-Hz signal, as shown pictorially in Figure 3-1.

3.5 SEC Vidicon

During three observing periods, September, November, and December 1970, a SEC Vidicon system operated by NASA/Huntsville was used at the Sidell site as a companion to the image orthicon. The SEC is notably superior to the image orthicon for faint objects in that almost the entire target charge is read out by a single pass of the scanning beam. Both fainter meteors and higher velocity meteors can be observed with a much improved signal-to-noise ratio. A total of 30 probable SIMOBS were observed with the SEC. Reduction of these recent data has been postponed until the completion of the best image-orthicon SIMOBS, since we were hesitant to undertake the development of a new photometric procedure during the last months of our contract. Very recent and preliminary results indicate that our basic photometric techniques will be applicable to the SEC data.

4. ANTENNA CALIBRATION AT HAVANA

Zdenek Sekanina and Richard B. Southworth

4.1 Introduction

Careful calibration of the entire Havana radar system was at least as important to the value of its observations as the size or sensitivity of the system. Measurement of the antenna-gain patterns was an important but laborious part of this calibration. We aimed for an accuracy of 0.2 db within the main lobe of the antenna, in order to have ionization curves comparable in accuracy to photographic (or image-orthicon) light curves. Consultants (Chu Associates, Harvard, Massachusetts) recommended an air-borne measuring program on the actual antennas to replace the existing measures made on the designer's scale model.

4.2 Measurements

The primary measurements of the antenna pattern were performed under the direction of Dr. C. S. Nilsson in the spring of 1968. A lignt airplane, flying more than 1 km from the antenna, so as to be in its far field, towed a battery-powered transmitter and a quarter-wave dipole on a long rope. On half the flights, the dipole was kept approximately horizontal by a further length of rope and a drogue (a light wood and canvas cone with high air resistance). On the other flights, the dipole was held partly vertical by a further length of rope and a heavy weight with little air resistance. The airplane made a slowly ascending spiral about 1 mi in radius around the antenna up to a height over 1 mi, and then spiraled in at that height. Successive turns were spaced 2° to 3° as seen from the radar station. The towed transmitter emitted a continuous signal at the radar frequency, which was received through the antennas under test. A radar tracking system lent by NASA/Langley and operated by NASA personnel tracked a small microwave transmitter carried on the airplane.

Antenna measures were made at sites 3 and 4 of the Havana system. The north and south troughs were measured both separately and together at both sites, because separate troughs were regularly used for reception at site 3 and because a theoretical combination of the troughs could be compared with the measured combination for a check. In addition, a vertical half-wave dipole and a horizontal half-wave dipole mounted above a ground plane were measured at site 3 for a control on the flying transmitter, and a horizontal dipole and the Yagi from site 7 were measured at site 4.

Meteor radar receivers from the Havana and Wallops systems were connected to the antennas and fed chart recorders. Calibration signals were supplied to the receivers from signal generators and step attenuators. Time signals from the radar tracking system and visual observers were also placed on the chart records. Selected charts were later read in Cambridge on film-viewing equipment that converts cursor settings to punched cards. The reduction of these primary measurements is discussed below.

An additional set of measurements of the antenna was obtained to evaluate the importance of the circular component of the polarization of the trough antenna gains, since purely linear polarization was not to be expected except in the axial azimuth. Any appreciable circular component relative to the linear component of polarization causes a large change in the radar system's response to a meteor. Measures with the flying dipole antenna could not reveal circular polarization.

To measure both linear and circular polarization, a special flying antenna, shown in Figure 4-1, was towed behind a heliocopter. Two half-wave dipoles intersecting at their centers were driven 90° out of phase by a battery-powered transmitter. A rope from the helicopter to a weight at one end of the thicker dipole supported the system; fins at the other end of the thicker dipole kept it approximately horizontal in flight. The fins were canted to spin the cross about the thicker dipole at approximately 1 revolution sec^{-1}. Thus the cross radiated alternately right- and left-circularly polarized signals when the thinner dipole was normal to the line of sight, and horizontal linearly polarized signals when the thinner dipole was projected onto the thicker dipole. Two sun sensors viewing the sky through slits in the thicker dipole were connected to

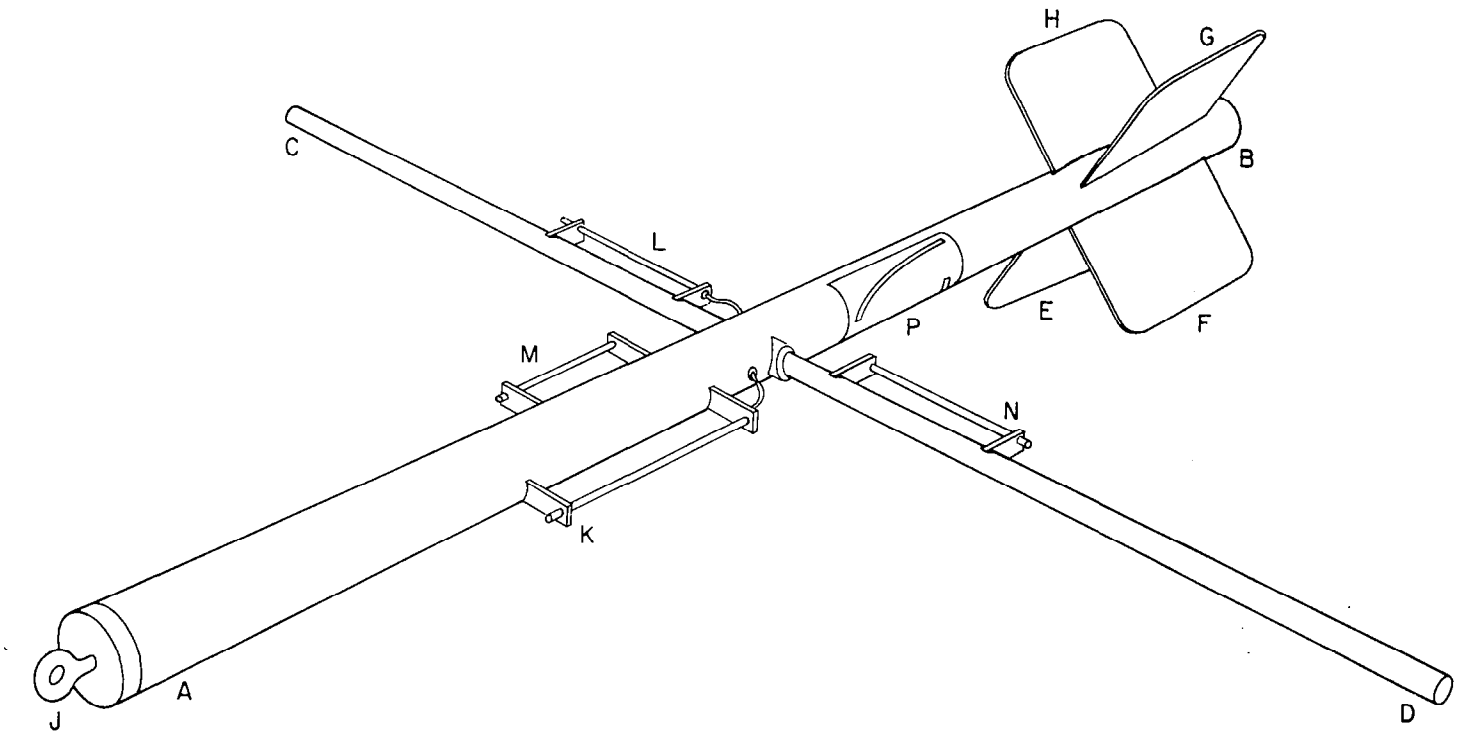

Figure 4-1. Flying cross antenna. An aluminum tube AB, 6 inches by 12 ft, formed one dipole; another aluminum tube CD, 1.5 inches by 12 ft, formed the second dipole. CD passed completely through AB and was insulated from it by a plastic sleeve. Plywood fins E, F, G, H held AB roughly horizontal in flight and rotated the entire assembly. A helicopter pulled the assembly by a rope through ring J, which turned on a bearing within AB. A 60-lb lead weight and a battery-powered transmitter were located within tube AB at A. The transmitter was connected to the dipoles through gamma-matches K and L. M and N were dummy gamma-matches for aerodynamic balance. The sun sensors viewed the sky through slits in cover P.

relays that attentuated the transmitter when the sensors viewed the sun. The slits were oriented so that the interval between attenuations indicated the angle between the thicker dipole and the direction to the sun.

The helicopter flew in a slowly ascending spiral approximately 1 km in radius about the station to a height of about 2 km; then it covered the top of the pattern by straight horizontal flights back and forth. The helicopter was tracked by the NASA/Langley radar, and the signals were received and recorded, essentially as with the single-dipole source towed by the airplane.

The combination of signals from the rotating crossed dipoles permits complete determination of the gain and polarization of the antenna under test. Figure 4-2 shows the results of an approximate reduction for the combined troughs at site 3. The ratio of the amplitude of the circular component to that of the linear component does not reach a factor of 0.3 in any part of the main lobe or the two principal side lobes. This amount of circular polarization has a negligible effect on meteor observations. Consequently, an exact reduction of the crossed-dipole measures was not completed, since the single-dipole reductions were much less time consuming.

The crossed-dipole reductions, and later the single-dipole reductions, showed that the gain patterns of the actual antennas were quite similar at sites 3 and 4, but significantly different from the designer's scale model. In particular, the centers of the main lobes were 3° lower than the model, and the side lobes were 6 db stronger.

4.3 Reduction of the Antenna-Pattern Measures

The remainder of this discussion concerns the reduction of the measures made using a dipole towed behind an airplane. A fuller report on the reduction is available on request from Z. Sekanina.

Obtained from this experiment were the positions of the aircraft at all-second intervals, details on the towed equipment, and the power of the signal from the flight antenna recorded by various units of the tested radar.

The net gain in power of the tested radar is given as the ratio between the recorded and the "expected" powers of the flight antenna at the location of the tested

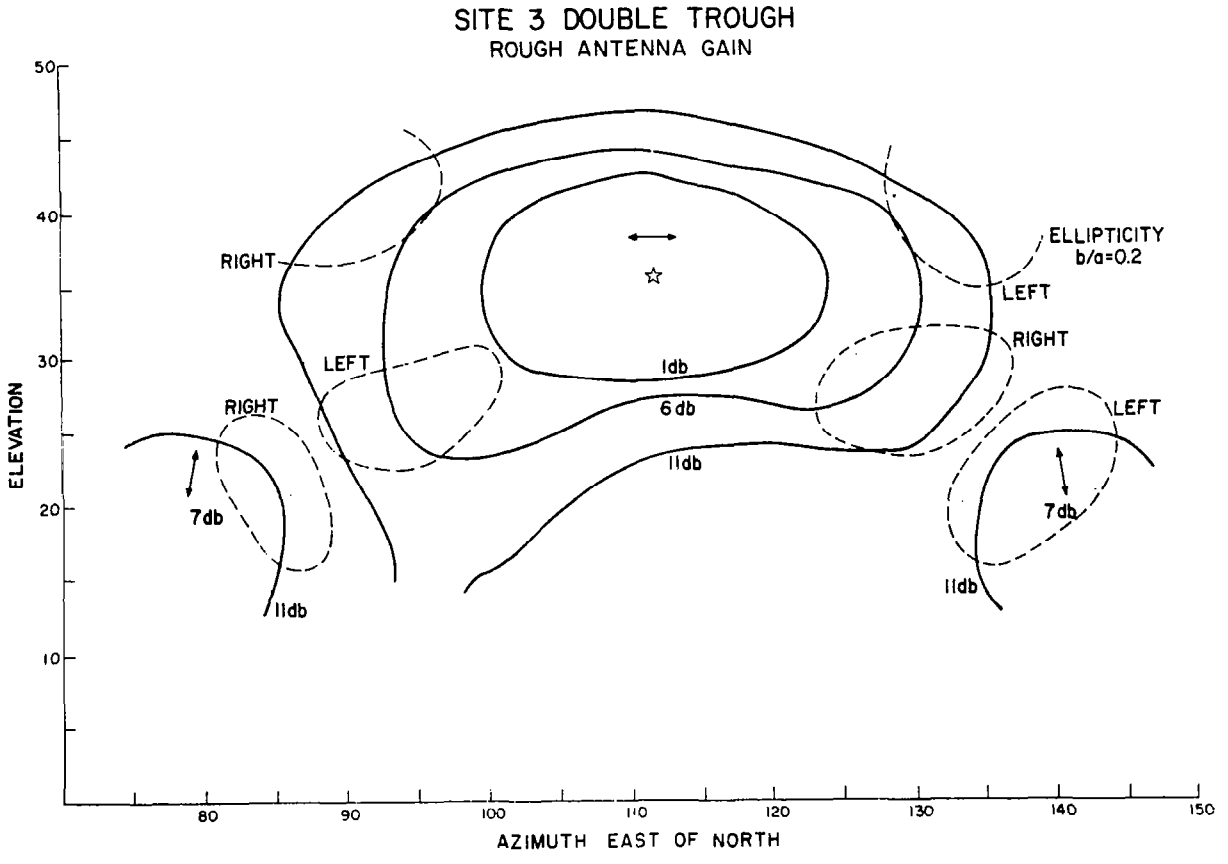

Figure 4-2. Rough antenna-gain pattern. This figure shows an approximate field reduction of one set of measures at station 3 of the two troughs connected together, obtained by using the flying-cross antenna. It has not been corrected for the nonhorizontal orientation of the thicker dipole and is therefore not symmetric about the azimuth of the troughs. The ratio of the minor axis to the major axis of the polarization ellipse is 0.2 on the dashed contours; it does not exceed 0.3 at any point with significant gain. This degree of ellipticity is negligible for our purposes. Peak antenna gained is marked by the star; the peaks of the principal minor lobes are 7 db lower and are located at the 7-db marks. Contours for gain 1, 6, and 11 db below the peak are shown.

units of the ground radar. The expected power of the flight antenna is the power that would be received by the radar if the radar antenna were isotropic and unpolarized; it can be calculated if the geometrical and aerodynamic conditions of the flight are known.

4.3.1 Speed of the aircraft

The speed of the aircraft relative to the ground has been computed from the aircraft's positions. Its speed relative to air, an essential quantity for determining the antenna's position, has been determined from the speed of the wind and that of the aircraft relative to the ground. The wind speed could not be computed for any particular time; however, since the pilot had been instructed to keep the air speed constant in magnitude, it was possible to calculate at least a smoothed effect of wind on the aircraft's speed.

4.3.2 Aerodynamics of the towing line

Three forces are considered to act upon the line and equipment towed by the aircraft:

A. The drag force of the air.
B. The gravity.
C. The centrifugal force due to the curvature of the aircraft's trajectory.

The flights were performed in two modes – "horizontal" and "vertical." The aerodynamic properties of each were determined basically by a piece of equipment, fixed at the very end of the line, of extreme aerodynamic characteristics in terms of the drag-to-weight ratio. The weight was very small compared to the drag for the horizontal mode (drogue), while the drag was very small compared to the weight for the vertical mode (bomb).

The shape of the line carrying the equipment has been determined by numerical integration of the effects of all three forces along the line. The computed vertical profile of the line for zero centrifugal acceleration and an aircraft-to-air speed of 220 km hr^{-1} is plotted in Figure 4-3. Inspection of photographs taken from an ancillary aircraft proved that the computed profiles approximated the observed ones quite well. Thus, the position of the flight antenna relative to the aircraft and the orientation of the antenna's axis were fairly confidently established at any time.

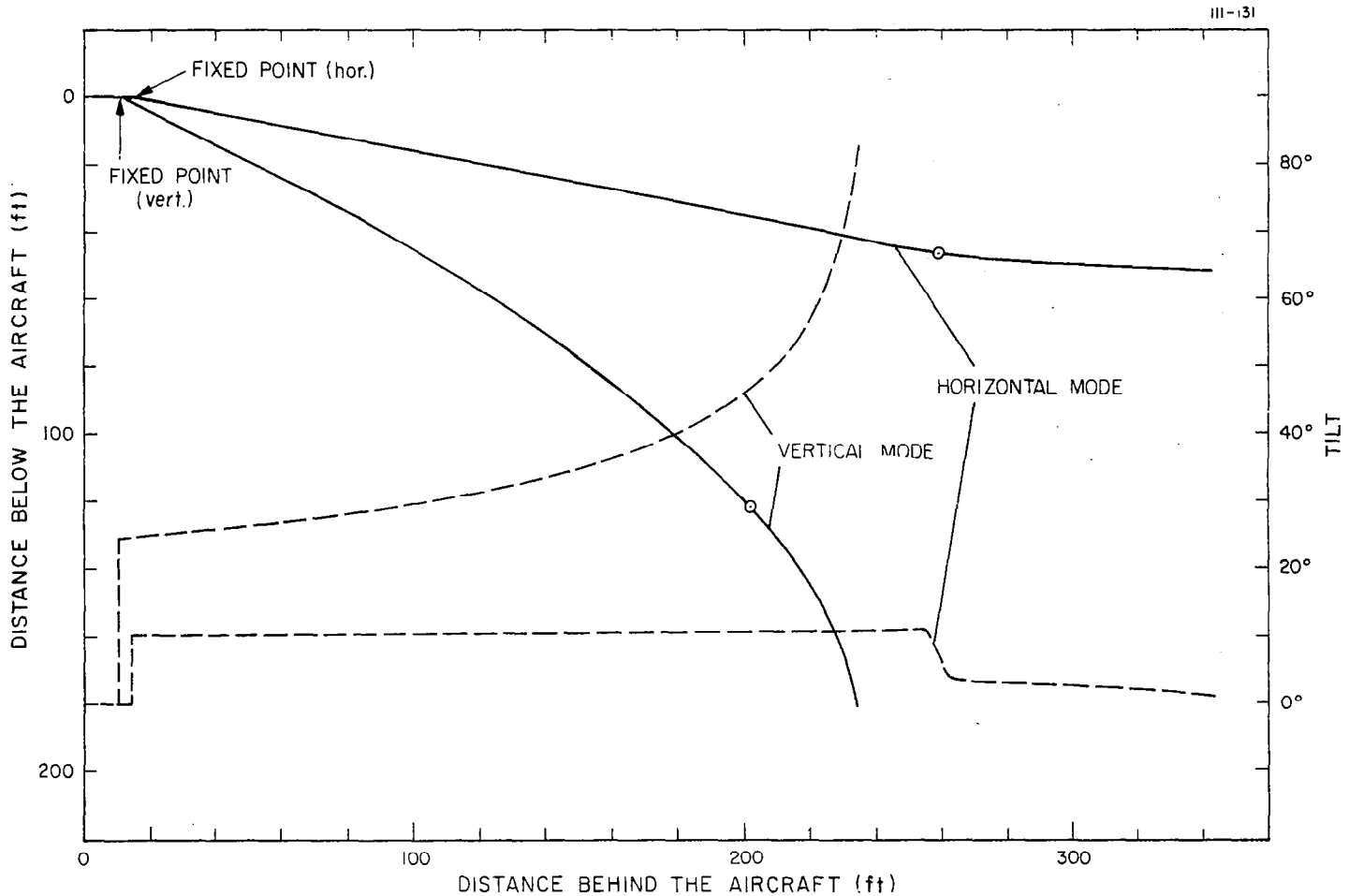

Figure 4-3. The calculated profile of the towing line with the flight transmitter for zero centrifugal force and an aircraft-to-air speed of 220 km hr^{-1}. Solid curves, the shape of the line (in feet); broken curves, tilt of the line to a horizontal plane (given separately for the horizontal and the vertical modes). The position of the transmitter on the line is marked by a circled point.

4.3.3 Power and power gain

Since the flight antenna can be mathematically taken as a thin dipole linearly polarized, the expected power of signals from it at the ground radar is fully described by the antenna's length, its working wavelength, the distance from the ground radar, the angle between the direction of the flight-antenna axis and that toward the radar, and the polarization angle. The aerodynamic analysis described leaves only the polarization ambiguity unresolved; this can, however, be removed by combining data from the vertical-mode flight with data from two horizontal-mode flights, carried out in clockwise and counterclockwise senses, respectively (see Figure 4-4). Since the power gain is given by comparing the recorded power with the expected one, the determination of the power-gain pattern is a matter of routine calculations once the polarization ambiguity is resolved.

4.3.4 Presentation of the results

The power-gain pattern has been determined for the north, south, and joint troughs of sites 3 and 4, as well as for superposed separate troughs of the two sites. The results are available in diagram form for general information (see Figures 4-5a to 4-5h) and on computer printout for detailed analysis; they are also stored on SAO tapes. The printout, much too bulky to be reproduced here, is available upon request.

The following table lists the SAO tape numbers for the results stored on tapes:

	SAO Tape Number	
Trough	Site 3	Site 4
South	7139	7188
North	7140	7189
Joint	7141	7195
Superposition (South and North)	7167	7252

The information is coded in binary and consists of the following:

A. For south, north, and joint troughs:
   1. azimuth, east of north (degrees)
   2. altitude above the horizon (degrees)
   3. power gain (db)
   4. probable error of the gain (db)
   5. position angle of the polarization plane (degrees)
   6. probable error of the angle (degrees)
   7. ambiguity solution (integer; see Figure 4-4).

B. For the trough superposition:
   1. azimuth, east of north (degrees)
   2. altitude above the horizon (degrees)
   3. power gain (db)
   4. probable error of the gain (db)
   5. position angle of the polarization plane of the south trough (degrees)
   6. ambiguity solution (integer) for the south trough
   7. position angle of the polarization plane of the north trough (degrees)
   8. ambiguity solution (integer) for the north trough.

Both types of data are sorted first by the azimuth (1°5 steps decreasing from 360° to 0° inclusive) and then by the altitude (1° steps increasing).

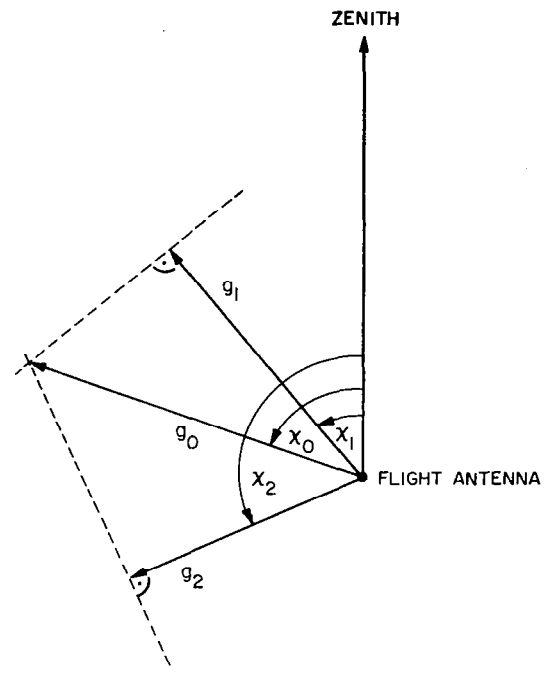

Figure 4-4. Voltage gain vs. polarization. The polarization plane can conveniently be characterized by a position angle χ_0. If the voltage gain g is known for two different position angles χ_1 and χ_2, the gain at χ_0 can be determined from the figure. In practice, however, such a solution is ambiguous, because χ_1 and χ_2 are ambiguous (first or third quadrant; second or fourth quadrant). To solve the ambiguity, the voltage gain must be available in more than two directions. The best fit of all such least-squares solutions is then taken as the correct solution. We have used three different flight modes, so there are four possible solutions (taking χ_0 in the first or second quadrant only):

	Flight Mode		
Ambiquity solution	Horizontal counterclockwise	Horizontal clockwise	Vertical
1	$0° < \chi < 180°$	$0° < \chi < 180°$	$0° < \chi < 180°$
2	$0° < \chi < 180°$	$0° < \chi < 180°$	$180° < \chi < 360°$
3	$0° < \chi < 180°$	$180° < \chi < 360°$	$0° < \chi < 180°$
4	$0° < \chi < 180°$	$180° < \chi < 360°$	$180° < \chi < 360°$

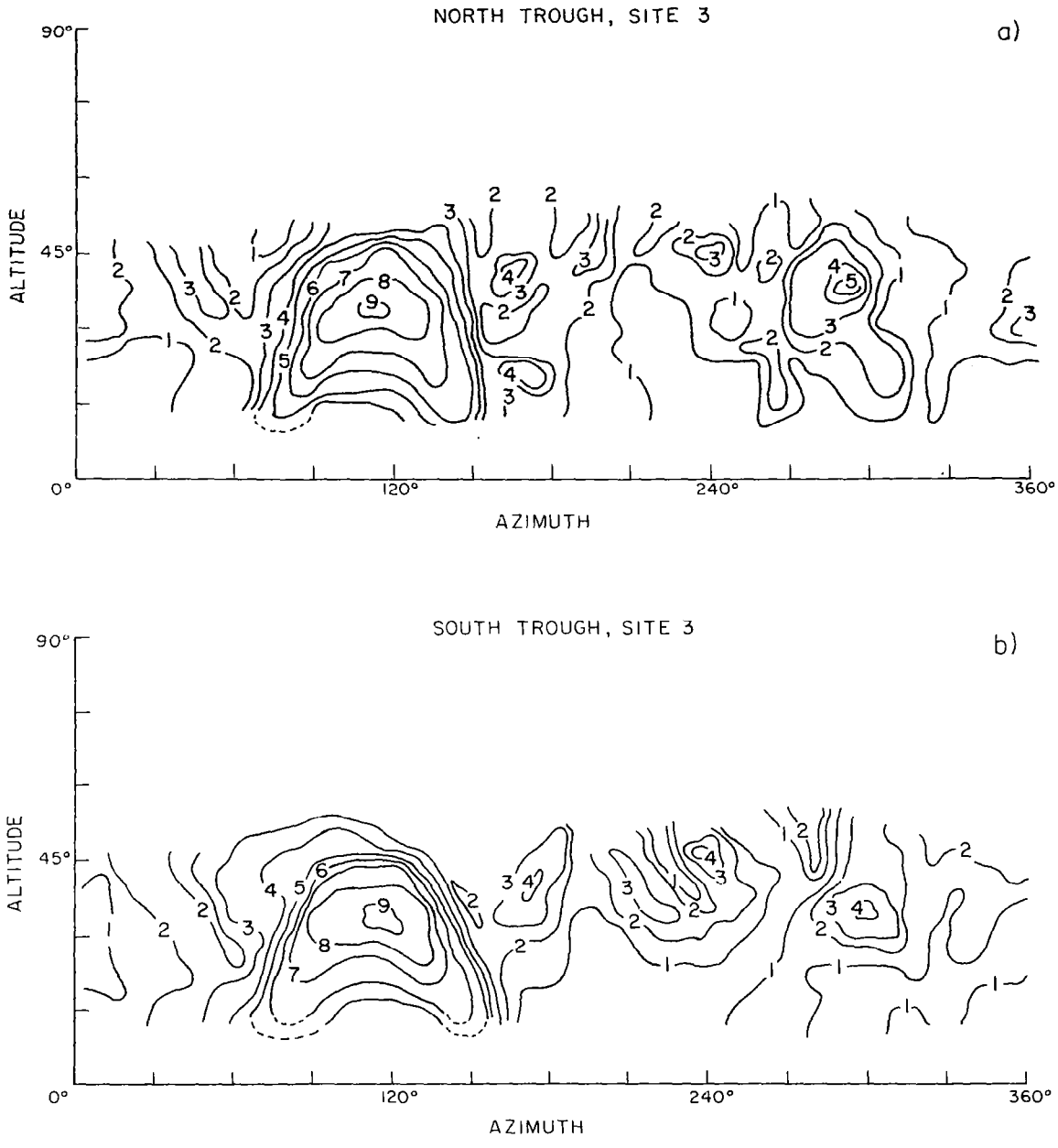

Figure 4-5. Antenna patterns. The power gain is expressed on a scale of 1 to 9, with a step +1 indicating an increase of 4 db (= 1 mag) in the gain.

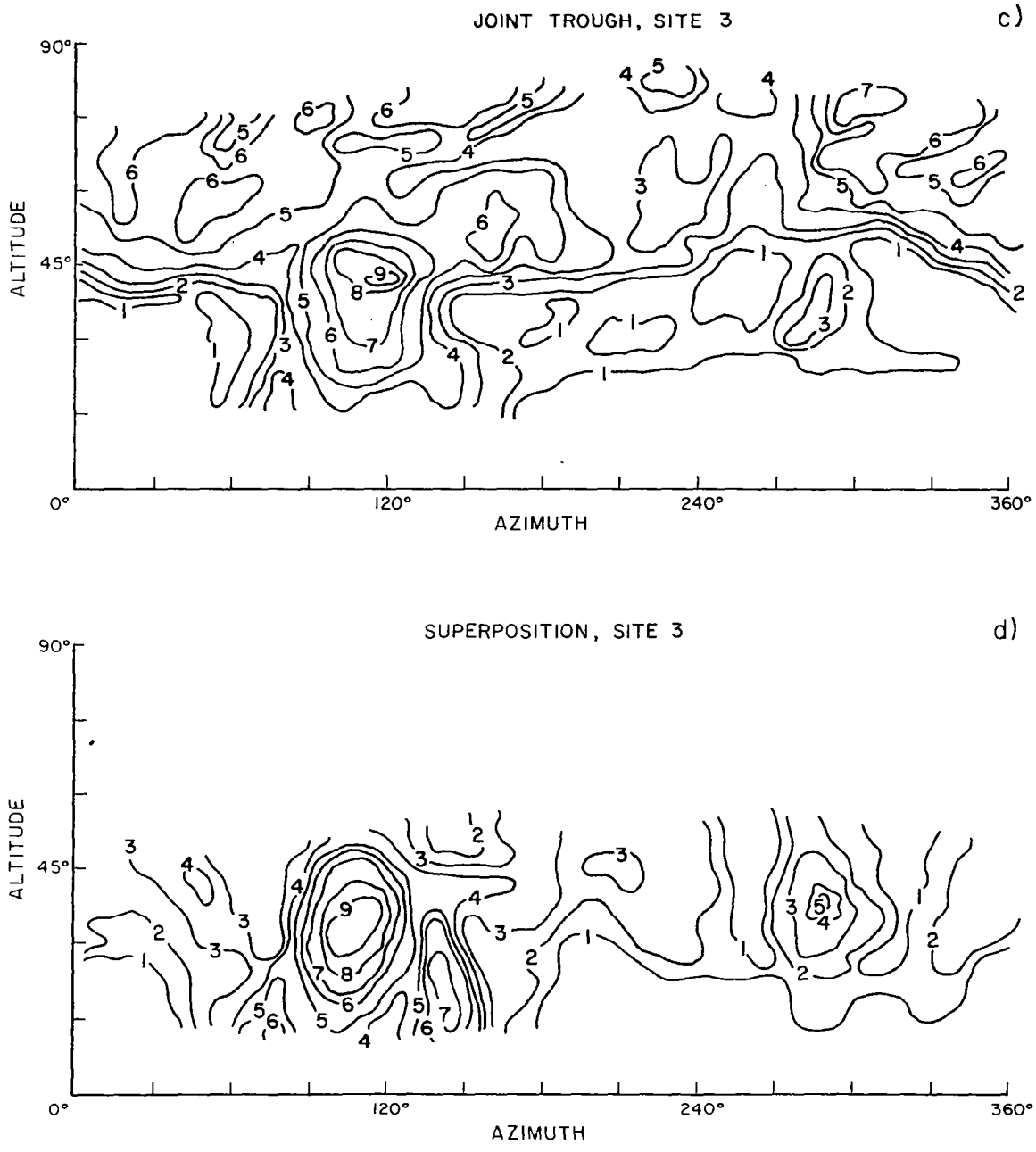

Figure 4-5. (Continued)

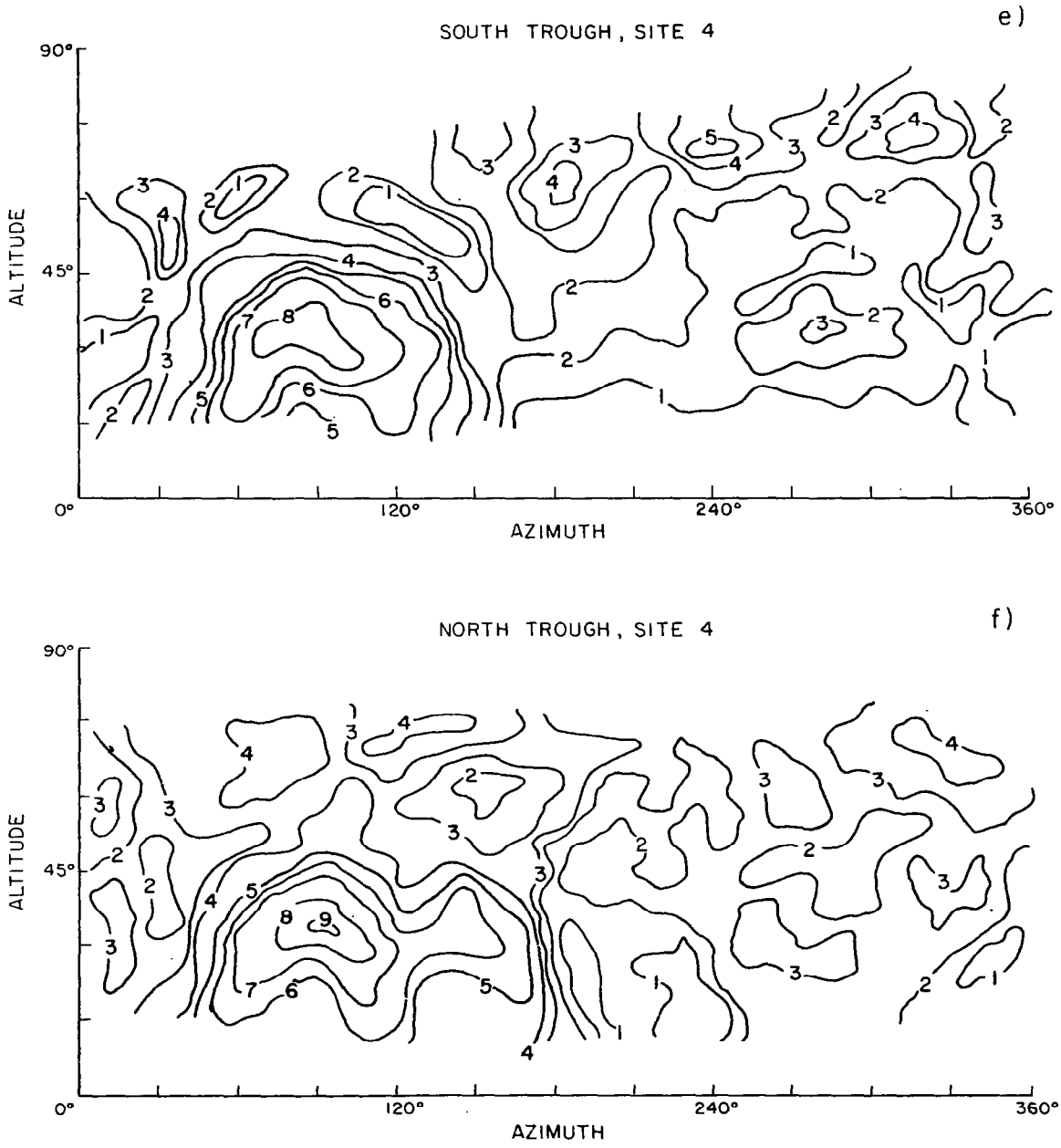

Figure 4-5. (Continued)

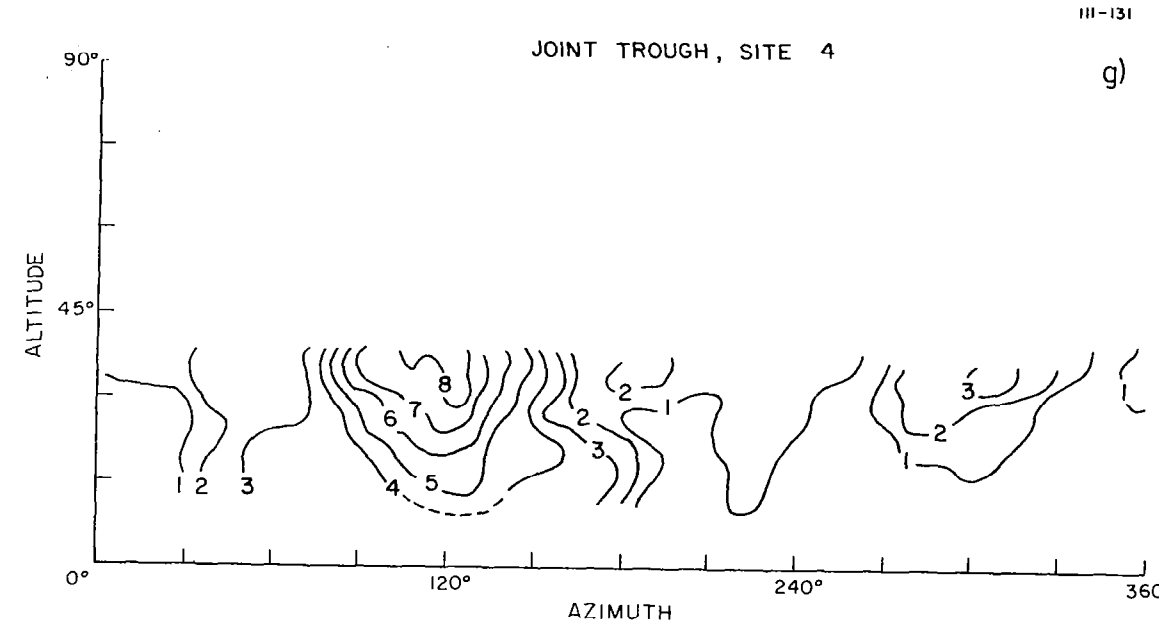

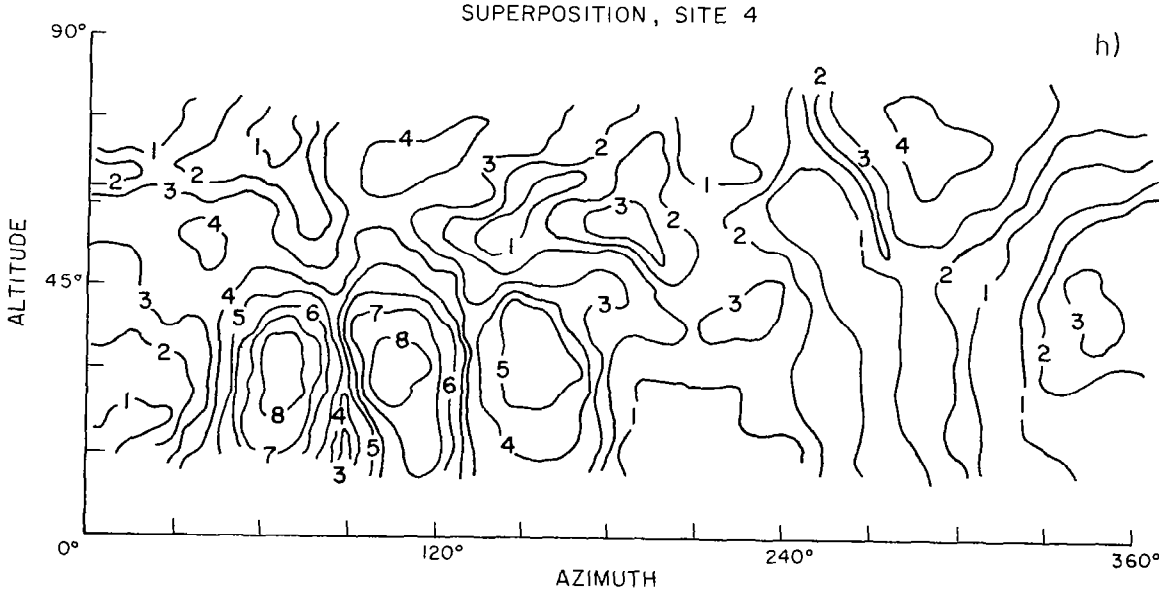

Figure 4-5. (Continued)

5. ANALYSIS PROCEDURE FOR RADAR OBSERVATIONS

Richard B. Southworth

5.1 Theoretical Model of Radar Information

The radar echo received from the ionized column left behind a moving meteoroid is, for practical purposes, entirely scattered back to the observer by free electrons in the column, since scattering by free ions or the solid surface is negligible. Kaiser (1955), among others, has discussed the echo from a meteor; some additional features are described by Southworth (1962a). The amplitude and phase of the observable echo are the integrated vector sum of the echoes from individual elements of the column. In an "underdense" column, such as are mostly observed by the Radio Meteor Project, we can consider separate electrons as these elements. In a denser column, it is necessary either to consider secondary scattering by nearby electrons of radar waves already once scattered by other electrons or else to use some approximation involving continuous media. Nonetheless, the assumption that the column is underdense yields reasonable approximations to the meteoroid's speed and trajectory, although not to its size.

For underdense meteors, it is correct and convenient to divide the column into independent elements distributed along the column and to consider each element as located exactly on the column axis. The effective number of electrons in each element will then be variable; in an underdense column, the effective number decreases exponentially with time because the electrons diffuse away from the axis, so that echoes from electrons on different sides of the column become out of phase with each other and interfere. A complication for a few of the brighter underdense meteors is a resonant scattering effect dependent on the polarization of the incident wave and the orientation of the column (Kaiser, 1955). In a resonant column, the effective number may first increase and then decrease, and some phase shifts may be superposed, both depending on the polarization. Fortunately, whenever this phase shift is large, it takes a form that cannot arise from winds of the type considered below, so we are able to reject it automatically in the reduction process.

The phase of the radar echo from each element of the column, with respect to the phase of the transmitted wave, is determined by the distance from the radar station to the element (neglecting effects of resonance or of overdense trails). Consider first the case where the radar transmitter and receiver are at the same point; separate transmitter and receivers will be treated later.

Let the trajectory of the meteor be the x axis, and let the radar station lie on the negative y axis at a distance R, so that R is the minimum distance from the station to the meteor trajectory. The distance D from any point (x, y) to the radar station is

$$D = \left[(R+y)^2 + x^2\right]^{1/2} = R + y + \frac{x^2}{2R} - \frac{x^2 y}{2R^2} - \frac{x^4}{8R^3} + \ldots \quad . \tag{5-1}$$

For the small values of y and moderate values of x to be used here, it will always be sufficient to limit equation (5-1) to three terms. The phase (now taken with respect to an element at the origin of coordinates and differing only by a constant from the phase with respect to the transmitted wave) is

$$\phi = \frac{4\pi}{\lambda}(D - R) = \frac{2\pi x^2}{\lambda R} + \frac{4\pi y}{\lambda} \quad . \tag{5-2}$$

Atmospheric winds will have negligible effect on the meteoroid but will carry the ionized column away from the meteor trajectory. Only the component of the wind along the y axis (i.e., along the radar beam) need be considered. We will assume that the radial component of the wind depends linearly on x within the part of the ionized column that reflects radar waves to any one receiving station. This assumption is necessary because it will not usually be possible to derive sufficient information from the received echo to specify any more complicated wind field. In particular, we do not resolve wind variations within the principal Fresnel zone, roughly 1 km long. Ultimate justification for the assumption must come from our results, but the observed absence of turbulence at the heights where we measure (Layzer and Bedinger, 1969) supports our use of it. Accordingly, let the radial wind speed be of the form

$$\dot{y} = a(x - x_w)\ \mathrm{m\ sec}^{-1} \quad , \tag{5-3}$$

so that $\underline{a}$ represents the wind shear (m sec^{-1} m^{-1}, or radian sec^{-1}) and x_w represents a point (perhaps extrapolated) on the trajectory where there is no radial wind. Let time $\underline{t}$ be measured from the moment the meteoroid passes the origin; then the coordinates of the meteoroid are (Vt, 0), where V is its velocity.

The y coordinate of any element of the column can then be found from its radial speed and the interval τ since it was generated by the meteoroid:

$$\begin{aligned} y &= \dot{y}\tau \\ &= a(x - x_w)\left(t - \frac{x}{V}\right) \\ &= -\frac{a}{V}\left[x^2 - (x_w + Vt)x + x_w Vt\right] \quad . \end{aligned} \tag{5-4}$$

Equation (5-4) shows that the ionized column takes a time-dependent parabolic form.

The phase of the echo from an element at x is found by substituting equation (5-4) into equation (5-2):

$$\phi = \frac{2\pi}{\lambda R}\left(1 - \frac{2aR}{V}\right)\left(x + \left\{\frac{aR[t + (x_w/V)]}{1 - (2aR/V)}\right\}\right)^2 - \frac{2\pi a^2 R}{\lambda}\left\{\frac{[t + (x_w/V)]^2}{1 - (2aR/V)} + \frac{2x_w t}{aR}\right\} \tag{5-5}$$

(which corrects equation (17) of Southworth, 1962a). It is convenient to define a parameter α that represents the importance of the wind shear (discussed further below) as

$$\alpha \equiv \frac{aR}{V} \tag{5-6}$$

and to rewrite equation (5-5) as

$$\begin{aligned} \phi = {} & \frac{2\pi}{\lambda R}(1 - 2\alpha)\left[x + \left(\frac{\alpha}{1 - 2\alpha}\right)(x_w + Vt)\right]^2 \\ & - \frac{2\pi}{\lambda R}\alpha\left[\left(\frac{\alpha}{1 - 2\alpha}\right)(x_w + Vt)^2 + 2x_w Vt\right] \quad . \end{aligned} \tag{5-7}$$

The second line of equation (5-7) is independent of x and therefore applies directly to the phase of the integrated radar echo (from all the elements at all values of x). Remarkably, the first line of equation (5-7) is the phase that would be observed if the station were in fact at a different distance from the meteor and moving, with coordinates

$$\left[-\frac{R}{1-2a}\ ,\quad -\left(\frac{a}{1-2a}\right)(x_w+Vt)\right]\ . \tag{5-8}$$

Thus, the amplitudes (which are determined by the first line of equation (5-7)) have the form of the Fresnel pattern of a meteor of velocity V′ that crosses the specular reflection point at a time δt after the real meteor does, where

$$V' = V(1-a)(1-2a)^{-1/2}\ , \tag{5-9}$$

$$\delta t = \frac{-ax_w}{(1-a)V}\ . \tag{5-10}$$

Measuring time t′ from the apparent crossing of the specular reflection point, we have

$$t' = t - \delta t = t + \frac{ax_w}{(1-a)V}\ . \tag{5-11}$$

The second line of equation (5-7) represents a variation in phase superposed on the normal Fresnel variation and is the observable phase variation due to wind. Denoting this observable wind phase by Φ, we have, in terms of V′ and t′,

$$\Phi = \frac{-2\pi}{\lambda R}\left(\frac{a}{1-a}\right)^2 (V't')^2 - \frac{4\pi}{\lambda R}\left[1-\left(\frac{a}{1-a}\right)^2\right]\frac{ax_w}{\sqrt{1-2a}}\ V't' + \text{constant}\ . \tag{5-12}$$

Observation of the Fresnel pattern in amplitude yields V′ and t′ (i.e., the origin of t′ in the system used for observing time). The quantities R and λ are already known; thus, observation of the phase yields the coefficients

$$\left(\frac{a}{1-a}\right)^2 \quad \text{and} \quad \frac{ax_w}{\sqrt{1-2a}} \quad . \tag{5-13}$$

These furnish the necessary factors for correcting the apparent velocity and time of passing the specular reflection point, since

$$\frac{V}{V'} = \left[1 - \left(\frac{a}{1-a}\right)^2\right]^{1/2} \tag{5-14}$$

and

$$\delta t = -\left(\frac{1}{V'}\right) \frac{ax_w}{\sqrt{1-2a}} \quad . \tag{5-15}$$

The actual geometry of the ionized column is quite different from the geometry that would be deduced directly from the apparent Fresnel pattern or from the geometry when there is no wind shear. The curvature of the ionized column is 2a times the curvature of the radar wavefront. To have only a single point of tangency (specular reflection point) between the wavefront and the column, we must have

$$2a < 1 \quad . \tag{5-16}$$

Other cases will give very anomalous Fresnel patterns, which can easily be rejected. Previous observations of winds at meteor heights show that the most probable value of a is of the order of ± 0.1 but that occasional meteors may not satisfy inequality (5-16).

The actual point of tangency between the radar wavefront and the ionized column (produced if necessary) is at

$$\begin{aligned} x_0 &= -\left(\frac{a}{1-2a}\right)(x_w + Vt) \quad , \\ y_0 &= (a-1)\frac{x_0^2}{R} - a x_w \frac{Vt}{R} \quad , \end{aligned} \tag{5-17}$$

which describes a parabola concave toward the station. The negative coefficient of t^2 in the first term of equation (5-12) is the result of this parabola.

When the Fresnel oscillations are empirically smoothed out, the remaining phase Φ and amplitude A variations refer to the principal Fresnel zone centered on the moving point (x_0, y_0). Irregularities in the ion column within the length of the principal Fresnel zone are averaged out; its length is

$$F = \sqrt{\frac{R\lambda}{1-2a}} \quad , \tag{5-18}$$

which is of the order of 1 km.

Observations of the wind phase at a station yield the value of the wind at one point, as well as two possibilities for the derivative of the wind, as follows. The observed coefficients of t and t^2 in equation (5-12) give the values of

$$G = \left|\frac{a}{1-a}\right| \quad ,$$

$$H = \frac{V}{V'} \frac{a x_w}{\sqrt{1-2a}} = \frac{a x_w}{1-a} \quad , \tag{5-19}$$

from which either

$$a = \frac{VG}{R(1+G)} \quad , \qquad x_w = \frac{H}{G} \quad , \tag{5-20a}$$

or

$$a = -\frac{VG}{R(1-G)} \quad , \qquad x_w = -\frac{H}{G} \quad . \tag{5-20b}$$

The value of the wind at one point

$$x = -H \quad , \qquad \dot{y} = -\frac{HV}{R} \tag{5-21}$$

is common to both equations (5-20a) and (5-20b). This is the point where the moving meteor crosses the point of tangency between the radar wavefront and the ionized column; i.e., it is the actual specular reflection point.

The derivative $\underline{a}$ of the wind is primarily useful for interpolation between the points observed by different stations. When the ambiguity between equations (5-20a) and (5-20b) is significant – that is, when $|\underline{a}|$ is appreciable – we can usually resolve it by selecting the derivative that makes a better fit to neighboring measures.

The case where the transmitter and the receiver are at different sites is very similar to that where they are at the same site, particularly for the meteors observed on this project. The essential difference is that the wind component observed is the component along the direction bisecting the angle between the directions from the two stations to the specular reflection point. Stations 1 to 6 and their antenna beams are so arranged that the distance along an observable meteor track between the feet of perpendiculars dropped from station 3 (the transmitter) and any other station cannot generally exceed 15 km. The specular reflection point is roughly halfway between these perpendiculars. Since echoes at station 7 or 8 will be analyzed only when they are reflected from parts of the meteor track observed at other stations, perpendiculars from station 7 or 8 will also be within 15 km of the perpendicular from station 3. In these circumstances, equation (5-2) and all subsequent developments remain valid with three substitutions: 1) the origin of x and ϕ is shifted to the new specular reflection point; 2) the perpendicular distance R from the station to the track is replaced by the harmonic mean of either the perpendicular distances from the two stations or the distances of the stations from the specular reflection point; and 3) the wind displacement y is replaced by y cos $(\psi/2)$, where ψ is the angle between the directions from the stations to the specular reflection point.

5.2 Geometrical Reduction

This section outlines the principles and procedure for finding a meteor's position and vector velocity from observed data.

The amplitude and phase of the Fresnel pattern generated by a meteor of constant magnitude, without diffusion, can be expressed in terms of the Fresnel integrals of classical analysis (e.g., McKinley, 1961); but numerical integrations are necessary to predict the effects of diffusion or varying magnitude (Loewenthal, 1956; Southworth, 1962a). When, as with our stations, the "range" (distance to the meteor trail) is much larger than the distance between the transmitting and the receiving stations, it is convenient and entirely adequate to use the concept of an "effective station." This is the position that would receive the same signal by direct back scatter as the actual receiving station receives by forward scatter at a small angle; it is located on the bisector of the angle between lines joining the specular reflection point with the transmitting and the receiving stations, and its range R from the meteor is the harmonic mean of the transmitting and receiving ranges. The position and speed of the meteor are deduced primarily from the times of maxima and minima (collectively, "extrema") of the Fresnel pattern; diffusion, radar magnitude, and other physical quantities are deduced primarily from the amplitudes of the extrema. The times of the extrema are the times when the meteoroid is at known multiples of the length F (equation (5-18)) of the "principal Fresnel zone" from the specular reflection point. From the numerical integrations cited above, we find that the "known multiples" depend on apparent diffusion, but not much on other likely events. Diffusion shifts maxima earlier and minima later than in a pattern without diffusion. However, the time of the first maximum also depends on the slope of the ionization curve (Southworth, 1962a, Table 3). From the integrations, an empirical expression for the distance x_1, from the specular reflection point to the point corresponding to the first maximum of the Fresnel pattern, is

$$\frac{F[0.861 - 1.535C + 2.75C^2 - 3.0C^3 + (CS/\sqrt{2})]}{\sqrt{2}} \quad , \tag{5-22}$$

where S is the slope of the ionization curve in magnitudes per length F, and C is Loewenthal's "decay constant":

$$C = \frac{8\pi D}{\lambda^2 V}\sqrt{\frac{\lambda R}{2}} = \frac{T_F}{2\sqrt{2}\,\pi T_D} \tag{5-23}$$

Here, D is the diffusion constant, V is the meteor's velocity, T_F is the time for the meteor to cross the principal Fresnel zone, and T_D is the time for the voltage amplitude of the signal to decay by a factor e under diffusion. Equation (5-22) replaces the approximation given in Southworth (1962a), which was vulnerable to distortion of amplitudes by fragmentation of the meteoroid.

Unpublished continuations of the developments in Southworth (1962a) show that the amplitudes of the Fresnel patterns may be quite accurately analyzed by smoothing out the oscillations and then regarding first the smoothed curve as denoting the decaying amplitude from the principal Fresnel zone and second the oscillations from the smoothed curve as denoting the amplitudes of the later Fresnel zones as each is formed. Such an analysis yields C, S, and the radar magnitude at the specular reflection points and at the extrema. It also yields the phase corrections necessary for wind measurements in the Fresnel pattern.

The "radiant" (named for the point in the sky from which visual shower meteors appear to radiate) is the direction opposite to the direction of motion of a meteor and is the common way to denote the direction of motion. Evidence for the radiant is found in the time intervals between crossings of different specular reflection points, seen as time intervals between beginnings of Fresnel patterns. The distance traveled by the meteoroid in a given time interval is known from the velocity (found from the spacing of Fresnel oscillations). This distance is the projection of the distance between the corresponding effective stations onto the meteor trajectory. Given at least two such projections from noncolinear interstation distances, the radiant is determined. In the computation, we solve initially for two horizontal direction cosines of the radiant. We then infer the vertical direction cosine from the other two, since there is essentially no vertical distance between the stations. Nearly horizontal trajectories do not yield good radiants and are rejected.

The position in space of the specular reflection point from station 3 (the transmitting station) is determined from the radiant, the range (directly measured), and the difference in phase between the signals received at the two halves of the antenna at station 3. The difference in phase determines the angle between the direction from one-half of the antenna to the other and the direction to the meteor. There is an

ambiguity between two or three possible values of the angle, which can nearly always be resolved by requiring the meteor to be in the antenna beam and at a plausible height; any doubtful cases are discarded.

The reduction procedure begins by treating the range observations, i.e., the observed time intervals between the transmission of a pulse and its return to station 3 via the meteor, or via the meteor and another station. Discrepant values are discarded, and one average loop range is formed for each station with range measures.

The observed (amplitude) Fresnel patterns are measured by a specially devised semiempirical pattern-recognition program. This finds the time and amplitude of each extremum, thus giving the same data we previously read from analog film records. The program uses the spacing of extrema found at one station to predict the spacing at others. If it fails in an attempt to measure the pattern at any station, it will try again when it gets a better prediction from some other station. The oscillations from a smoothed curve are found for each pattern.

The wind phase Φ is next measured at each station for which an amplitude pattern was measured. The recorded phase data are an analog representation of s = amplitude $\times$ sin (phase) at odd pulses and c = amplitude $\times$ cos (phase) at even pulses. (These are the outputs of the phase detectors.) Initially, the missing alternate values are interpolated. For a first approximation to the phase variation, the phases are found at the Fresnel maxima, multiples of 2π being added where necessary for continuity. These are then fitted with an expression of the form

$$\Phi = E_0 + E_1 p + E_2 p^2 \quad , \tag{5-24}$$

where p is the pulse number (measuring time). Next, the phase at each observed pulse after the first maximum is corrected for the oscillating part of the Fresnel pattern by subtracting a rotating vector

$$\begin{aligned} s_{corr} &= s - C_F \sin (\phi_F + E_0 + E_1 p + E_2 p^2) \\ c_{corr} &= c - C_F \cos (\phi_F + E_0 + E_1 p + E_2 p^2) \\ \tan \phi_{corr} &= \frac{s_{corr}}{c_{corr}} \quad . \end{aligned} \tag{5-25}$$

Here, C_F is the amplitude of the oscillating part, interpolated between extrema, and ϕ_F is the phase of the oscillating part, defined to be 0 at the first extremum, π at the second, 2π at the third, etc., also interpolated. The corrected phases are fitted with equation (5-24), and the process is then iterated once more. If E_2 is inadequately determined or significantly positive, it is rejected, and

$$\Phi = E_0 + E_1 p \tag{5-26}$$

is fitted instead.

The amplitude Fresnel pattern is next analyzed at each station by using a provisional value of the range. This yields velocities and times at specular reflection points, for the geometric reduction proper, as well as various physical data such as diffusion.

The geometric reduction proper (determining the position and velocity) follows next; it proceeds by iteration. First, the effective station positions are estimated. Next, the velocities and times at specular reflection points are corrected by using equations (5-14) and (5-15). Then, the velocities V and times t are fitted to an expression of the form

$$V = B + C\overline{K} \exp(\overline{K}t) \quad . \tag{5-27}$$

Whipple and Jacchia (1957) have shown that this form is suitable for the analysis of photographic (Super-Schmidt) meteors. Since it does not yet appear practical to attempt to evaluate $\overline{K}$ from individual radar meteors, we use a value characteristic of faint photographic meteors – namely, 5/4 the value expected for unfragmenting meteoroids in an exponential atmosphere. Accordingly,

$$\overline{K} = \frac{1.25\,\overline{V}}{5.3} \cos Z_R \quad , \tag{5-28}$$

where $\overline{V}$ is the mean observed velocity, Z_R is the zenith distance of the radiant, and the atmospheric scale height is taken to be 5.3 km. We do not impute great accuracy

to equation (5-27), but consider that it is a more reasonable bridging formula than most others, especially polynomials. The distances between specular reflection points are now found by integrating equation (5-27), and the radiant is fitted to these and the effective stations. Finally, the specular reflection point from station 3 is found by fitting the position of the whole trail (not varying the radiant) to the difference of phase at station 3 and to all observed ranges.

Successive iterations begin by computing the effective stations using the newly computed position of the trail and continue by correcting velocities for the difference between the original provisional ranges and the latest values. The iteration is carried to convergence (or failure).

Throughout the reduction, it is general practice to "fit" by least squares and to carry an estimate of the uncertainty of nearly every quantity deduced. This estimate is kept as realistic as possible and usually depends on both the internal scatter in a least-squares fit and the previously estimated uncertainties of the data fitted. In case of doubt, we try not to underestimate the errors.

5.3 Orbit

The meteor's preatmospheric velocity V_∞, radiant, and date of observation fully determine its orbit before it strikes the earth. We estimate the difference between V_∞ and the observed velocity V by using the simplified meteor theory (McKinley, 1961) and the observed deceleration $\dot{V}$ at the maximum of the observed portion of the ionization curve. The theoretical deceleration at the point of maximum ionization is (McKinley, 1961, equation (7-20))

$$\dot{V}_{(max)} = -\frac{3 \cos Z_R}{2 \sigma H} , \qquad (5\text{-}29)$$

where H is the atmospheric scale height, and σ is a constant characteristic of meteor material. We use H = 5.3 km, and $\log_{10} \sigma = -11.8$ (cgs) as an effective value estimated from the meteors themselves (Southworth, 1962b). We can combine McKinley's equations (7-1), (7-16), (7-19), and (7-28) to show that

$$V_\infty^2 = V^2 + \frac{6}{\sigma} \ell n \left[1 + \frac{\dot{V}}{2\dot{V}_{(max)}} \right] \quad . \tag{5-30}$$

In effect, we use $\dot{V}$ to determine where in the ionization curve V is measured and do not assume that the entire ionization curve is observed. However, when $\dot{V}$ is not well determined, we substitute an empirical mean value from

$$\frac{\dot{V}}{\dot{V}_{(max)}} = \frac{V^2}{540} \left(1 - \frac{V}{108} \right) \quad , \tag{5-31}$$

where V is in km sec^{-1}, which was derived by averaging well-determined values of $\dot{V}$. Equation (5-31) is consistent with a hypothesis that we fail to observe the early parts of the ionization curves of fast meteors, presumably because of diffusion, and the later parts of the ionization curves of slow meteors, presumably because of recombination and fragmentation.

Having found V_∞ from equations (5-29) and (5-30), we compute the orbit by standard methods (Whipple and Jacchia, 1957).

5.4 Physical Quantities

Apparent diffusion rates are computed for every reflection point on every meteor from the decay of the Fresnel amplitudes. These are also combined into an atmospheric scale height and a "diffusion height." The diffusion height is the meteor's height above sea level as found by fitting the observed diffusions to Greenhow and Neufeld's (1955) relation

$$\log_{10} D = 0.068\ h - 1.67 \quad , \tag{5-32}$$

where D is diffusion ($cm^2\ sec^{-1}$) and h is height (km).

The ionization curve is plotted for each meteor, giving the radar magnitude as a function of time and of height above sea level. A magnitude is computed from the

amplitude of the smoothed Fresnel curve at each station and also from the amplitude of each extremum except the first and last.

The mass of the meteor is computed by fitting a parabola to the observed points of the ionization curve and applying Verniani and Hawkins' (1964) value of the ionizing probability β:

$$\beta = 1 \times 10^{-8} V^4 \quad . \tag{5-33}$$

Care is taken not to let the fitted parabola include large amounts of hypothetical unobserved ionization; as a result, the masses are doubtlessly systematically a little small. However, revisions for recombination, and for reevaluation of β, have yet to be included.

The characteristic constant σ is evaluated from the basic "mass equation" (Hawkins and Southworth, 1958, equation (5)):

$$\frac{\dot{m}}{m} = -\sigma V \dot{V} \quad , \tag{5-34}$$

where m is the mass. A formal estimate of the meteoroid density, assuming that the meteoroid is a homogeneous sphere, is also computed from the observed deceleration, velocity, atmospheric density, and computed mass.

5.5 Computing Procedure

5.5.1 Introduction

As described in Section 2, the radar network records meteor echoes on film in analog form and on magnetic tape in digital form suitable for further processing by a digital computer.

A computer program (called MANAGE) to reduce meteor echoes has been written, debugged, and tested. This program can read the data and complete the final reduction

without intervention. Often, however, it is more convenient and reliable to divide the reduction into several partial steps that can be separately supervised in the event of inaccurate recorded data.

The reduction process can be divided into four steps: 1) a visual search of the films for meteor echoes that are likely to give results (although the program rejects unsuitable echoes, this preliminary search saves considerable computer time); 2) reading and analyzing the calibration data; 3) reduction of Fresnel (diffraction) patterns and phase data; and 4) final reduction of the meteor data.

5.5.2 Calibration data

Each receiving station has its own calibrator, and calibrations are usually recorded every hour. Precisely controlled signal generators insert pulsed signals, at the system pulse-repetition rate, through precision attenuators into the receivers. One digitizer and film record is made at each of 11 attenuator steps (5 db step^{-1}) when a central control unit advances the attenuators and starts the signal generators at all sites. Both phase and amplitude data are recorded simultaneously, so that both are calibrated over their full dynamic ranges, about 60 db for amplitude and 35 db for phase. These calibrations are recorded on both the film and the magnetic tape.

The reduction of calibration data is divided into two parts; the first deals with amplitudes, the second with phase data. Phases are reduced only if amplitudes are successful. From all the recorded amplitudes, a table of input voltages against digital output is produced, stored, and punched for each individual station. Depending on the setting of the equipment, there are usually 10 or 11 calibrating values, so it is possible to use linear interpolation among them. When this table has been successfully produced, another table of input voltages against phase outputs is stored and punched for further use.

5.5.3 Reduction of diffraction patterns and phase data

This segment of the program takes most of the computer time necessary to reduce a meteor from a magnetic tape. The partial output produced, which is the

input for the final part of the reduction, is the same kind of output that was generated in the past by people reading film, but it is much more accurate and reliable.

At each station, the amplitude data are treated first. The signal at each pulse is converted to microvolts at the antenna, using the results of calibration; saturated signals are rejected. The maxima and minima of the Fresnel patterns are sought by a special pattern-finding procedure. The first maximum is initially recognized as the first group of high amplitudes in the record at that station, the first minimum as a following group of lower amplitude pulses, and so forth. Then the first two maxima and the first minimum are more definitely recognized by virtue of good least-squares fits to empirical expressions of the proper shapes. Finally, all maxima and minima that can be reliably detected are measured in order from the first maximum, by similar least-squares fits.

If five or more points are measured in the amplitudes, the phase data are converted to volts and analyzed. The received phase is computed at every suitable pulse and corrected for the phase shifts caused by the Fresnel diffractions. They are finally fitted by a set of phase coefficients used to find atmospheric winds and wind shear.

This kind of analysis is performed for each receiving station and also for an extra set of phase data collected at the main station, where the pulsed-radar transmitter is located. Here there are two separate receiver channels connected to two antennas. The additional set of phase data recorded at this station gives an interferometric measure of the angle of arrival, which is necessary to determine the height of the meteor. The additional amplitudes are not digitized, but they are used for other studies.

When three or more of these stations successfully give amplitude data, punched and printed output is produced, which can be examined or used for further reduction. Range measurements (not yet analyzed) are included in this output.

5.5.4 Final reduction

When enough data are generated in the partial reduction described earlier, they are used to derive all the information about the meteor and the atmosphere.

The amplitude diffraction data and the range furnish the velocity of the meteor. A measure of the velocity is given at each specular reflection point, as well as the time at which the point was reached. These velocities and times give the direction cosines of the radiant, which are necessary to compute the orbit and the meteor height. When the direction cosines are computed and there is a good measure of the angle of arrival of the echo from the interferometric data recorded at the main station, the height of the meteor is computed. The phase data are used at this stage of the reduction to correct the direction cosines and height of the meteor. After this correction is applied, the phase data are used to produce a wind profile along the meteor path in one dimension. Printed output and punched cards are generated for further use. The antenna patterns and the received and transmitted power are used to compute the magnitude of the meteor at different times. An ionization curve is fitted through these magnitudes, and a graph of it is printed. Then the density and the mass of the meteoroid are computed, as well as the atmospheric density and the scale height.

A summary of all geometric and physical quantities is printed during the reduction, so that all the information about each meteor and the adjacent atmosphere is easily found. Most of these results are punched on cards, which can be used in different studies on the atmosphere and on the meteors themselves.

5.6 References

Greenhow, J. S., and Neufeld, E. L. (1955). The diffusion of ionized meteor trails in the upper atmosphere. Journ. Atmos. Terr. Phys., vol. 6, pp. 133-140.

Hawkins, G. S., and Southworth, R. B. (1958). The statistics of meteors in the earth's atmosphere. Smithsonian Contr. Astrophys., vol. 2, pp. 349-364.

Kaiser, T. R. (1955). The interpretation of radio echoes from meteor trails. In Meteors, ed. by T. R. Kaiser, Pergamon Press, New York, pp. 55-64.

Layzer, D., and Bedinger, J. F. (1969). Upper-atmosphere winds and their interpretation – II. Planet. Space Sci., vol. 17, pp. 1891-1911.

Loewenthal, M. (1956). On meteor echoes for underdense trails at very high frequencies. Lincoln Lab. Tech. Rep. No. 132, MIT, December.

McKinley, D. W. R. (1961). Meteor Science and Engineering. McGraw-Hill Book Co., New York, 309 pp.

Southworth, R. B. (1962a). Theoretical Fresnel patterns of radio meteors. Harvard College Observatory Radio Meteor Project Res. Rep. No. 14, 60 pp.

Southworth, R. B. (1962b). Deceleration of radio meteors (abstract). Astron. Journ., vol. 67, p. 283.

Verniani, F., and Hawkins, G. S. (1964). On the ionizing efficiency of meteors. Harvard-Smithsonian Radio Meteor Project Res. Rep. No. 5, 23 pp.

Whipple, F. L., and Jacchia, L. G. (1957). Reduction methods for photographic meteor trails. Smithsonian Contr. Astrophys., vol. 1, pp. 183-206.

6. ANALYSIS PROCEDURE FOR TELEVISION OBSERVATIONS AND SIMULTANEOUS OBSERVATIONS

Allan F. Cook, II

The procedure we employed in the analysis of television and simultaneous observations is one in which the position read from a plot of the meteor on a copy of a portion of a chart of the Atlas des Nördlichen Gestirnten Himmels (Schönfeld and Krüger, 1899) is combined with the radar observations to find the trajectory in the atmosphere. The zero points of the time scales for the radar and optical records as established by the start of the radar return recorded on the audio channel of the video tape are exhibited on the light curve. The threshold for the kinescoped film is established to fit the duration on the film so that the epochs of beginning and end of the meteor as kinescoped are found. We then have positions (beginning of meteor, beginnings and ends of frames, end of meteor) at specified epochs. The reduction requires that two well-determined positions and their epochs be selected. These are often the beginning and end and will be referred to by those terms for convenience.

The linear velocity of the meteor is taken from results of the processing of the Fresnel patterns or of the complete radar reduction. Then a series of values of the range from Sidell, Illinois, to the end point of the meteor is introduced. A solution for the trajectory (rectangular coordinates and radiant) is found for each of these end ranges. The bisector of the directions of the transmitter and receiver from the meteor is also found for the minimum range epoch of each radar return. The cosine of the angle between this direction and the radiant is then determined. The correct solution is that at which this angle is a right angle and its cosine vanishes and is found by interpolation with respect to the end range. Errors of observation cause these values of the end range to vary from one radar station to another. An appropriate mean is adopted. Also, the loop ranges are computed from each station as a check, and the phase is computed for site 3 (the transmitter). Comparison of this phase with that measured between the two troughs at site 3 and of the computed loop ranges with their observed values serves to eliminate chance coincidences between a radar observation

of one meteor and an optical observation of another. The computed loop range is usually near a minimum with respect to end range from Sidell and so cannot be used to determine that end range.

We are given at two epochs (beginning and ending) the right ascension and declination of the meteor as observed from Sidell: t_b, α_b, δ_b; t_e, α_e, δ_e. We are also given for each radar station n the epoch t_n of the first Fresnel maximum, the loop range R_{3n}, and the velocity V deduced from the Fresnel pattern. We further know the alt-azimuth coordinates x_n, y_n, z_n (to the East, North, and zenith, respectively) of each station referred to site 3 as the origin, and the coordinates of Sidell x_s, y_s, z_s.

We initially find the Greenwich Sidereal Time from the American Ephemeris and subtract the longitude of Havana ($+6^h0^m5^s.27$) to determine the Local Sidereal Time θ_0. Also, we find the epochs of specular reflection t_n at each site by application of the correction

$$\Delta t'_n = -0.4 \frac{\sqrt{\lambda(R_{3n}-R_{G3n})}}{V} \quad , \quad t_n = t'_n + \Delta t'_n \quad , \tag{6-1}$$

where R_{G3n} is the range of site n from site 3:

$$R_{G3n} = (x_n^2 + y_n^2 + z_n^2)^{1/2} \quad . \tag{6-2}$$

We commence by transforming our optical directions to hour angle and declination for the meridian of Havana as seen from Sidell:

$$t = \theta_0 - \alpha \quad . \tag{6-3}$$

The direction cosines on the local equatorial system are

$$\begin{aligned} \ell_E &= -\cos\delta \sin t \quad , \\ m_E &= -\cos\delta \cos t \quad , \\ n_E &= \sin\delta \quad . \end{aligned} \tag{6-4}$$

Here the x_E axis is directed to the East, the y_E axis to the intersection of the meridian and the equator below the horizon, and the z_E axis to the north celestial pole, as in Figure 6-1.

III-131

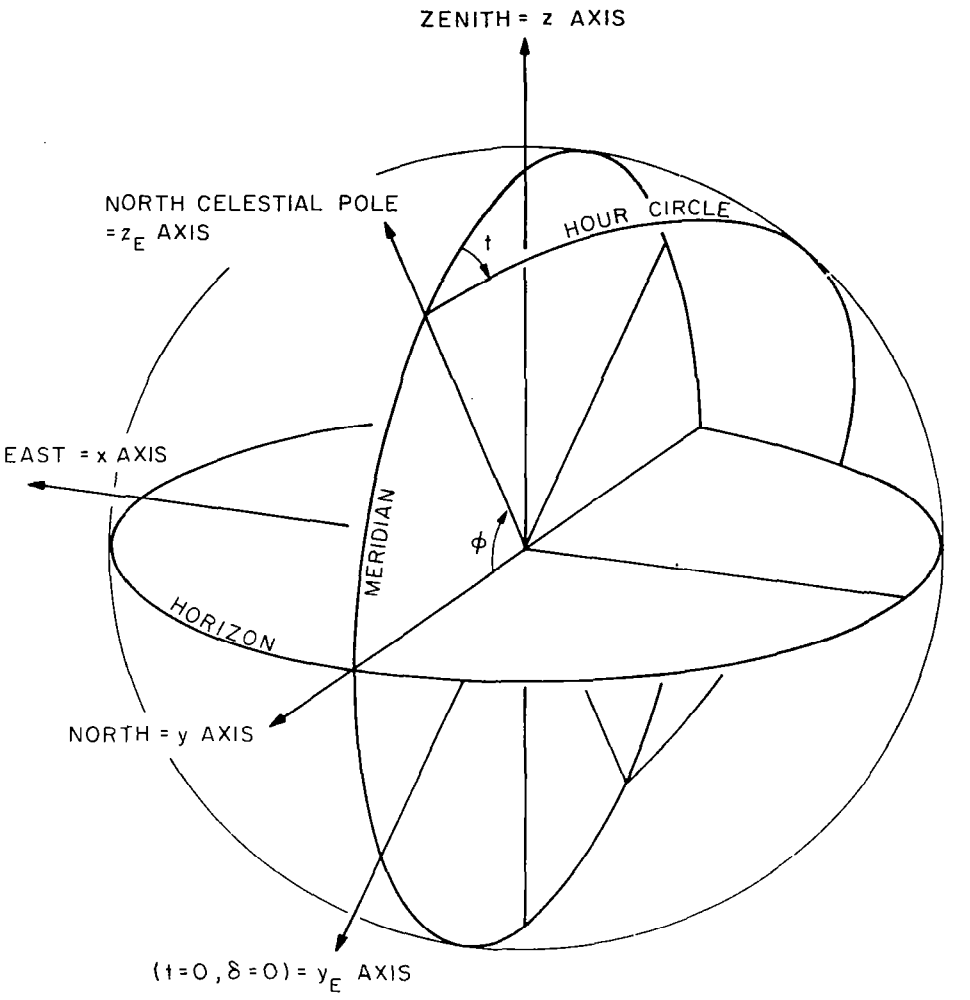

Figure 6-1. Coordinate transformation.

We next rotate to the alt-azimuth system of Havana:

$$\begin{aligned} \ell &= \ell_E \quad , \\ m &= m_E \sin\phi + n_E \cos\phi \quad , \\ n &= -m_E \cos\phi + n_E \sin\phi \quad . \end{aligned} \tag{6-5}$$

At Havana, the latitude $\phi = +40°\,15'$, $\sin\phi = +0.6457$, and $\cos\phi = +0.7636$. These directions are from Sidell at

$$x_s = +185.38 \text{ km} \quad , \qquad y_s = -28.45 \text{ km} \quad , \qquad z_s = -2.67 \text{ km} \quad .$$

We choose as an independent variable the range R_e at the end point of the meteor from Sidell. For such a chosen value, the end point lies at

$$x_{me} = R_e \ell_e + x_s \quad , \qquad y_{me} = R_e m_e + y_s \quad , \qquad z_{me} = R_e n_e + z_s \quad . \tag{6-6}$$

Next we require the various angles in the triangle formed by Sidell and the meteor (see Figure 6-2). The pole of the trail is given by

$$\begin{aligned} \ell_p \sin\alpha_{be} &= m_b n_e - m_e n_b \quad , \\ m_p \sin\alpha_{be} &= \ell_e n_b - \ell_b n_e \quad , \\ n_p \sin\alpha_{be} &= \ell_b m_e - \ell_e m_b \quad , \end{aligned} \tag{6-7}$$

where α_{be} is the angular distance from the beginning to the end. Then we have, by application of the law of sines,

$$\sin\theta_b = \frac{R_e}{V(t_e - t_b)} \sin\alpha_{be} \quad , \tag{6-8}$$

$$\theta_e = \theta_b + \alpha_{be} \quad . \tag{6-9}$$

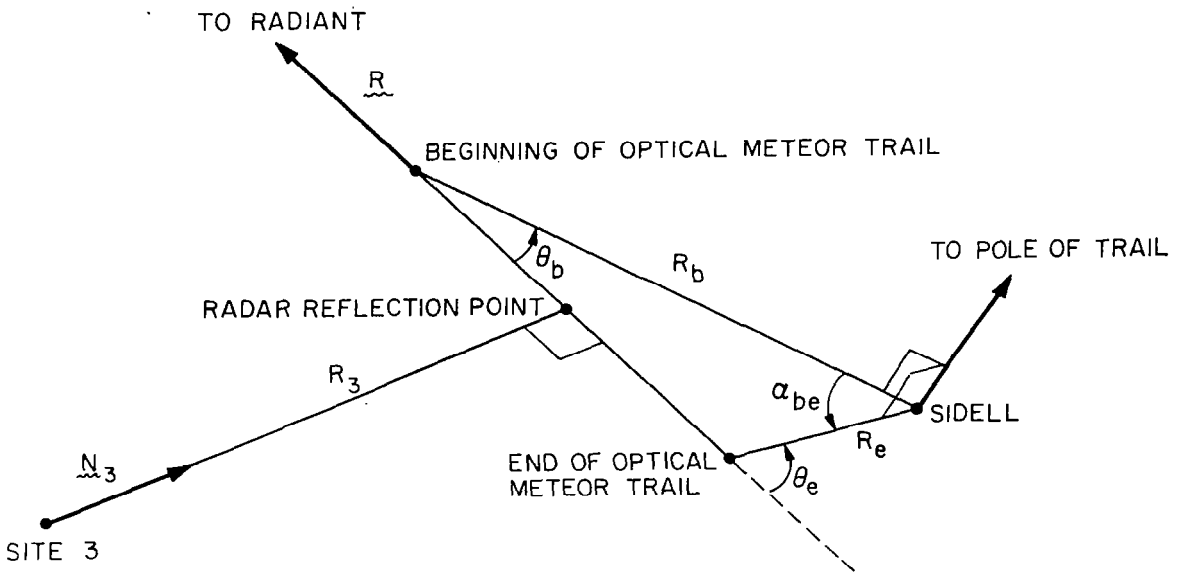

Figure 6-2. Geometry for analysis of simultaneous observations.

Here we can use either solution of equation (8), i.e., $0 \leq \theta_b \leq 90°$ or $90° \leq \theta_b \leq 180°$. In either case,

$$R_b = V(t_e - t_b) \frac{\sin \theta_e}{\sin \alpha_{be}} \quad . \tag{6-10}$$

The beginning of the meteor then lies at

$$x_{mb} = R_b \ell_b + x_s \quad , \quad y_{mb} = R_b m_b + y_s \quad , \quad z_{mb} = R_b n_b + z_s \quad . \tag{6-11}$$

The radiant has the direction cosines

$$\ell_R = \frac{x_{mb} - x_{me}}{V(t_e - t_b)} \quad , \quad m_R = \frac{y_{mb} - y_{me}}{V(t_e - t_b)} \quad , \quad n_R = \frac{z_{mb} - z_{me}}{V(t_e - t_b)} \quad .$$

At the epochs of specular reflection t_n, the meteor was at

$$x_{mn} = x_{me}\,\frac{t_n - t_b}{t_e - t_b} + x_{mb}\,\frac{t_e - t_n}{t_e - t_b} \quad ,$$

$$y_{mn} = y_{me}\,\frac{t_n - t_b}{t_e - t_b} + y_{mb}\,\frac{t_e - t_n}{t_e - t_b} \quad , \tag{6-13}$$

$$z_{mn} = z_{me}\,\frac{t_n - t_b}{t_e - t_b} + z_{mb}\,\frac{t_e - t_n}{t_e - t_b} \quad .$$

The loop range from sites 3 and n is given by

$$\begin{aligned} R_{3n} &= R_3 + R_n + R_{G3n} \quad , \\ R_n &= \left[(x_{mn} - x_n)^2 + (y_{mn} - y_n)^2 + (z_{mn} - z_n)^2\right]^{1/2} \quad , \\ R_3 &= (x_{mn}^2 + y_{mn}^2 + z_{mn}^2)^{1/2} \quad . \end{aligned} \tag{6-14}$$

Finally, we wish to determine how close the meteor was to minimum loop range. This can be done by formation of the derivative

$$\frac{dR_{3n}}{dt} = \frac{dR_3}{dt} + \frac{dR_n}{dt} \quad ,$$

$$\frac{dR_n}{dt} = \frac{(x_{mn} - x_n)(dx/dt) + (y_{mn} - y_n)(dy/dt) + (z_{mn} - z_n)(dz/dt)}{R_n} \quad .$$

The derivatives are

$$\frac{dx}{dt} = -V\ell_R \quad , \qquad \frac{dy}{dt} = -Vm_R \quad , \qquad \frac{dz}{dt} = -Vz_R \quad .$$

Then we have

$$\frac{dR_n}{dt} = -\frac{V}{R_n}\left[(x_{mn}-x_n)\ell_R + (y_{mn}-y_n)m_R + (z_{mn}-z_n)n_R\right] ,$$

$$\frac{dR_{3n}}{dt} = -\frac{V}{R_3R_n}\left\{R_n(x_{m3}\ell_R + y_{m3}m_R + z_{m3}n_R) + R_3\left[(x_{mn}-x_n)\ell_R + (y_{mn}-y_n)m_R + (z_{mn}-z_n)n_R\right]\right\} , \tag{6-15}$$

$$\frac{dR_{33}}{dt} = -\frac{2V}{R_3}(x_{m3}\ell_R + y_{m3}m_R + z_{m3}n_R) \quad . \tag{6-16}$$

To put these on a dimensionless basis, we divide by (-2V):

$$\underset{\sim}{R}\cdot\underset{\sim}{N}_n = \frac{1}{2R_3R_n}\left\{R_n(x_{mn}\ell_R + y_{mn}m_R + z_{mn}n_R) + R_3\left[(x_{mn}-x_n)\ell_R + (y_{mn}-y_n)m_R + (z_{mn}-z_n)n_R\right]\right\} , \tag{6-17}$$

$$\underset{\sim}{R}\cdot\underset{\sim}{N}_3 = \frac{1}{R_3}(x_{m3}\ell_R + y_{m3}m_R + z_{m3}n_R) \quad . \tag{6-18}$$

Here $\underset{\sim}{R}$ is a unit vector toward the radiant, $\underset{\sim}{N}_n$ is the unit vector bisecting the directions to the meteor from sites 3 and n, and $\underset{\sim}{N}_3$ is the unit vector toward the meteor from site 3.

The observation of phase gives us $\sin\phi_A$, where ϕ_A is the phase angle from the trough at site 3. The direction cosines from station 3 are

$$\ell_{33} = \frac{x_{m3}}{R_3} = \frac{2x_{m3}}{R_{33}} \quad , \quad m_{33} = \frac{y_{m3}}{R_3} = \frac{2y_{m3}}{R_{33}} \quad , \quad n_{33} = \frac{z_{m3}}{R_3} = \frac{2z_{m3}}{R_{33}} \quad , \tag{6-19}$$

and the direction cosines of the southerly perpendicular to the trough are (direction toward A = 203°) - sin 23°, - cos 23°, 0, or - 0.3907, - 0.9205, 0.0000. The scalar product of these two unit vectors is sin ϕ_A:

$$\sin \phi_A = -0.3907 \frac{x_{m3}}{R_3} - 0.9205 \frac{y_{m3}}{R_3} \quad ,$$

$$= - \frac{0.7814\, x_{m3} + 1.8410\, y_{m3}}{R_{33}} \quad . \tag{6-20}$$

We repeat this process at successive ranges. We commence at R_e = 80 km and increase in 10-km steps to 180 km and then stop. Interpolation in R_e to fit the condition $\underset{\sim}{R} \cdot \underset{\sim}{N}_n = 0$ is then carried out and a suitable compromise made between the various stations in arriving at a final end range R_e. Finally, the computation is repeated at the adopted end range, and the height above mean sea level is found in the usual way from the deduced rectangular coordinates of the meteor.

The deduced ranges are used with the apparent light curve to find the light curve in absolute magnitude (standard range 100 km). The observed radar magnitude (a line density of 10^{12} cm^{-1} corresponds by definition to a meteor of radar magnitude +5) is then corrected for the antenna pattern established by Z. Sekanina (see Section 4).

Reference

Schönfeld, E., and Krüger, A. (1899). Atlas des Nördlichen Gestirnten Himmels. 2nd. ed., ed. and corr. by F. Küstner, Marcus und Weber, Bonn.

7. RESULTS FROM THE SYNOPTIC YEAR

Richard B. Southworth

In mid-December 1971, reduction was completed at Langley Research Center of 19,698 meteors observed by the Havana radar system during the "synoptic year," October 1968 to December 1969. A few more remain to be reduced, so the total sample may exceed 20,000.

The synoptic year constitutes the largest body of meteor data in existence. Its homogeneity is second to none, and its selection biases can be more reliably assessed than those of any other sample. Its accuracy is second only to the best photographic meteor data, which are far smaller in quantity (less than 400 meteors) and which pertain to much larger meteors of potentially different properties. The synoptic year data are sure to be the subject of further analyses for many years.

Copies of magnetic tapes containing condensed results from the reductions will be filed with the Analysis and Computation Division of Langley Research Center. Inquiries concerning these tapes should be directed to T. Dale Bess, Space Technology Division, Langley Research Center, Hampton, Virginia 23365.

Researchers intending to use the results in the form currently available should be aware, however, of certain limitations. As it has not yet been possible to examine the results fully, there may be errors of reduction. It is not practicable to publish all auxiliary data, including hourly calibrations and operating logs, that may be necessary to some interpretations. Any statistical study would need to consider the numerous selection effects, depending on station locations, antenna gains, TR-ATR switches, recognition logics, receiver and recorder dynamic limits, and reduction-program data requirements, in addition to the physical selection factors discussed elsewhere in this report. We are studying these effects under a current contract with NASA. Finally, a very small proportion of the "meteors" observed must in fact

be composite observations of two (or more) meteors, one meteor at one or more stations, the other at other stations.

We give below some statistics of observing times and masses and of orbits. The physical observations (heights, diffusions, ionization curves, indications of recombination and fragmentation, etc.) need further study before they can be usefully tabulated.

Approximately 60, 000 observations were selected for computer reduction from the film records. The computer program rejected two-thirds of these as inadequate, inconsistent, or otherwise unsatisfactory for reduction. The yield of successful reductions is therefore smaller than we had anticipated, although ample for our purposes. (We projected that 10, 000 to 15, 000 would be needed; and we expected to reduce only half or less of the data actually collected.) We will need to see whether the rejection process introduced significant selection effects. Our initial hypothesis is that phases were not reliably found on the faint meteors near the noise level; this would lead to rejection of observations for internal inconsistency, especially when there were appreciable wind shears in the meteor region. This mode of selection would not bias the data, except by decreasing the fraction of apparently faint meteors reduced. This does not affect the final statistics, since the distribution of apparent magnitudes must in any event be found from the hourly rate data, not from the eight-station reductions.

Table 7-1 shows the distribution by month of observation of 14, 941 synoptic-year meteors with radiants north of the ecliptic. This follows the normal trend of meteor rates in northern midlatitudes, except for a dip caused by a lack of observations in November 1968. Actual observing time will be taken into account in later statistical discussions. Table 7-2 shows the distribution by hour of observations. This agrees generally with previous Havana distributions, and also with theory (Elford and Hawkins, 1964).

Table 7-1. Synoptic-year observations by month.

January	7.9%	May	4.1%	September	15.9%
February	3.8	June	4.7	October	13.8
March	5.7	July	14.9	November	6.4
April	4.9	August	12.8	December	5.0

Table 7-2. Synoptic-year observations by hour (CST).

0^h-1^h	2.3%	6^h-7^h	6.6%	12^h-13^h	4.6%	18^h-19^h	2.4%
1 −2	3.2	7 −8	7.1	13 −14	3.6	19 −20	1.9
2 −3	4.9	8 −9	6.4	14 −15	3.9	20 −21	1.6
3 −4	5.9	9 −10	6.5	15 −16	4.0	21 −22	1.6
4 −5	6.9	10 −11	5.1	16 −17	3.1	22 −23	1.7
5 −6	6.8	11 −12	5.4	17 −18	3.0	23 −24	1.7

Figure 7-1 shows the distribution of meteoroid masses observed in the synoptic year, computed with the ionizing efficiency heretofore used on this project (Verniani and Hawkins, 1964). We expect to revise these masses upward by approximately a factor of 10. Figure 7-1 also shows the distribution of masses in a 1962 sample (Hawkins, Southworth, and Rosenthal, 1964) of Havana radio meteors, observed with the same transmitter power and antennas as the synoptic year but with much less sensitive receivers and recording equipment. The limited dynamic range of the system, however, has eliminated some of the largest masses observed in 1962 from the synoptic-year sample.

Figures 7-2 to 7-5 show the distributions of velocity, inverse semimajor axis, eccentricity, and inclination in synoptic-year meteors. These figures also show the corresponding distributions in a 1961 sample (Harvard Radio Meteor Project, 1961), similar to the 1962 sample shown in Figure 7-1. Above 35 km sec^{-1}, the synoptic-year velocity distribution is nearly proportional to the earlier sample, although normalization to 100% has made the absolute percentages different. However, below 25 km sec^{-1}, the synoptic year includes many more meteors than the earlier one does. Recombination caused most of this observed difference, if not all of it. Any real difference in the velocity distributions of bright and faint radar meteors has yet to be found (but these data are the place to look).

Figures 7-3 to 7-5 show the qualitative differences in the distribution of orbital elements that would be expected from the velocity-distribution differences in Figure 7-2, but no other differences. To a first approximation, we can conclude that the orbital distribution of radio meteors does not depend appreciably on mass.

References

Elford, W. G., and Hawkins, G. S. (1964). Meteor echo rates and the flux of sporadic meteors. Harvard-Smithsonian Radio Meteor Res. Rep. No. 9, 24 pp.

Harvard Radio Meteor Project (1961). Final Report on Contract CST-7282, December 13, 1957, to June 30, 1961.

Hawkins, G. S., Southworth, R. B., and Rosenthal, S. (1964). Preliminary analysis of meteor radiants and orbits. Harvard-Smithsonian Radio Meteor Res. Rep. No. 7, 32 pp.

Verniani, F., and Hawkins, G. S. (1964). On the ionizing efficiency of meteors. Astrophys. Journ., vol. 140, pp. 1590-1600.

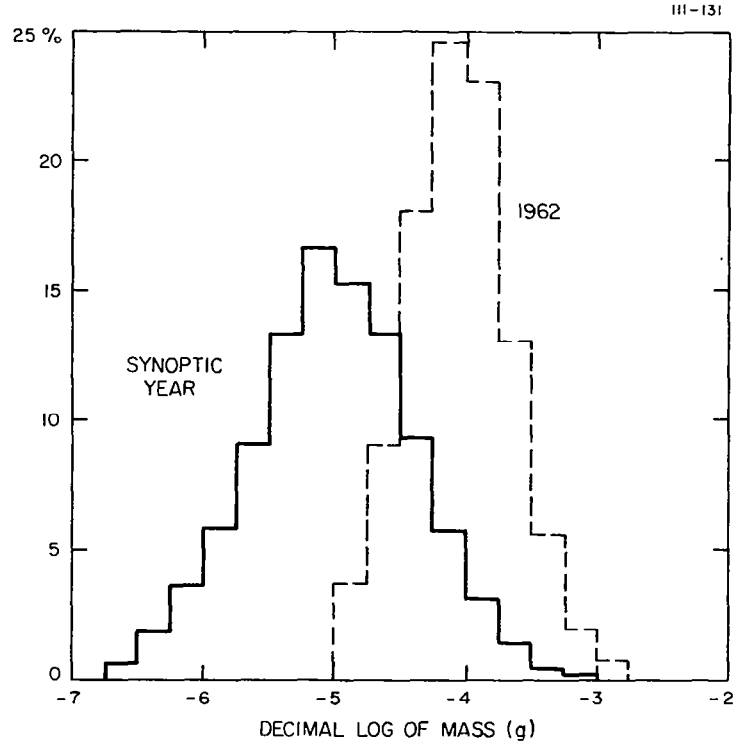

Figure 7-1. Mass distribution, using Hawkins and Verniani's ionizing probability. Revision of the ionizing probability will increase the masses by roughly a power of 10.

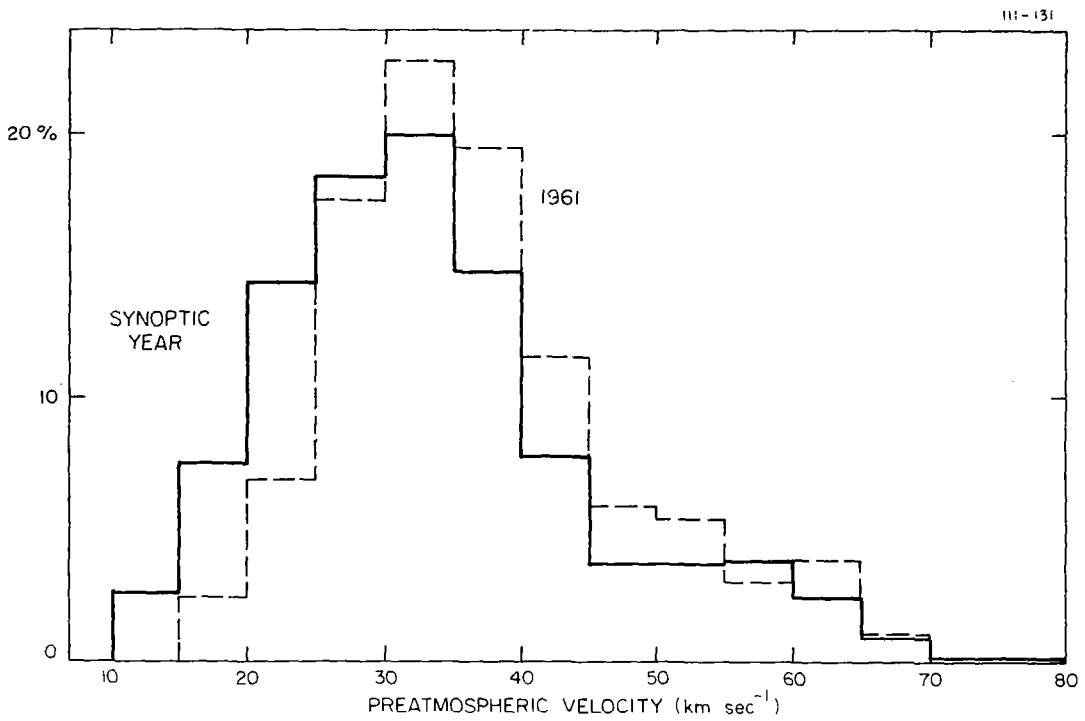

Figure 7-2. Velocity distribution.

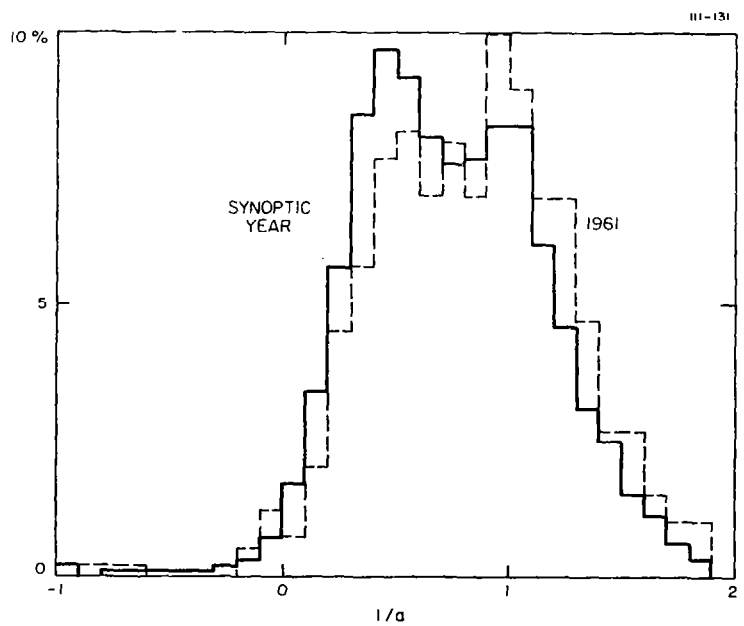

Figure 7-3. Distribution of inverse semimajor axis.

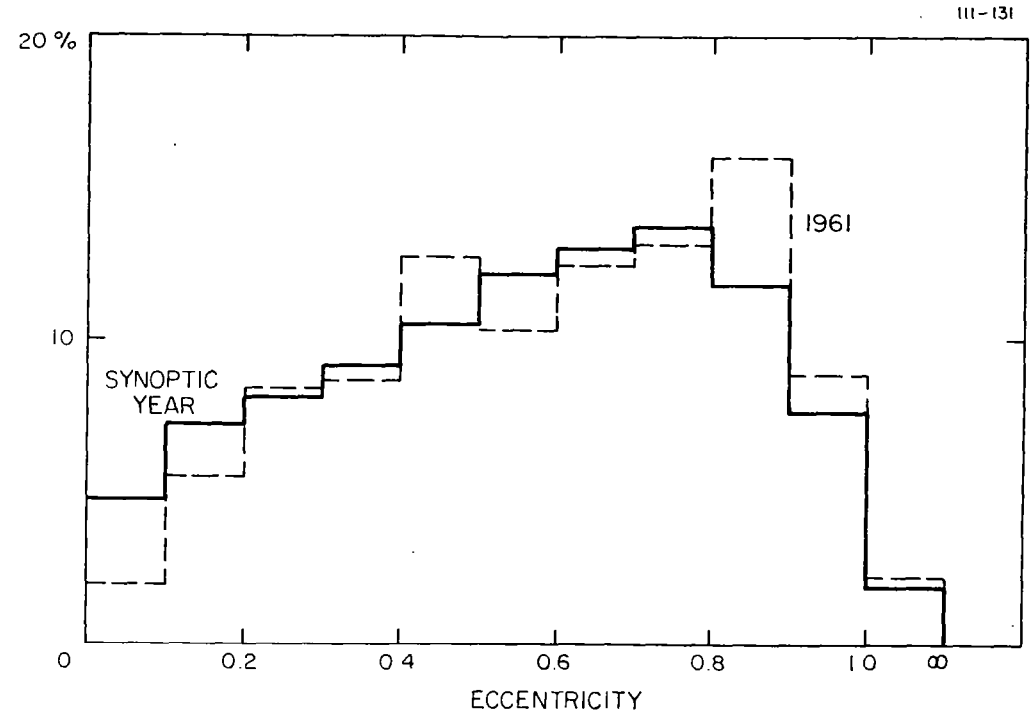

Figure 7-4. Distribution of eccentricity.

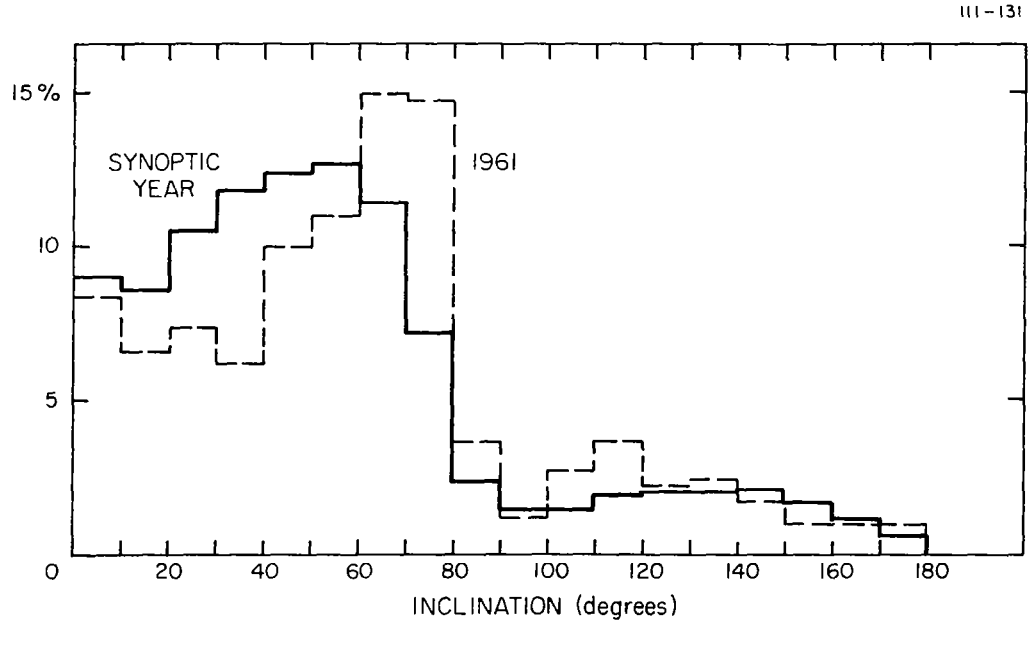

Figure 7-5. Distribution of inclination.

8. RESULTS FROM SIMULTANEOUS RADAR-TELEVISION OBSERVATIONS

Allan F. Cook, II, J. T. Williams, and C.-Y. Shao

Twenty-nine meteors were observed and reduced simultaneously by radar and television from February 1969 through June 1970. Tables 8-1 to 8-5 list the results of these observations. The following quantities are presented in the tables:

V is the velocity of the meteor;

h_B and h_E are the beginning and end heights;

$M_{p\,max}$ denotes the image-orthicon magnitude (approximately panchromatic) at maximum brightness;

$$\int_{-\infty}^{+\infty} I_p \, dt \quad , \qquad I_p \equiv 10^{-0.4\,M_p} \quad ,$$

is the integrated brightness (including linear extrapolations of magnitude versus time below threshold), where I_p denotes the instantaneous panchromatic brightness in units of zero absolute magnitude (reference range of 100 km);

Z_R is the zenith distance of the radiant from the zenith at Havana;

Ceplecha's (1968) class with respect to beginning height is read from his Figure 1;

α_R and δ_R are the right ascension and declination of the geocentric radiant (cleared of zenith attraction and diurnal aberration);

V_G is the geocentric velocity of the meteor;

M_R denotes the radar magnitude; and

M_p is the image-orthicon magnitude.

The observed velocity was used for the velocity outside the atmosphere without correction for deceleration by atmospheric drag. The orbital elements are denoted by the usual symbols (semimajor axis, eccentricity, distance from the sun at perihelion, argument of perihelion, longitude of the ascending node, inclination, and longitude of perihelion, respectively). The designations of the showers are those in Attachment A. Heights are referred to mean sea level. Magnitudes below threshold are indicated by an inequality sign.

Velocities are probably uncertain by a few tenths of a kilometer per second (none of these relatively bright radar meteors is a first-class example of a well-observed radar meteor); no measurable decelerations were found. Heights are uncertain by a kilometer or two, or occasionally three. The threshold absolute magnitude quoted is an average for the beginning and end of the trail if both were observed, or it refers to the beginning alone if only it was observed and the meteor left the field while under observation. Masses are based on the suggested luminous efficiency of stone by Ayers, McCrosky, and Shao (1970).

Most of the observations appear to have been affected by fragmentation. Unmistakable evidence can be seen for this in the light curves shown in Figures 8-1 and 8-2. In particular, a fast rise followed by an exponential decay suggests mutual shadowing of droplets from the air stream leading to mutual coalescence. This process has already been discussed by Cook (1968) as an explanation for exponential decay in terminal blending. The process requires that the droplets group about a few trajectories or even one trajectory, so that late in such a light curve, we can look for radar returns unattenuated by fragmentation. Also, near the beginning, before severe fragmentation can spread the particles much, we can again look for little attenuation. Fragmenting meteors caught near the beginning that show relatively small values of $M_R - M_p$ are nos. 7, 12, and 19. Fragmenting meteors caught in exponential decay that exhibit relatively small values of $M_R - M_p$ are nos. 9, 15, and 23. One meteor, no. 24, has a light curve everywhere too close to threshold to allow recognition of a light curve typical of fragmentation; this meteor also yields relatively small values of $M_R - M_p$. The light curves of meteors nos. 1, 2, 14, 21, and 25 all look classical, except that nos. 1, 2, 21, and 25 show behavior similar to terminal blending near

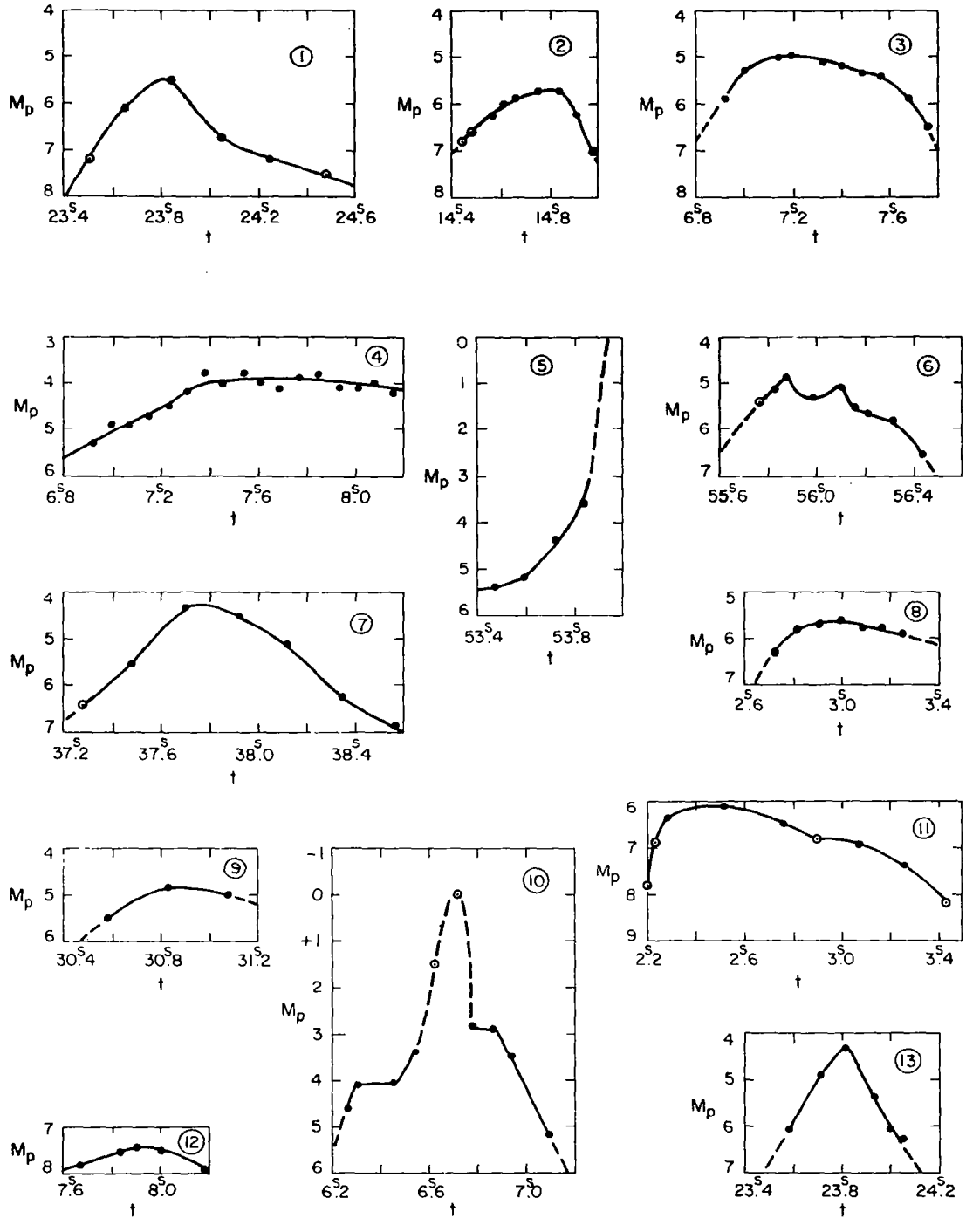

Figure 8-1. Light curves of meteors nos. 1 to 13.

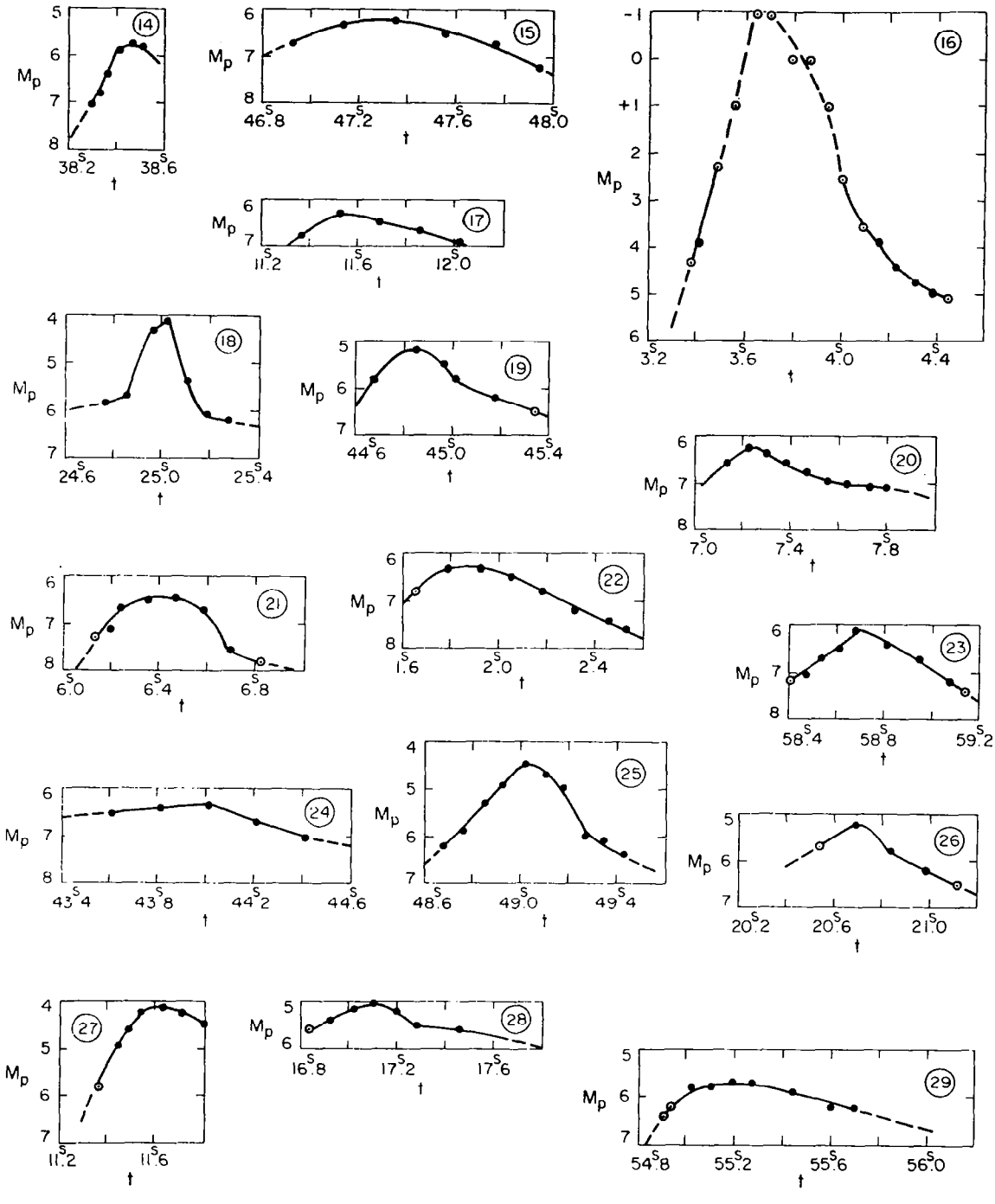

Figure 8-2. Light curves of meteors nos. 14 to 29.

their end points. This occurred after the radar observations in these cases. Meteor no. 14 left the field too early to show terminal blending.

Twelve meteors appear not to have had all their radar returns weakened by fragmentation. These are no. 1 (sites 3, 4, 5), no. 2 (all sites), no. 7 (sites 4, 5), no. 9 (sites 3, 4), no. 12 (sites 3, 4), no. 14 (all sites), no. 15 (sites 4, 5), no. 19 (site 8), no. 21 (all sites), no. 23 (both sites), no. 24 (both sites), and no. 25 (all sites).

Average values were formed for $M_R - M_p$ for each meteor. Means for two obvious groups in velocity (meteors nos. 2, 7, 12, 25 and meteors nos. 1, 9, 14, 15, 19, 21, 23, 24) yield a difference of higher-velocity group minus lower-velocity group of -0.8 ± 0.3 (standard deviation) mag. A linear fit with standard deviations was, therefore, found:

$$M_R - M_p = \underset{\pm 0.19}{+2.77} - \underset{\pm 1.5}{4.0} (\log V - 6.408) \quad ,$$

with the standard deviation for a single meteor being ± 0.6 mag. We note that measures consistent with this result are found over the range in height from 81.7 to 100.7 km above sea level. No measurements at all are found below these heights. This floor is presumably imposed by dissociative recombination. Meteor no. 9 was measured above this height with an underdense echo that was affected either by fragmentation or by a large initial radius, or by both. For meteor no. 16, the observation at 109.2 km (site 8) must have been affected by the initial radius, and all the others must have been points at which the electron trail was overdense. Estimates of the strength of the radar return that should have occurred suggest that the known uncertainty of the antenna pattern at higher altitudes has taken its toll here. Meteors nos. 5 and 25 were also vulnerable to this difficulty. These data suggest that the size of the initial radius affects measurements above a height of 101 km.

We must combine these results with the two really numerous comparisons between visual and radar meteors. The Geminids and Perseids were studied by Millman and McKinley (1956), who found a relationship between $\log T_D$ and M_V (T_D is the duration of an overdense echo in seconds, and M_V is the visual absolute magnitude). McKinley (1961, pp. 228-230) has discussed these results on the basis of Greenhow and Neufeld's

(1955) relation for the coefficient of ambipolar diffusion of electrons and ions. He finds for the Geminids

$$M_V = 39.76 - 2.87 \log q \quad ,$$

where q here is in electrons per centimeter. The definition of radar magnitude M_R is (McKinley, 1961, pp. 230-231)

$$M_R = 35 - 2.5 \log q \quad ,$$

and thus we have

$$M_V = -0.42 + 1.148\, M_R \quad .$$

For the Perseids, McKinley derives the expression

$$M_V = 35.1 - 2.45 \log q \quad ,$$

from which we have

$$M_V = +0.8 + 0.98\, M_R \quad .$$

The lines of regression, log T_D vs. M_V and M_V vs. log T_D, cross at $M_V = +0.4$, $M_R = -0.4$ for the Perseids. For the Geminids, this point lies at $M_V = +0.8$, $M_R = +1.0$. The deviation from unity of the coefficient of M_R for the Geminids is not significant, as it amounts to less than the unit of a half-magnitude used in quoting magnitudes even over a range of ±3 mag from $M_V = +0.8$.

Lindblad (1963) found for the Perseids

$$\log T_D = -0.50\, M_V + 1.08 \quad ,$$

where the echo duration T_D is in seconds. He also quotes

$$q = \frac{T_D}{4.5 \times 10^{-14}} \quad .$$

Combination of these equations yields

$$\log q = 14.427 - 0.50\ M_V \quad ,$$

$$M_R = -1.07 + 1.25\ M_V \quad .$$

Lindblad's lines of regression cross at $M_V = +1.1$, $M_R = +0.3$. We have two alternatives. In the first we accept Millman and McKinley's coefficient of M_V; i.e., it is taken as unity. Then we have

Authority	log V	M_R	M_V	$M_R - M_V$
McKinley	6.556	+1.1	+0.8	+0.2
McKinley	6.781	-0.4	+0.4	-0.8
Lindblad	6.781	+0.3	+1.1	-0.8

A linear fit through these two points (the second and third points coincide) yields

$$M_R - M_V = -0.3 - 4.4\ (\log V - 6.668) \quad .$$

Our two points from the groups of radar and television meteors are

log V	$M_R - M_p$
6.234	$+3.5 \pm 0.2$
6.496	$+2.4 \pm 0.3$

The mean of the higher of these values of log V and that for the Geminids falls at log V = 6.526. We extrapolate both fits to that value to find $M_R - M_V = +0.3$, $M_R - M_p = +2.3$. The former value requires adjustments to panchromatic magnitudes via the color index (photographic minus visual) of -1.0 mag for faint Super-Schmidt meteors (Jacchia, 1957) and of -0.2 mag for the panchromatic index (Millman and Cook, 1959). This yields $M_R - M_p = +1.5$.

This discrepancy in $M_R - M_p$ of +0.8 mag, going from the visual observations of overdense radar meteors to the television observations of underdense radar meteors, drives us to our second alternative, which is to adopt Lindblad's coefficient of M_V for overdense meteors, although not for underdense. The overdense fit intersects the Geminid and Perseid values of $M_R - M_p$ at $M_V = +0.8$ and joins the underdense fit 3.2 mag fainter at $M_V = +4.0$, $M_{ph} = +3.0$, $M_p = +2.8$, where M_{ph} is the photographic absolute magnitude. Accordingly, we suggest the following very tentative fits:

$$\log V \leq 6.526,\ M_p \geq +2.8\ , \qquad M_R - M_p = +2.8 - 4.0\ (\log V - 6.408)\ ,$$

$$\log V \geq 6.526,\ M_p \geq +2.8\ , \qquad M_R - M_p = +1.7 - 4.4\ (\log V - 6.668)\ ,$$

$$\log V \leq 6.526,\ M_p \leq +2.8\ , \qquad M_R - M_p = +2.8 - 4.0\ (\log V - 6.408) + 0.25\ (M_p - 2.8)\ ,$$

$$\log V \geq 6.526,\ M_p \leq +2.8\ , \qquad M_R - M_p = +1.7 - 4.4\ (\log V - 6.668) + 0.25\ (M_p - 2.8)\ .$$

A physical argument for such a behavior is that ionization should increase as we move with increasing brightness into a regime of slip flow of a meteor's own vapors. Use of these expressions for M_p brighter than -4 is at the reader's peril, as the visual magnitude scale fails for such bright objects.

Attention is called to the large number of light curves exhibiting a fast rise and exponential decay. This pattern suggests mutual shadowing of droplets vis-à-vis the air stream leading to mutual coalescence, a process discussed by Cook (1968) as an explanation of exponential decay in terminal blending. In this picture, no solid meteoroid is left.

Finally, a comparison is in order between the above results and the estimated relation between ionization and luminosity by Verniani and Hawkins (1964). It can be shown that their relation can be expressed in the form

$$M_R - M_p = +0.2\ ,$$

independent of velocity. The following short table compares the two results for faint meteors ($M_p \geq +2.8$):

log V	$M_R - M_p$		Correction to Verniani and Hawkins
	This paper	Verniani and Hawkins	
6.234	+3.5	+0.2	+3.3
6.496	+2.4	+0.2	+2.2
6.556	+2.1	+0.2	+1.9
6.781	+1.0	+0.2	+0.8

Multiplication of the last column by -0.4 yields the correction to the logarithms of the masses obtained in the routine reduction of the radar observations. (Further corrections are necessary when either recombination or fragmentation occurs.)

Meteors Not Yet Reduced

There remain more than 50 meteors not yet reduced. These were observed from July to December 1970, and many are of higher quality than those already reduced. We plan to begin with 22 more meteors from the nights of November 6-7 and December 1-2. We hope to complete this work by the summer of 1972. A few of these meteors may yield measurable decelerations. If this happens, then a full analysis in terms of the parameters in the deceleration and luminosity equations would be possible and would yield fundamental information about the structure of the meteoroids at a size much smaller than has been reached heretofore. The remaining 30-odd meteors should also be reduced if funds can be found.

References

Ayers, W. G., McCrosky, R. E., and Shao, C.-Y. (1970). Photographic observations of 10 artificial meteors. Smithsonian Astrophys. Obs. Spec. Rep. No. 317, 43 pp.

Ceplecha, Z. (1968). Discrete levels of meteor beginning height. Smithsonian Astrophys. Obs. Spec. Rep. No. 279, 54 pp.

Cook, A. F. (1968). The physical theory of meteors. In Physics and Dynamics of Meteors, IAU Symp. No. 33, ed. by L. Kresák and P. M. Millman, D. Reidel Publ. Co., Dordrecht, Holland, pp. 149-160.

Greenhow, J. S., and Neufeld, E. L. (1955). The diffusion of ionized meteor trails in the upper atmosphere. Journ. Atmos. Terr. Phys., vol. 6, pp. 133-140.

Jacchia, L. G. (1957). On the color index of meteors. Astron. Journ., vol. 62, pp. 358-362.

Lindblad, B.-A. (1963). The relation between visual magnitudes of meteors and the durations of radar echoes. Smithsonian Contr. Astrophys., vol. 7, pp. 27-39.

McKinley, D. W. R. (1961). Meteor Science and Engineering. McGraw-Hill Book Co., New York, 309 pp.

Millman, P. M., and Cook, A. F. (1959). Photometric analysis of a spectrogram of a very slow meteor. Astrophys. Journ., vol. 130, pp. 648-662; also in Contr. Dominion Obs. Ottawa, vol. 2, no. 30.

Millman, P. M., and McKinley, D. W. R. (1956). Meteor echo durations and visual magnitudes. Can. Journ. Phys., vol. 34, pp. 50-61.

Verniani, F., and Hawkins, G. S. (1964). On the ionizing efficiency of meteors. Astrophys. Journ., vol. 140, pp. 1590-1600.

Table 8-1. Circumstances of the observed meteors.

Meteor number		1969 UT	Radar	Optical	V (km sec^{-1})	Radar h_B (km)	Radar h_E (km)	Optical h_B (km)	Optical h_E (km)
1	Feb.	$14^d10^h57^m$	$23^s.50-24^s.48$	$23^s.76-24^s.13$	$23^s.50-24^s.48$	31.5	91.0–83.2	96.5–	75.7
2	Apr.	20 8 19	14.12–15.00	14.12–14.83	14.44–14.99	14.7	102.1–94.6	98.8–	93.1
3	July	19 7 44	6.88– 7.86	7.13– 7.50	6.88– 7.86	17.1	86.4–82.6	89.0–	79.5
4	July	19 8 30	6.87– 8.16	7.81– 8.16	6.87– 8.16	19.8	92.5–90.6	97.6–	(90.6)
5	Aug.	18 7 42	53.16–54.66	53.72–53.95	53.16–54.66	26.0	105.3–91.4	110.8–	(86.0)
6	Sept.	18 8 52	55.65–56.48	55.65–55.91	55.72–56.48	20.4	97.1–93.8	96.2–	86.7
7	Oct.	8 6 18	37.20–38.86	37.42–37.82	37.20–38.86	17.9	94.1–88.7	97.1–	74.6
8	Oct.	15 8 52	2.70– 3.25	2.72– 3.09	2.70– 3.26	21.8	97.6–92.1	97.9–	(88.6)
9	Oct.	15 9 55	30.54–31.08	30.66–30.98	30.54–31.08	28.8	105.3–98.8	106.4–	(97.0)
10	Oct.	22 10 44	6.03– 7.25	6.21– 6.59	6.03– 7.25	32.9	98.5–90.6	102.2–	77.0
11	Nov.	8 8 43	2.15– 3.43	2.77– 2.85	2.15– 3.43	19.3	84.6–83.4	94.3–	74.4
12	Nov.	16 7 33	7.42– 8.25	7.42– 7.87	7.60– 8.25	16.2	93.4–87.7	91.1–	82.8
13	Nov.	16 9 45	23.58–24.10	23.83–23.99	23.58–24.10	30.2	96.7–93.2	102.3–	90.7
14	Dec.	13 11 11	38.29–38.50	38.29–38.50	38.29–38.50	36.0	87.7–81.7	87.7–	(81.7)
15	Dec.	16 9 45	46.89–48.02	46.94–47.24	46.89–48.02	30.1	100.9–92.3	101.4–	74.4
		1970 UT							
16	Jan.	10 10 26	3.38– 4.43	3.38– 3.75	3.38– 4.43	44.5	110.0–103.0	(110.0)–	(91.7)
17	Feb.	12 7 50	11.22–12.04	11.22–11.92	11.35–12.04	16.9	97.8–89.2	96.2–	(87.7)
18	Feb.	12 9 24	24.48–25.28	24.48–24.74	24.66–25.28	25.5	96.3–92.0	93.4–	83.4
19	Feb.	12 10 11	44.62–45.39	45.04–45.39	44.62–45.34	30.4	102.3–95.4	110.5*–	94.4
20	Feb.	12 10 16	7.08– 7.82	7.15– 7.26	7.08– 7.82	19.3	91.1–89.6	92.0–	82.2
21	Feb.	12 10 36	6.12– 6.82	6.12– 6.45	6.14– 6.82	32.0	95.8–88.2	95.3–	79.6
22	Feb.	12 10 52	1.60– 2.53	1.75– 1.93	1.60– 2.53	23.5	96.2–93.9	99.8–	86.7
23	Mar.	16 10 40	58.47–59.14	58.54–59.10	58.47–59.14	35.7	93.6–83.7	94.8–	83.2
24	Apr.	3 9 59	43.50–44.59	43.53–43.72	43.50–44.59	27.1	94.1–89.9	94.7–	76.8
25	Apr.	7 7 48	48.43–49.55	48.43–49.22	48.61–49.55	20.2	95.1–84.5	92.7–	80.1
26	Apr.	7 9 55	20.38–21.11	20.53–20.75	20.38–21.11	35.5	102.6–96.8	106.6–	87.2
27	Apr.	10 8 9	11.32–12.07	11.36–12.07	11.32–11.84	20.2	100.3–91.1	100.8–	(94.1)
28	May	5 9 19	16.73–17.50	16.73–17.28	16.80–17.50	17.5	94.2–87.0	93.3–	84.1
29	May	7 5 36	54.63–56.03†	54.63–55.07	54.91–56.03†	14.7	94.6–90.6	92.1–	81.7†

*Extrapolated out of field.

†Light curve extrapolated to threshold. Ending could have been as early as $55^s.69$.

Table 8-2. Radiant and photometric data for the observed meteors.

Meteor number	$M_{p\,max}$	$\int_{-\infty}^{+\infty} I_p\,dt$ (0 mag sec)	cos Z_R	Ceplecha's class	Threshold M_p	α_R	δ_R	V_G (km sec^{-1})
1	+5.5	3.4×10^{-3}	0.618	B	+7.4	166°	+11°	29.4
2	+5.3	2.7×10^{-3}:	0.745	above C_1	+6.6	166	+83	10.0
3	+5.0	7.7×10^{-3}	0.612	B	+7.2	273	0	13.3
4	+3.9	–	0.273	C_1	+5.8	299	-35	16.6
5	$\ll$ 0	–	0.705	above C_1	+5.8	281	+54	23.7
6	+4.9	6.2×10^{-3}:	0.613	C_1	+7.2	302	+65	17.2
7	+4.3	1.27×10^{-2}	0.751	above C_1	+7.1	332	+18	14.4
8	+5.6	–	0.628	C_1	+6.8	23	+ 7	19.1
9	+4.9	–	0.656	above C_1	+6.2	30	+16	26.9
10	~ 0	–	0.629	C_1	+7.4	46	+17	31.3
11	+6.1	2×10^{-3}::	0.807	C_1	+7.8	47	+19	16.0
12	+7.4	–	0.790	C_1	+7.8	27	+25	12.2
13	+4.3	5.6×10^{-3}:	0.738	C_1	+6.6	67	+18	28.4
14	+5.7	–	0.805	below A	+7.1	120	+23	34.5
15	+6.2	–	0.778	C_1	+6.8	94	+27	28.2
16	~ 0	–	0.438	above C_1	+6.5	130	- 9	43.3
17	+6.3	–	0.736	C_1	+6.9	123	+12	13.1
18	+4.6	–	0.635	B	+6.6	140	+13	23.2
19	+5.2	5.4×10^{-3}:	0.652	above C_1	+6.4	159	+ 8	28.6
20	+6.3	–	0.751	B–C_1	+7.0	137	+56	16.0
21	+6.5	2.1×10^{-3}:	0.731	B	+7.6	164	+20	30.2
22	+6.3	2.7×10^{-3}:	0.764	C_1	+7.4	166	+25	20.9
23	+6.1	2.1×10^{-3}:	0.497	A–B	+7.2	211	-14	34.1
24	+6.3	–	0.820	B	+6.9	207	+30	25.0
25	+4.5	8.2×10^{-3}:	0.673	C_1	+6.6	178	+ 5	17.2
26	+5.2	7.0×10^{-3}::	0.744	above C_1	+6.2	207	+23	34.0
27	+4.1	–	0.654	above C_1	+6.0	187	+ 2	17.1
28	+5.0	6×10^{-3}:	0.764	C_1	+5.8	214	+33	13.8
29	+5.7	6×10^{-3}:	0.640	C_1	+6.6	111	+64	9.9

Uncertain integrated intensities are indicated by a colon (10 to 25% contribution by extrapolated parts of light curve) and very uncertain values by two colons (25 to 50% contribution).

Table 8-3. Orbits of the observed meteors.

Meteor number	a (a.u.)	e	q (a.u.)	ω	Ω	i	π	Shower
1	1.55	0.82	0.28	306°	325°	7°	272°	Northern Virginid
2	2.31	0.57	1.00	190	30	10	220	
3	2.09	0.58	0.88	231	116	9	347	
4	1.56	0.56	0.68	85	296	8	21	
5	5.1	0.81	0.99	198	145	36	342	κ Cygnid
6	1.39	0.30	0.97	212	175	30	27	
7	3.53	0.74	0.90	219	195	10	54	
8	1.60	0.64	0.58	95	22	2	116	
9	1.93	0.81	0.37	294	202	4	135	Northern Piscid
10	1.75	0.87	0.23	131	29	1	160	Southern Taurid
11	1.29	0.53	0.60	278	226	1	144	
12	1.80	0.54	0.84	236	234	4	109	
13	1.88	0.82	0.33	118	54	5	172	Southern Taurid
14	0.97	0.94	0.06	341	261	7	242	
15	2.51	0.84	0.40	288	264	4	192	Northern X Orionid
16	56	0.99	0.31	112	110	55	221	
17	1.98	0.57	0.84	53	143	3	196	
18	3.79	0.84	0.62	79	143	2	222	Southern δ Leonid?
19	1.71	0.81	0.32	120	143	0	263	
20	2.54	0.66	0.87	225	323	16	188	
21	2.11	0.84	0.34	296	323	15	259	
22	1.20	0.60	0.47	293	323	14	256	
23	0.88	0.95	0.05	164	175	4	339	
24	3.57	0.80	0.73	247	13	27	260	
25	3.68	0.78	0.82	234	17	2	251	
26	-3.01	1.21	0.64	250	17	30	267	
27	2.49	0.69	0.78	243	20	2	263	σ Leonid
28	2.04	0.55	0.93	219	44	16	263	
29	2.10	0.53	0.99	159	46	10	205	

Table 8-4. Radar and optical measurements of the observed meteors.

Meteor number	Site	Epoch	Height (km)	M_R	M_p	$M_R - M_p$	Remarks
1	1	$23^s.81$	88.8	+ 9.7	+5.6	+4.1	Fragmentation
	2	23.91	86.9	+10.3	+5.8	+4.5	Fragmentation
	3	23.99	85.4	+ 9.3	+6.2	+3.1	Perhaps only a few fragments
	5	24.11	83.1	+ 9.0	+6.8	+2.2	
	4	24.13	82.7	+10.0	+6.8	+3.2	
2	4	14.37	99.5	+ 8.8*	>+6.8	<+2.0	
	3	14.44	98.8	+ 9.4*	+6.8	+2.6	
	5	14.69	96.1	+ 8.0	+5.8	+2.2	
	7	14.83	94.6	+ 9.9	+5.7	+4.2	
3	3	7.17	86.0	+10.4	+4.9	+5.5	All stations appear to be affected by fragmentation (see light curve)
	5	7.27	84.9	+10.8*	+5.1	+5.7	
	4	7.39	83.7	+12.2	+5.2	+7.0	
	6	7.50	82.6	+11.0	+5.3	+5.7	
4	3	8.04	91.3	+ 8.4	+4.1	+4.3	Strong fragmentation
	6	8.16	90.6	+ 9.1	+4.1	+5.0	
5	5	53.78	99.4	+ 9.9*	+4.0	+5.9	
	7	53.80	99.1	+10.9*	+3.9	+7.0	
	6	53.95	96.4	+ 8.6	-0.5::	+9.1::	
6	8	55.91	93.8	+11.2	+4.9	+6.3	Fragmentation and broad flares
7	4	37.57	92.0	+ 7.8	+5.0	+2.8	
	5	37.58	91.8	+ 8.2	+4.7	+3.5	
	6	37.82	88.7	+ 8.5	+4.4	+4.1	Fragmentation
8	1	2.78	96.7	+10.5	+6.0	+4.5	Fragmentation throughout
	2	2.86	95.6	+10.2	+5.8	+4.4	
	3	2.92	94.7	+ 9.8	+5.7	+4.1	
	4	3.09	92.1	+ 9.5	+5.7	+3.8	
9	1	30.71	103.6	+ 8.3	+5.0	+3.3	Fragmentation (rapid brightening, slow decline)
	8	30.81	101.7	+ 9.1	+4.9	+4.2	
	2	30.82	101.5	+ 8.7	+4.9	+3.8	

Table 8-4 (Cont.)

Meteor number	Site	Epoch	Height (km)	M_R	M_p	$M_R - M_p$	Remarks
9	3	$30^s.90$	100.0	+ 8.0	+4.9	+3.1	
	4	30.98	98.5	+ 7.0	+5.0	+2.0	
10	7	6.59	90.6	+ 9.8	+2.3:	+7.5:	Pronounced flare
11	1	2.85	83.4	+10.6	+6.8	+3.8	
12	3	7.66	90.3	+11.4	+7.8	+3.6	
	4	7.69	89.9	+10.4	+7.7	+2.7	
	5	7.87	87.7	+11.6	+7.5	+4.1	Fragmentation
13	8	23.99	93.2	+ 9.6	+5.9	+3.7	Fragmentation
14	1	38.34	86.3	+ 7.6	+6.6	+1.0	
	2	38.42	84.0	+ 8.1	+6.0	+2.1	
	3	38.50	81.7	+ 8.5	+5.8	+2.7	
15	2	47.04	96.9	+11.0	+6.5	+4.5	Light curve indicates
	8	47.12	95.1	+12.0	+6.4	+5.6	fragmentation; last two
	3	47.13	94.9	+10.6	+6.4	+4.2	values of $M_R - M_p$ imply
	4	47.19	93.5	+ 8.6	+6.3	+2.3	relative proximity
	5	47.24	92.3	+ 7.9*	+6.3	+1.6	among fragments
16	8	3.43	109.2	+ 9.5:*	+3.5	+6.0	Undoubtedly an overdense
	1	3.56	106.6	+ 7.9:*	+1.1	+6.8	echo undergoing rapid
	3	3.64	105.1	+ 7.3:*	-0.7::	+8.0::	diffusion
	4	3.75	103.0	+ 6.4:*	-0.6::	+7.0::	
17	2	11.44	95.1	+10.2	+6.5	+3.7	
	3	11.54	93.9	+10.8	+6.3	+4.5	Fragmentation
	6	11.92	89.2	+10.3	+6.8	+3.5	
18	3	24.59	94.4	+10.2	(+6.5)	(+3.7)	Large flare
	5	24.69	92.8	+11.0	(+6.4)	(+4.6)	
	4	24.74	92.0	+10.4	+6.4	+4.0	
19	8	45.12	100.7	+ 9.0	+6.2	+2.8	
	3	45.29	97.4	+11.6	+6.6	+5.0	Fragmentation (rapid rise, slow fall)
	5	45.35	96.2	+11.1	+6.6	+4.5	
	4	45.39	95.4	+10.9	(+6.7)	(+4.2)	

Table 8-4 (Cont.)

Meteor number	Site	Epoch	Height (km)	M_R	M_p	$M_R - M_p$	Remarks
20	8	$7^{s}.20$	90.1	+10.7	+6.4	+4.3	Fragmentation (near
	6	7.26	89.3	+ 8.9	+6.3	+2.6	peak), rapid rise,
	7	7.26	89.3	+10.6	+6.3	+4.3	slow fall
21	2	6.15	95.1	+10.5	+7.2	+3.3	
	8	6.18	94.4	+10.5	+7.0	+3.5	
	3	6.23	93.2	+ 9.4	+6.8	+2.6	
	4	6.31	91.4	+ 8.3	+6.6	+1.7	
	5	6.31	91.4	+ 8.9	+6.6	+2.3	
	6	6.45	88.2	+ 8.6	+6.5	+2.1	
22	2	1.81	96.0	+ 9.8	+6.2	+3.6	Maximum of strongly
	8	1.93	93.9	+11.4	+6.3	+5.1	fragmenting meteor
23	1	59.03	84.9	+ 9.0	+7.1	+1.9	Very near turning down
	5	59.10	83.7	+ 9.8	+7.2	+2.6	end after slow fall; drops reconsolidated?
24	1	43.62	92.1	+10.2	+6.5	+3.7	Echoes from stations
	2	43.72	89.9	+ 9.4	+6.5	+2.9	8, 4, 5, 6 give wild velocities, so either they are overdense (unlikely) or wind field spoils them
25	1	48.61	92.7	+11.6*	+6.4	+5.2	
	3	48.78	90.4	+ 8.8*	+5.8	+3.0	
	5	48.87	89.2	+ 9.0:*	+5.2	+3.8:	
	4	48.98	87.7	+ 8.3*	+4.7	+3.6	
	6	49.22	84.5	+ 9.6:*	+5.6	+4.0:	
26	8	20.75	96.8	+12.2:*	+5.3	+6.9:	Fragmentation
27	3	11.79	94.7	+ 8.8	+4.5	+4.3	Fragmentation
	6	12.07	91.1	+10.1	>+4.6	< +5.5	
28	1	16.78	93.6	+12.6*	(+5.7)	(+6.9)	Fragmentation?
	8	17.28	87.0	+ 8.9	+5.5	+3.4	Fragmentation
29	4	54.63	94.6	+12.0	$\gg$+6.4	$\ll$ +5.6	
	3	54.81	93.0	+12.0	>+6.4	< +5.6	
	5	55.07	90.6	+ 9.4	+5.8	+3.6	Fragmentation

Parentheses denote magnitudes extrapolated from observed light curves. Uncertain magnitudes are indicated by a colon and very uncertain values by two colons.

*Steep gradient in antenna pattern or noise in pattern.

Table 8-5. Masses of the observed meteors.

Meteor number	Initial mass (g)	Meteor number	Initial mass (g)
1	1.0×10^{-3}	16	–
2	4.9×10^{-3}:	17	–
3	8.3×10^{-3}	18	–
4	–	19	1.8×10^{-3}:
5	–	20	–
6	5.3×10^{-3}:	21	6×10^{-4}:
7	1.43×10^{-2}	22	1.7×10^{-3}:
8	–	23	4×10^{-4}:
9	–	24	–
10	–	25	7.2×10^{-3}:
11	2×10^{-3}::	26	1.4×10^{-3}::
12	–	27	–
13	1.9×10^{-3}:	28	7×10^{-3}:
14	–	29	1.1×10^{-2}:
15	–		

Uncertain mass (10 to 25% of total in extrapolations of light curve) is indicated by a colon; very uncertain mass (25 to 50% of total in extrapolations of light curve) is indicated by two colons.

9. HOURLY RATE DATA

Richard B. Southworth

9.1 Purpose

The mass-dependent influx of meteors to the earth is the single most important set of data for calculations of meteoroid hazard to spacecraft and provides essential information for any earth-based study of meteor distributions. Influx studies with a sensitive radar were indeed part of the primary mission of the Havana radar system. Nonetheless, the recording equipment for six- or eight-station observations of individual meteors was not suited to the unbiased counts of meteor echoes that are needed for influx determinations. The six- or eight-station recording (film and tape) was not continuous but was triggered only when the logics detected a fresh echo of adequate amplitude and when the recording apparatus was unoccupied. Without triggering, the entire project would have been economically unfeasible. But since it was not possible to state accurately how many meteors failed to trigger the recording, special recording apparatus was installed for counting all meteor echoes at one station (normally station 3). The first counting apparatus recorded analog signals on film; the second and third recorded digital counts on paper tape and magnetic tape, respectively.

9.2 Film Recording of Echo Rates

Intensity-modulated range-time film recording has been common in pulsed meteor radar systems. The intensity of the spot on a cathode-ray oscilloscope is made proportional to the strength of the radar signal received, and the horizontal position of the spot is made proportional to the time since the most recent pulse was transmitted, i.e., to the range from the station. The oscilloscope face is then imaged onto a film moving vertically. The film represents echo strength by image intensity, plotted with respect to range and time.

The Havana echo counting systems were connected to the output of the receiver from one of the troughs at station 3, before the logics. The first echo-counting system was an intensity-modulated range-time recording on 16-mm and later 35-mm film. The range sweep covered five pulse intervals beginning on the doubled transmitted pulse; the doubled echo of the doubled pulse served to resolve ambiguities of 200 km in range and to help differentiate genuine echoes from interference. Recording was normally performed for 5 min of each half hour that the radar system was in use.

This film echo-counting system was installed in 1962 and was used for most of the subsequent operation of the Havana radar system. Echo rates have been counted from part of the films, but the resulting data have been little used because of the difficulty of determining the limiting echo power of the counts. The six- or eight-station records were used to calibrate the intensity-modulated films, although a sufficiently exact calibration could not be obtained. The intensity-modulated film recording was continued, however, in order to have a record of the information that the logics eliminated from the six- or eight-station recordings.

9.3 Echo Analyzer

The "echo analyzer" devised by Dr. M. R. Schaffner was a logical descendant of the "logics" that he devised to eliminate interference and to trigger recording. Each received echo was represented by a digital word circulating in a delay line at the pulse-repetition frequency. As in the logics, a meteor echo was recognized (and counted) if it reached a threshold amplitude for at least eight (normally) consecutive repetitions, or 8 + x with x intermediate repetitions below threshold. After the disappearance of an echo, the word representing it was retained for a while (usually for the echo's lifetime) to prevent multiple counts of echoes that oscillated in amplitude. Echoes were also tracked in range.

Over half an hour, the threshold amplitude was cycled through four levels, distributed over the system dynamic range from near cosmic noise to near receiver saturation. The counts at each level were punched on paper tape. Satisfactorily reliable and precise measurements of the thresholds were also made with special calibrating equipment. This equipment counted echoes from July 1965 for much of the

operating time of the Havana system. Extensive tabulations of hourly rates have been published (Lacy, 1966; Southworth, 1967), and much later data have been partially analyzed.

The meteor influx to the earth was discussed, based on the echo-analyzer data by Nilsson and Southworth (1968). Further discussion has been postponed until we have better evaluated some of the physical observational biases (such as recombination) that we recognize as being important to a thorough interpretation of the data.

9.4 Echo Processor

The "echo processor" was the third piece of digital equipment designed by Schaffner for real-time processing of meteor radar echoes. Its operations were programed by punched cards and thus could be adapted to different purposes (Schaffner, 1966). The initial uses were joint distributions of meteor echoes in range, duration, and amplitude. Anticipated future uses included observations of head echoes, meteors simultaneously observed by the image orthicon, long-enduring echoes, the moon, and the sun.

The echo processor was not completed before the Havana system was dismantled, but a few observations in a preliminary operating state were obtained. The equipment is on loan at the Massachusetts Institute of Technology, where Schaffner is continuing its development for applications in radar meteorology.

9.5 References

Lacy, R. G. (1966). A tabulation of meteor-echo rates. Harvard-Smithsonian Radio Meteor Project Res. Rep. No. 13, 23 pp.

Nilsson, C. S., and Southworth, R. B. (1968). The flux of meteors and micrometeoroids in the neighborhood of the earth. In Dynamics and Physics of Meteors, IAU Symp. No. 33, ed. by L. Kresák and P. M. Millman, D. Reidel Publ. Co., Dordrecht, Holland, pp. 280-287.

Schaffner, M. R. (1966). The circulating page loose system, a new solution for data processing. Harvard-Smithsonian Radio Meteor Project Res. Rep. No. 15, 129 pp.

Southworth, R. B. (1967). A survey of the influx rates of major meteor streams. Final Report on Contract NAS 9-4873, 72 pp.

10. HEAD-ECHO DATA

Richard B. Southworth

Bright radar meteors are observed to scatter radar signals from a target moving with the meteoroid. This is the "head echo," distinguished from the echo of the ionized column left behind the meteoroid. Unlike the sharp aspect sensitivity of the ion column, the head echo represents nearly isotropic scattering, as if by a spherical or only mildly elongated body. The cross section of this body would be many times larger than the meteoroid's, however, and its nature is not well understood. Ionization of a large volume of air by ultraviolet radiation from the meteoroid has been widely discussed (McKinley and Millman, 1949; Cook and Hawkins, 1960; Rajchl, 1969).

Head echoes appear frequently on our intensity-modulated range-time films (Section 9.2) but are not recorded on our six- or eight-station recording, which contains only specular echoes from the ion columns behind the meteoroids. Furthermore, our stations are too closely spaced for reliable trajectory determinations from head echoes. However, we have made occasional special observations of head echoes during showers, at times when the shower radiant was not normal to the antenna beam, thus preventing us from making ordinary observations.

Four cathode-ray oscilloscopes were mounted to be photographed on 35- or 50-mm film. Two gave intensity-modulated range-time presentations from different stations; the other two gave amplitude-time presentations from the same stations, for more accurate amplitude measurements than were possible from the intensity modulation.

This recording system was used for the 1966 Leonids and for several later showers. The most valuable records for meteor physics concern Perseid and Geminid showers, which were simultaneously observed with the image-orthicon at Sidell. However, since we have not yet had an opportunity to reduce the image-orthicon measures, we have also deferred analysis of the radar data.

References

Cook, A. F., and Hawkins, G. S. (1960). The meteoric head echo. Smithsonian Contr. Astrophys., vol. 5, pp. 1-7.

McKinley, D. W. R., and Millman, P. M. (1949). A phenomenological theory of radar echoes from meteors. Proc. Inst. Radio Eng., vol. 37, pp. 364-375.

Rajchl, J. (1969). On the interaction layer in front of a meteor body. Bull. Astron. Inst. Czech., vol. 20, pp. 363-372.

11. SUPER-SCHMIDT METEORS

Richard E. McCrosky and C.-Y. Shao

In order to enlarge our sample of photographic meteoric data, we have carried out a precise reduction program of photographic Super-Schmidt meteors following the automatic star-identification method developed by Posen and McCrosky (1967).

A total of 314 meteors have been completely reduced; their trajectory and orbital results have been published in the Meteor Research Program Semiannual Technical Report Nos. 3, 4, 6, and 7. Of these meteors, 253 were photographed during 1956-1959 by the Harvard Meteor Project in New Mexico, and the remaining 61 were obtained during 1965-1967 by the Smithsonian meteor group in Wallops Island, Virginia.

In addition, about 40 meteors were at various stages toward completion when the reduction program was discontinued.

Reference

Posen, A., and McCrosky, R. E. (1967). A theoretical study of meteoric trajectories and processes, including examination of the incidence and characteristics of photographic meteors by reduction of about 600 data points. NASA Contractor Report, NASA CR-862, August, 45 pp.

12. ATOMIC AND MOLECULAR STUDIES

M. Raymond Flannery and Hiram Levy II

In order to increase our understanding of the physical processes involved in the collision of meteoroids with the upper atmosphere, the Radio Meteor Project initiated studies of the collisions of heavy particles. Dr. M. R. Flannery joined the Observatory staff to carry out these studies with Dr. H. Levy II, under the guidance of Dr. A. Dalgarno.

The optical and ionization phenomena produced by a meteor are caused by the impact of atoms evaporated from the meteor with the atmospheric atomic and molecular constituents. By use of the collision theory, one can determine the probability that a meteor atom excited by collisions will either emit a light quantum or produce an electron before reaching thermal equilibrium with the surrounding atmosphere.

In a description of the collision between a meteor atom and an atmospheric molecule, the probability of emission of a light quantum can be expressed roughly as Q_{ex}/Q_d, where Q_{ex} is the appropriate inelastic cross section to excited states that lead ultimately to light emission, and Q_d is the momentum-loss cross section. The probability that an electron will be produced is roughly Q_i/Q_d, where Q_i is the ionization cross section.

Flannery and Levy were developing theoretical methods for calculating cross sections valid for typical energies of the meteor (i.e., to about 100 ev) energy range. This energy range was not accessible to previous methods, which treated either higher or lower energies.

Dr. Flannery developed the following two approaches for treating the excitation and ionization arising from the impact of two neutral atoms:

A. The multistate impact-parameter treatment, which was basically an attempt to refine and include certain effects neglected in a high-energy treatment.

B. A semiquantal treatment, which had the advantage that reliable cross sections were obtained for complex systems with the same ease as those for simpler atomic systems.

These methods, with applications, are described in a number of publications (see Flannery, 1969a–e, 1970a–k; Flannery and Levy, 1969a, b, 1970).

Levy's work was directed toward the development of theoretical models that would determine those collision processes responsible for ionization and excitation in meteor trails.

The general problem, slow collisions of heavy atoms and molecules, has yet to be treated theoretically with high accuracy. The approach was first to study simple systems for which experimental results were available and then to develop semi-empirical models for the more complicated meteor system of many-electron metal atoms and atmospheric gases.

The first step was the development of a general analytic representation of the interaction potential in an atom–atom representation (Flannery and Levy, 1969a, b). This potential was then applied to the hydrogen-atom–hydrogen-atom collision system (Levy, 1969a; Flannery and Levy, 1970) by use of the impact-parameter approximation for the heavy-body motion.

This general form of the interaction potential was used to develop a first Born approximation for the collision between any two atoms that required only elastic and inelastic form factors (Levy, 1969b). First Born cross sections were then calculated for excitation and ionization of hydrogen and excitation of helium upon collision with He, Ne, Ar, Kr, N_2, and O_2 (Levy, 1969b, c, 1970a). Semiempirical scaling factors found for the many-electron target species gave good agreement between experiment and theory.

The same analytical potential was used to develop an impact-parameter approximation that could be applied to any atomic or molecular system for which elastic and inelastic form factors and generalized oscillator strengths were available. This technique was applied to a variety of excitation collisions between hydrogen and rare gases (Levy, 1969d, 1970b).

The final set of calculations was for quenching of metastable atomic hydrogen by rare gases (Levy, 1971).

At this point, the program was terminated as a result of a budget cut.

References

Flannery, M. R. (1969a). Impact-parameter treatment of hydrogen-hydrogen excitation collisions. I. Two-state approximation. Phys. Rev., vol. 183, pp. 231-240.

Flannery, M. R. (1969b). Impact-parameter treatment of hydrogen-hydrogen excitation collisions. II. Four-state approximation. Phys. Rev., vol. 183, pp. 241-244.

Flannery, M. R. (1969c). Approximations to the two-state impact parameter treatment of heavy particle collisions. Journ. Phys. B (Atom. Molec. Phys.), vol. 2, pp. 909-912.

Flannery, M. R. (1969d). Multi-state impact parameter treatment of hydrogen-helium excitation collisions. Journ. Phys. B (Atom. Molec. Phys.), vol. 2, pp. 913-922.

Flannery, M. R. (1969e). The 2s and 2p excitations of hydrogen by proton and helium-ion impact. Journ. Phys. B (Atom. Molec. Phys.), vol. 2, pp. 1044-1054.

Flannery, M. R. (1970a). Impact parameter and wave equations for direct excitation and electron capture processes. Journ. Phys. B (Atom. Molec. Phys.), vol. 3, pp. 21-28.

Flannery, M. R. (1970b). The $2\,^1S$ and $2\,^1P$ excitations of helium by proton and electron impact. Journ. Phys. B (Atom. Molec. Phys.), vol. 3, pp. 306-314.

Flannery, M. R. (1970c). Inclusion of higher state couplings in a multistate impact-parameter treatment of heavy-particle collisions. Journ. Phys. B (Atom. Molec. Phys.), vol. 3, pp. 798-803.

Flannery, M. R. (1970d). The $n \rightarrow n+1$ transition of atomic hydrogen induced by hydrogen-atom impact. Astrophys. Journ., vol. 161, pp. L41-L42.

Flannery, M. R. (1970e). Excitation and ionization of hydrogen by hydrogen-atom impact. Journ. Phys. B (Atom. Molec. Phys.), vol. 3, pp. L97-L100.

Flannery, M. R. (1970f). Long-range effects in the 2s and 2p excitations of hydrogen by proton and helium ion impact. Journ. Phys. B (Atom. Molec. Phys.), vol. 3, pp. 1083-1089.

Flannery, M. R. (1970g). Semi-quantal theory of heavy-particle excitation by neutral atoms. I. Low and intermediate energies. Ann. Phys. (N.Y.), vol. 61, pp. 465-487.

Flannery, M. R. (1970h). The excitation of atomic hydrogen from n to n+1 by electron impact. Astrophys. Lett., vol. 6, pp. 85-88.

Flannery, M. R. (1970i). Classical theory of excitation, de-excitation and ionization of atoms by charged particles. Journ. Phys. B (Atom. Molec. Phys.), vol. 3, pp. 1610-1619.

Flannery, M. R. (1970j). Impact parameter treatment of hydrogen-hydrogen excitation collisions. III. Electron-exchange and nuclear symmetry effects. Journ. Phys. B (Atom. Molec. Phys.), vol. 3, pp. 1600-1609.

Flannery, M. R. (1970k). Collisional quenching of metastable hydrogen by ground-state hydrogen atoms. Physica, vol. 53, pp. 28-31.

Flannery, M. R., and Levy II, H. (1969a). H-H interaction potentials. Journ. Phys. B (Atom. Molec. Phys.), vol. 2, pp. 314-321.

Flannery, M. R., and Levy II, H. (1969b). Simple analytic expression for general two-center Coulomb integrals. Journ. Chem. Phys., vol. 50, pp. 2938-2990.

Flannery, M. R., and Levy II, H. (1970). Single and double excitations in hydrogen-hydrogen collisions. Journ. Phys. B (Atom. Molec. Phys.), vol. 3, pp. L21-L23.

Levy II, H. (1969a). Impact-parameter calculation of hydrogen-hydrogen double-excitation collisions. Phys. Rev., vol. 184, pp. 97-101.

Levy II, H. (1969b). Born wave calculation of atom-atom inelastic cross sections: Description of target atom by elastic and inelastic X-ray form factors. Phys. Rev., vol. 185, pp. 7-15.

Levy II, H. (1969c). Born-wave calculation of atom-atom inelastic cross sections: Excitation of He(1^1S) to He(N^1L) by hydrogen atoms. Phys. Rev., vol. 187, pp. 130-135.

Levy II, H. (1969d). Multistate impact-parameter calculation of atom-atom excitation cross sections: Excitation of H(1s) by He(1^1S). Phys. Rev., vol. 187, pp. 136-142.

Levy II, H. (1970a). Born wave cross-section calculation for excitation of He(1^1S) to He(N^1L) by helium, neon, argon, and krypton. Journ. Phys. B (Atom. Molec. Phys.), vol. 3, pp. 1501-1509.

Levy II, H. (1970b). Multistate impact-parameter calculations of atom-atom excitation cross sections: Excitation of H(1s) by neon, argon, and krypton. Phys. Rev. A, vol. 1, pp. 750-754.

Levy II, H. (1971). Born wave cross-section calculation for quenching of metastable H(2s) by helium, neon, argon, and krypton. Phys. Rev. A, vol. 3, pp. 1987-1991.

13. DYNAMICS OF METEOR STREAMS AND NEW ASTEROID-METEOR AND COMET-METEOR ASSOCIATIONS

Zdenek Sekanina and Allan F. Cook, II

Between November 1961 and November 1965, a total of 19,303 radio meteor orbits were determined from systematic observations by the Havana network. On the average, the network operated about 6 hr each day for 5-day periods, alternating with 9-day rest intervals. The orbital data on the 19,303 meteors, called hereafter the sample meteors, served as the observational basis for a dynamical study of meteor streams.

13.1 Statistical Model of Meteor Streams

In contrast to all earlier methods of stream search and meteor-to-stream identification, the present method is statistical in nature and is based on the following:

A. The Southworth-Hawkins D-criterion, developed in 1963, tests the similarity of two Keplerian orbits in terms of the differences in their orbital elements and measures essentially the mean-perturbation-velocity increment that would make the two orbits identical. Here D is the radius vector in a five-dimensional phase space.

B. The appearance of any shower is contaminated to some extent by a sporadic background. Both the shower and the background have their own specific frequency distributions with respect to D.

The fundamental aim of the investigation was the analysis of the properties of the observed (i.e., contaminated) D-distribution of a number of meteor streams, both known and previously unknown. We followed four steps:

Step 1. Definition and calculation of the mean elements of the stream orbit and of the D-distribution of the sample meteors with respect to this "mean orbit."

We must have a set of orbital elements to which the D-values of the sample meteors can be referred. For this purpose, the mean orbit of the stream has been defined by the numerical procedure shown in Figure 13-1.

Step 2. Discussion of the contamination of the observed D-distribution curve by a sporadic meteor background and development of a model of the intrinsic D-distribution of the stream.

To estimate the contamination effect, we have calculated the D-distribution of a number of artificial samples of meteors with orbits randomly dispersed about the paths of some known streams. We have found that the expected frequency-density D-distribution of the sporadic background varies as $D^{2.8}$, and its cumulative D-distribution, as $D^{3.8}$. A few examples are given in Figure 13-2.

The stream's intrinsic D-distribution has been assumed to be Maxwellian in character. The proposed statistical model of meteor streams is represented in detail in Figure 13-3. The shape of the stream's intrinsic D-distribution is specified by its dispersion coefficient σ, whereas the stream's strength relative to the surrounding sporadic background is expressed by the population coefficient Λ. The two parameters define what we call the inner (D_I) and the outer (D_{II}) boundaries of the stream (see Figure 13-3). The proposed model gives the total number of the stream's members in the investigated sample but does not specify which meteors belong to it. Instead, the model attributes the degree of probability of stream membership to each of the sample meteors.

In Figure 13-4, the contaminated cumulative D-distribution curves, as derived theoretically from the model, are plotted on a logarithmic scale as a function of $D/\sigma\sqrt{2}$ with Λ as a parameter.

Step 3. Elimination of the sporadic background contamination and determination of the character of the intrinsic D-distribution of a stream.

Comparing graphically the theoretical curves in Figure 13-3 with the empirical contaminated D-distributions, we derived the dispersion and population coefficients for all the detected showers. The fits for some of the streams are given in Figures 13-5 and 13-6.

FLOW CHART FOR THE CALCULATION
OF THE MEAN ORBIT OF A STREAM

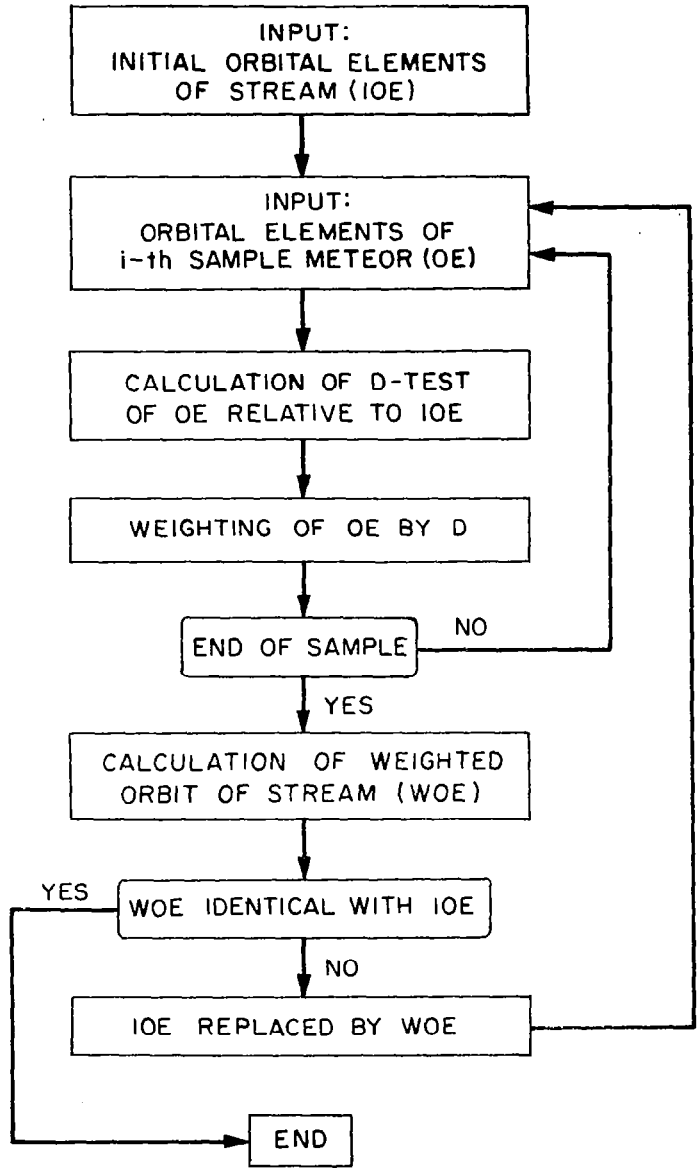

Figure 13-1. Flow chart for the calculation of the mean orbit of a stream.

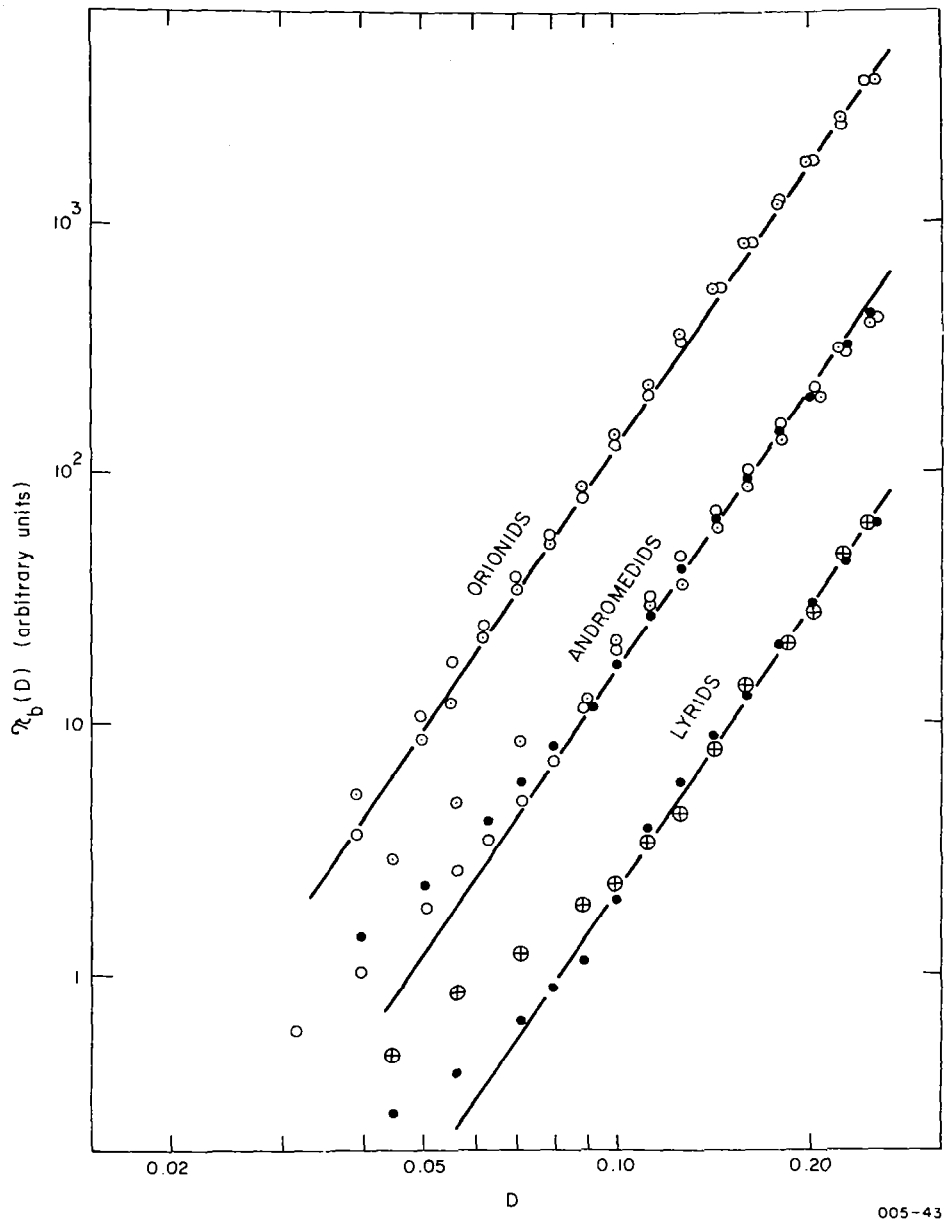

Figure 13-2. The D-distribution of an artificial sample of meteors moving in paths randomly dispersed about the mean orbit of the Orionids (top), the Andromedids (middle), and the Lyrids (bottom). The circled crosses denote a variation step of 1°.5 in angular elements and 0.026 a.u. in perihelion distance; the solid circles, 2°.0 and 0.035 a.u.; the open circles, 2°.5 and 0.044 a.u.; and the circled points, 3°.0 and 0.052 a.u. The lines indicate a slope of 3.8.

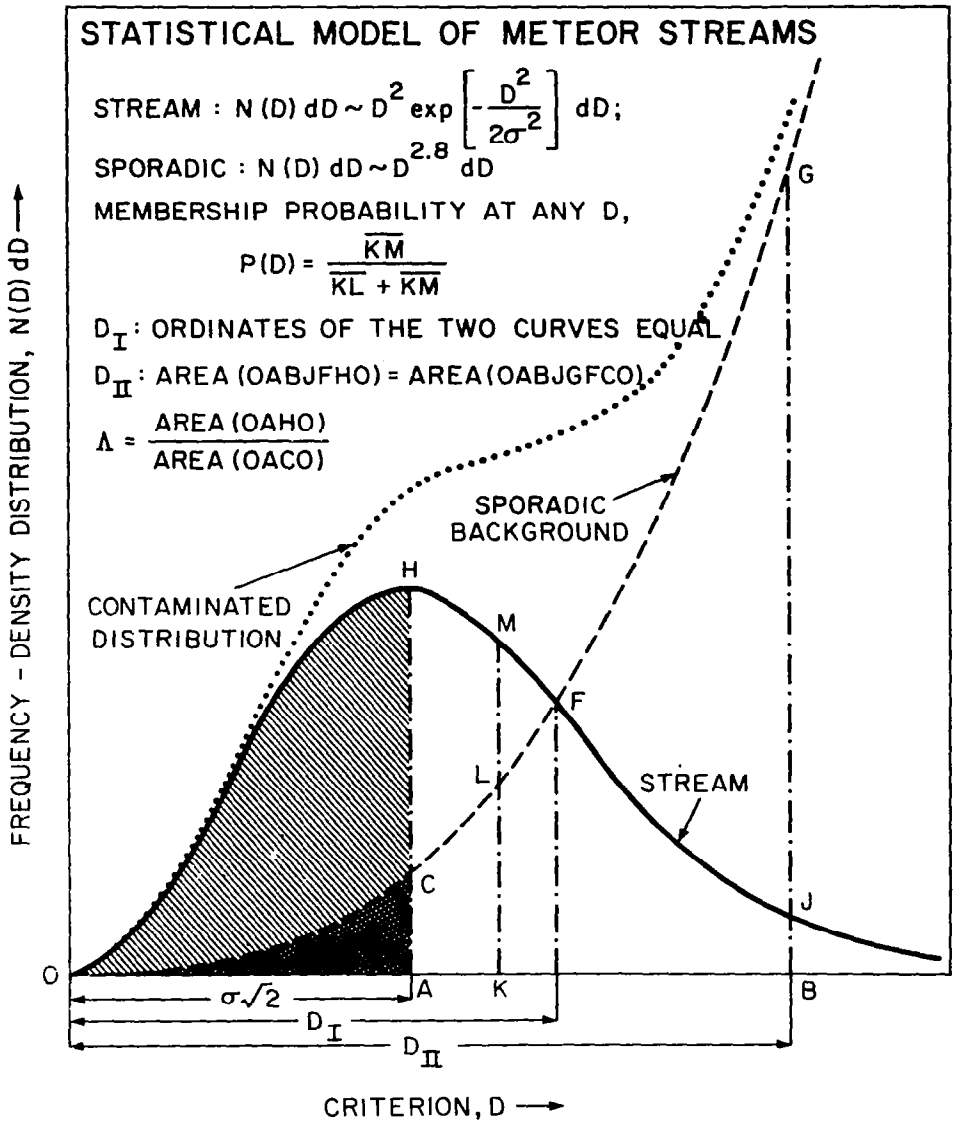

Figure 13-3. Density distribution of the statistical model of meteor streams. The intrinsic distribution (solid curve) is proportional to $D^2 \exp[-D^2/(2\sigma^2)]\,dD$, the sporadic background (dashed curve) increases as $D^{14/5}\,dD$, and the resultant contaminated distribution (dotted curve) is the sum of the two. The membership probability of a meteor with $D = \overline{OK}$ is $p(D) = \overline{KM}/(\overline{KL} + \overline{KM})$. The inner limit of the stream D_I is defined as the abscissa of the intersection point F of the intrinsic and sporadic distribution curves; the outer limit D_{II} is given by the abscissa $\overline{OB}$ such that areas (OABJFHO) and (OABJGFCO) are equal. The population coefficient Λ is defined by the ratio of area (OAHO) to area (OACO).

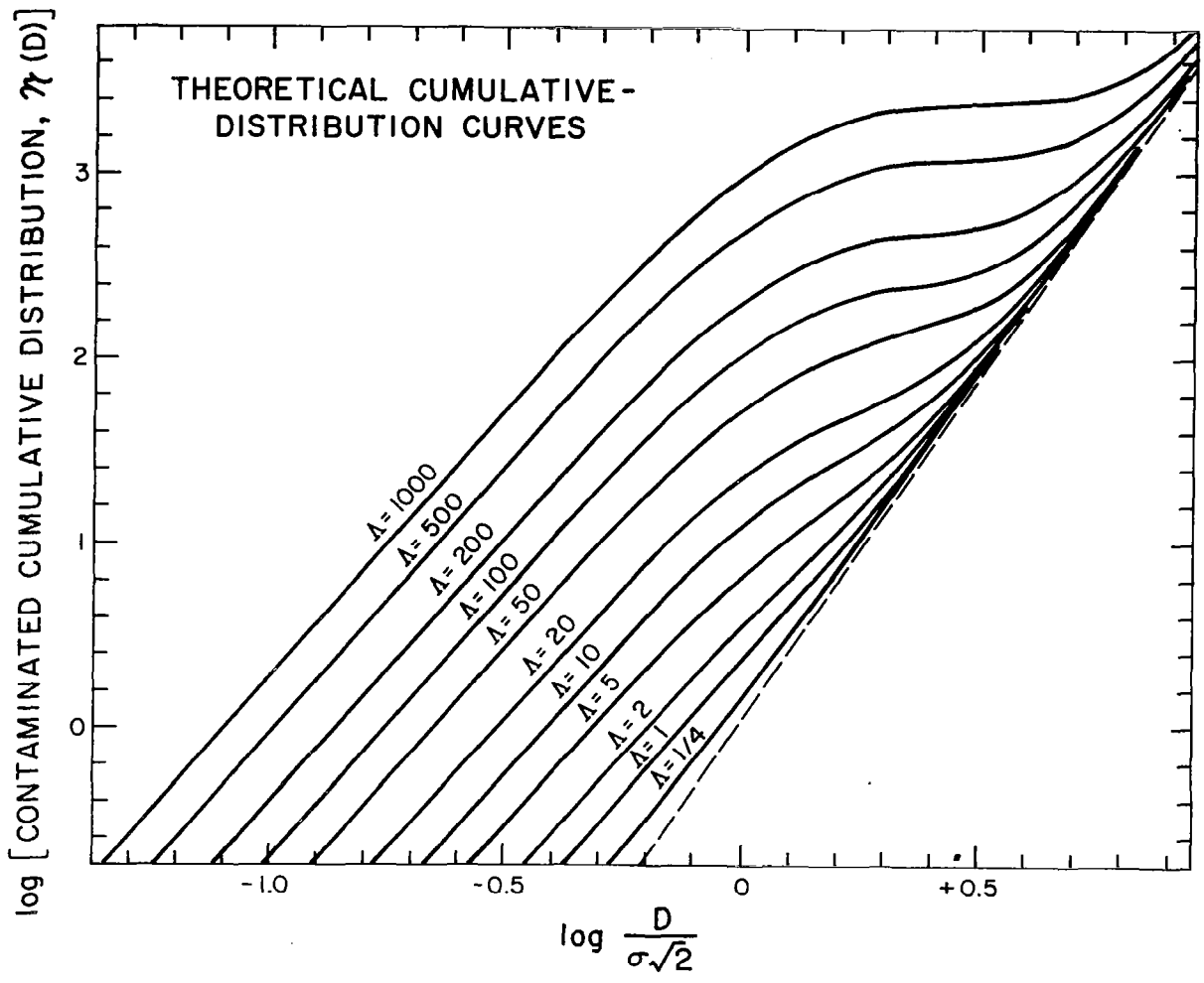

Figure 13-4. Theoretical curves of the contaminated cumulative D-distribution in meteor streams. The two parameters are the population coefficient Λ and the dispersion σ.

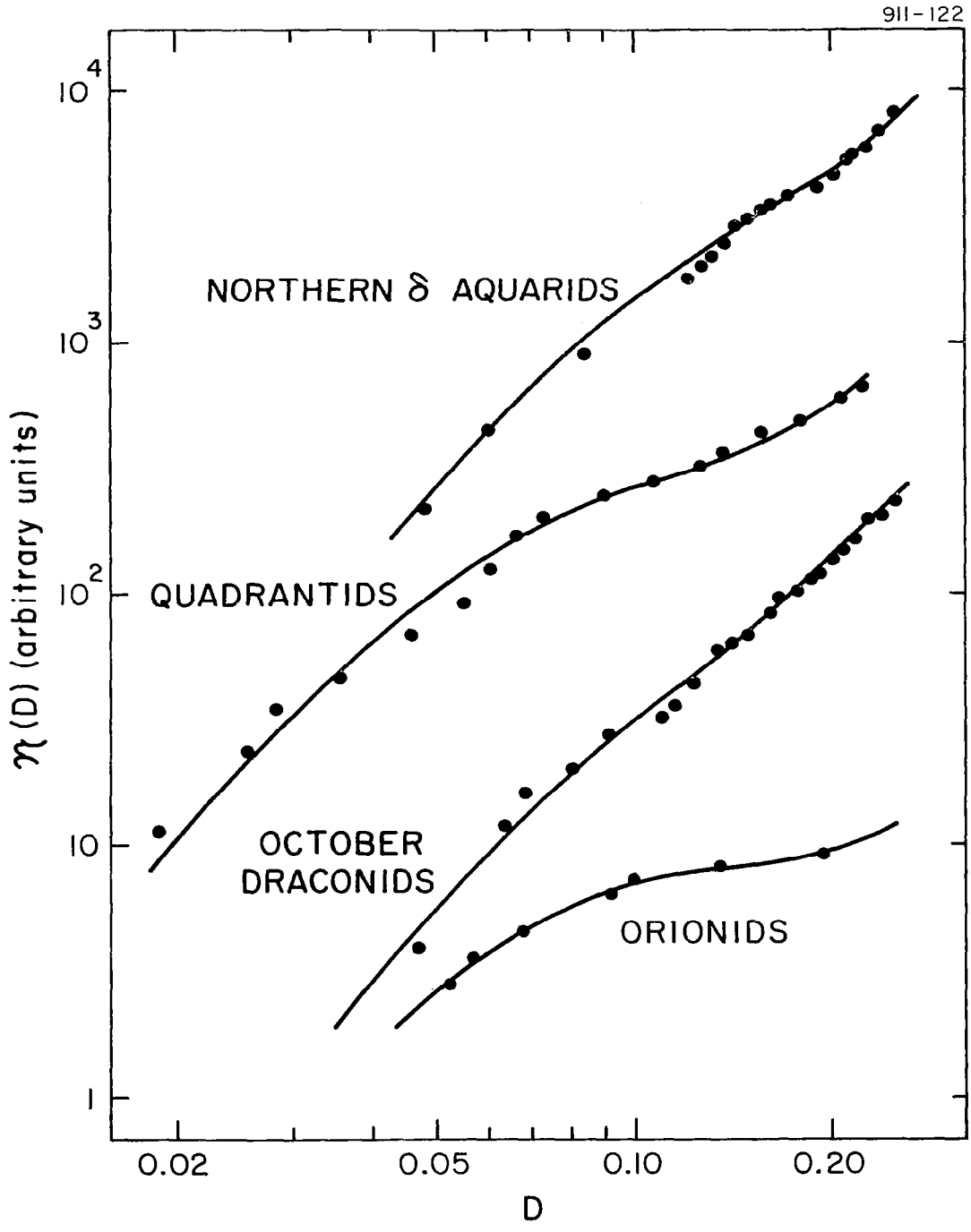

Figure 13-5. Fits of the normalized cumulative D-distribution $\Upsilon(D)$ for the Northern δ Aquarids, Quadrantids, October Draconids, and Orionids.

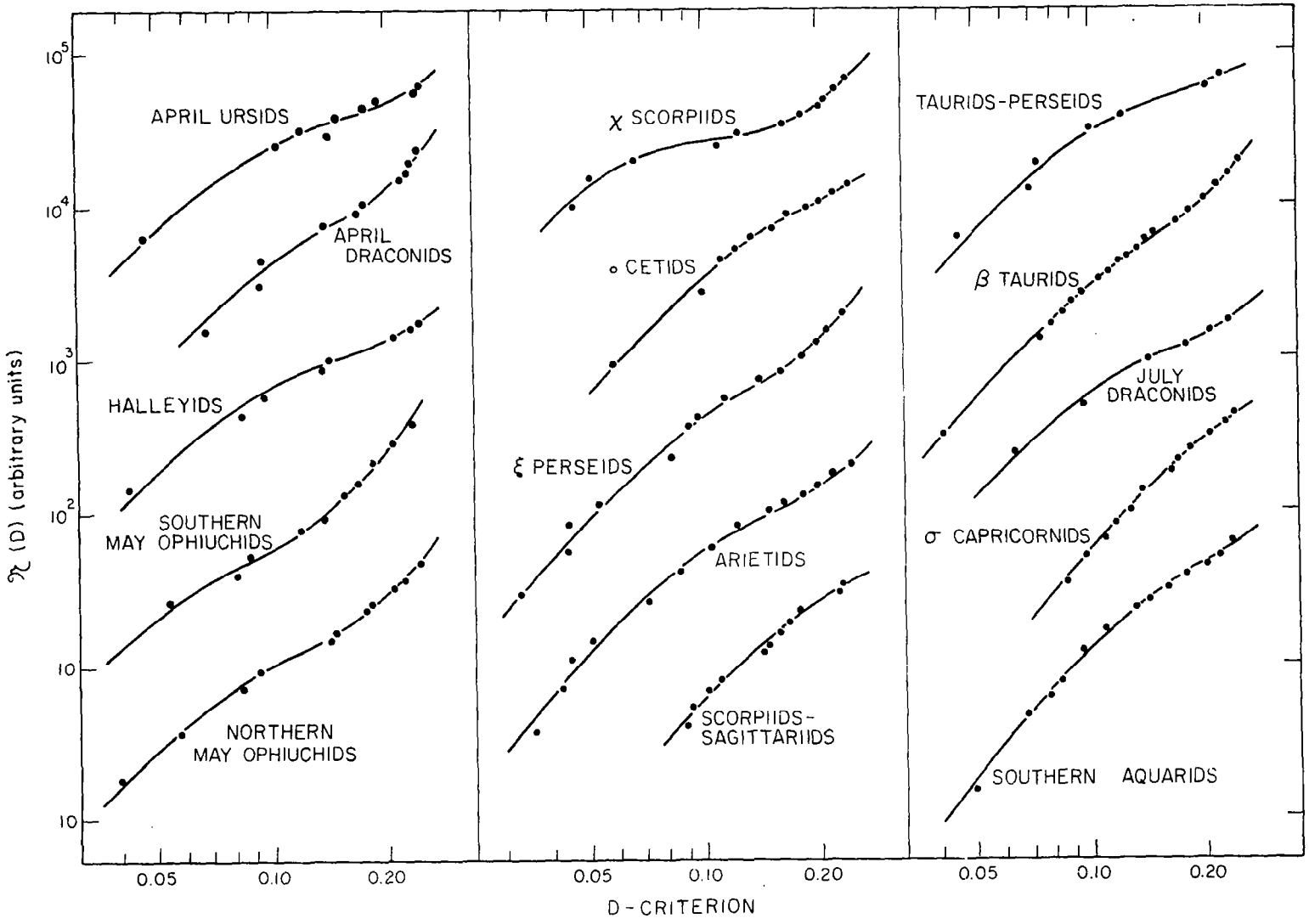

Figure 13-6. Normalized cumulative D-distribution $\mathcal{R}$ (D) for 15 radio streams of April to August.

Step 4. Discrimination between real streams and spurious ones and determination of possible comet-meteor and asteroid-meteor associations. Possible relation of the dispersion coefficient σ to the dynamical evolution of the streams.

Two criteria have been applied to the detected streams to find out whether they are real. One is based on the ratio of meteor population within D = 0.25 to that within D = 0.20. For a random sporadic distribution, this ratio is $(0.25/0.20)^{3.8} = 2.3$. The existence of a stream at low D's lowers this value, so the deviation from 2.3 measures the probability that the stream is real.

The other criterion says that a stream is real if the number of definite stream members within D is significantly greater than the square root of the number of sporadic meteors within the same D, for at least some D.

Both criteria rather consistently indicate that almost all the streams are very probably real.

13.2 Stream-Search Technique

Theoretically, to make the search absolutely complete, we should search for meteors dynamically associated with every single sample meteor. Because of the complexity of calculations associated with this statistical model, however, such a procedure would be in practice very inefficient and may become physically unfeasible even with the aid of a powerful computer. We therefore modified the first step of the search by substituting for the initial set of elements the orbits of all the objects of interest. These objects included visual, radio, and mainly photographic streams with known orbits previously detected by computer or conventional techniques, as well as comets and minor planets with orbits approaching the earth's orbit.

Except for spurious convergences, such a selection of initial orbits would make it impossible to detect radio streams not associated with any previously known object. We have therefore looked for high concentrations of meteor orbits in the sample, using a three-dimensional searching scheme, interrelating the longitude of perihelion with the longitude and latitude of the orbital pole. It is unlikely that we overlooked a major radio shower this way, but a number of minor streams could have escaped unnoticed in the fluctuating "noise" of the sporadic field. It must be these minor streams that are responsible for the stream-population bias mentioned below.

A total of 83 streams have been detected in the sample of 19,303 radio orbits. The number of definite stream members found in the sample is estimated at slightly over 1400, or about 7.5%. If the search were complete, this would be a very conservative figure by standards of the photographic samples.

13.3 Radiant Distribution of Radio Meteors and Streams

Computer plots of the ecliptical coordinates of our sample meteor radiants (radiant longitude λ vs. radiant latitude β in Figure 13-7; radiant longitude relative to the sun $\lambda - \lambda_{\odot}$ vs. β in Figure 13-8) suggests that the directions of the observed meteor trajectories are far from being uniformly distributed. The location and power-gain pattern of the radar system and selection due to the observing schedule account for part of the nonuniformity, particularly for the significant lack of radiants in high southern latitudes.

There is undoubtedly a definite concentration of radiants along the ecliptic, a decrease toward latitudes of +30° to +40°, and an increase in concentration at very high latitudes. The existence of frequent high-inclination, low-eccentricity orbits among radio meteors was reported previously by Davies (1957) and Hawkins (1963). We point out that some of the high-inclination showers we have detected suggest quite elongated orbits.

Figure 13-7 also shows the effect of annual variation in the meteor distribution.

In comparing the plots of individual radiants with those of mean radiants of the detected streams (Figures 13-9 and 13-10), we find a certain degree of resemblance. This is not a trivial statement since the detected streams make up less than 10% of the total population of Figures 13-7 and 13-8.

13.4 Differences between the Photographic and the Radio Components in the Streams

Possible relationships between the detected radio streams and previously known streams have been extensively studied. On the one hand, there are straightforward relations (e.g., the photographic and radio δ Cancrids); on the other, there are about

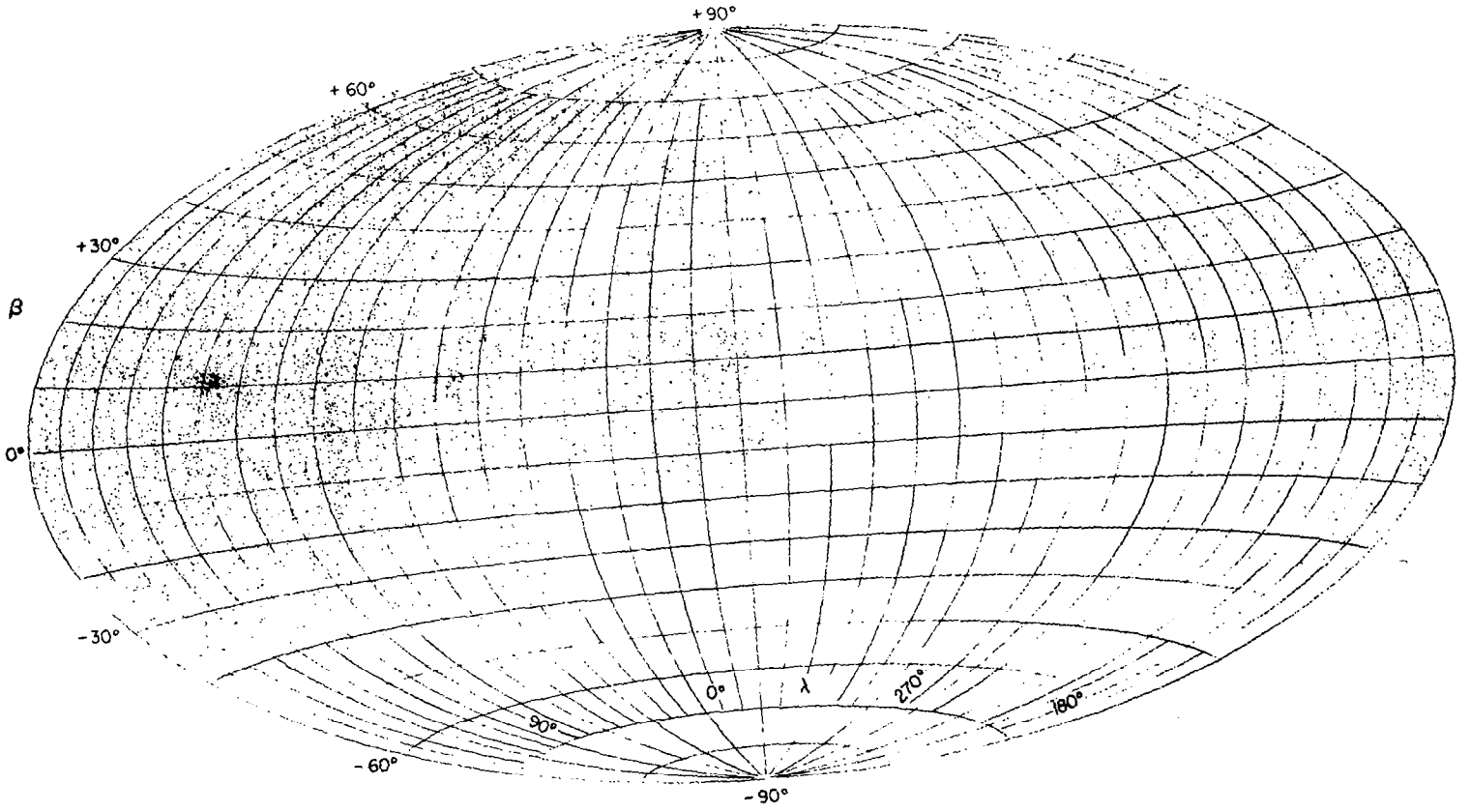

Figure 13-7. Computer plot of the ecliptical coordinates λ and β of 19,303 individual radio meteor radiants in Hammer's equal-area projection. The longitude increases leftward, the zero meridian being 20° left of the apparent central meridian; the two edge meridians thus indicate longitude 160°.

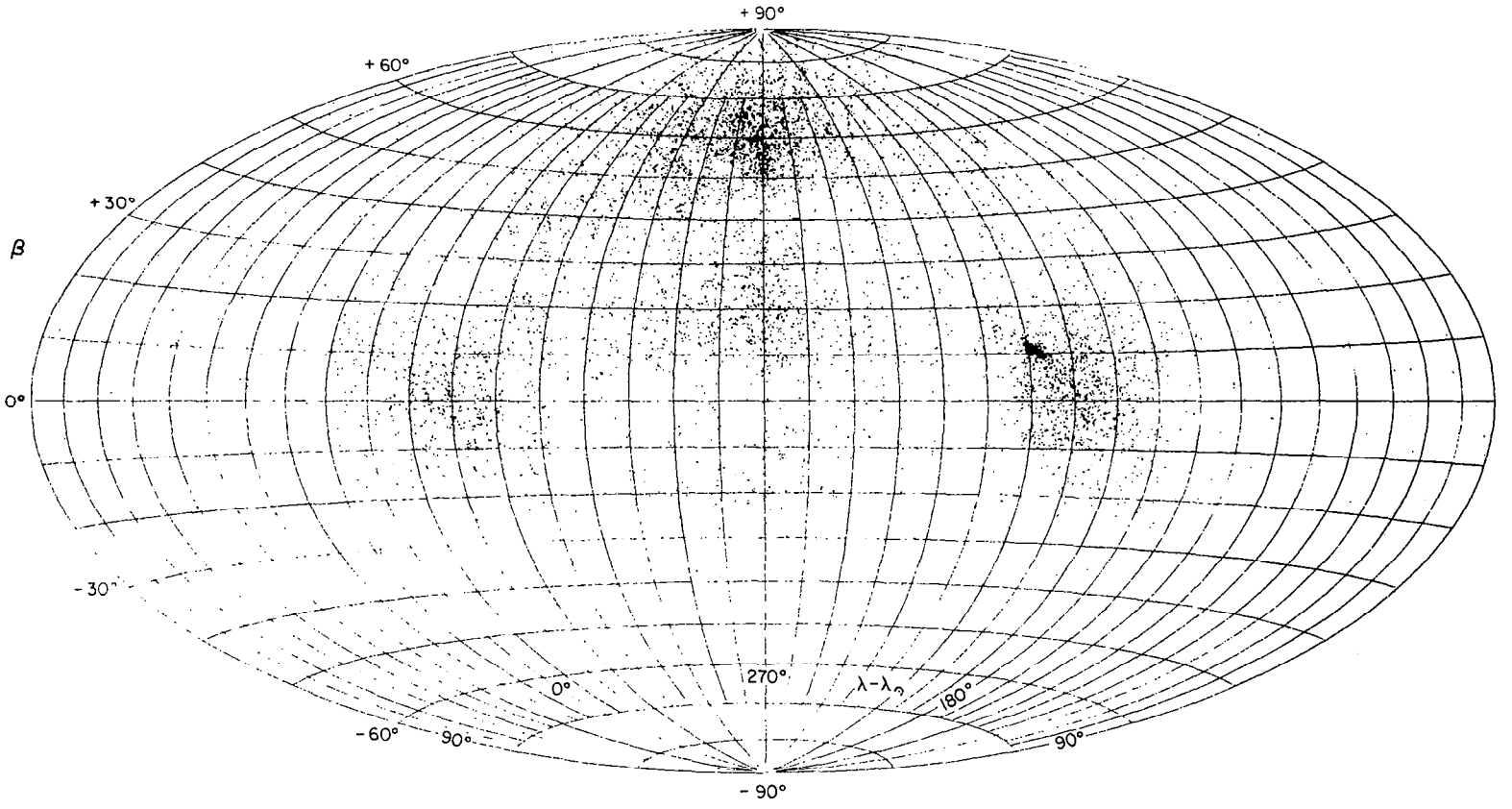

Figure 13-8. Computer plot of the sun-oriented ecliptical coordinates $\lambda - \lambda_{\odot}$ and β of 19,303 individual radio meteor radiants in Hammer's equal-area projection. The longitude increases leftward, the $\lambda_{\odot}$ meridian being 90° left of the apparent central meridian.

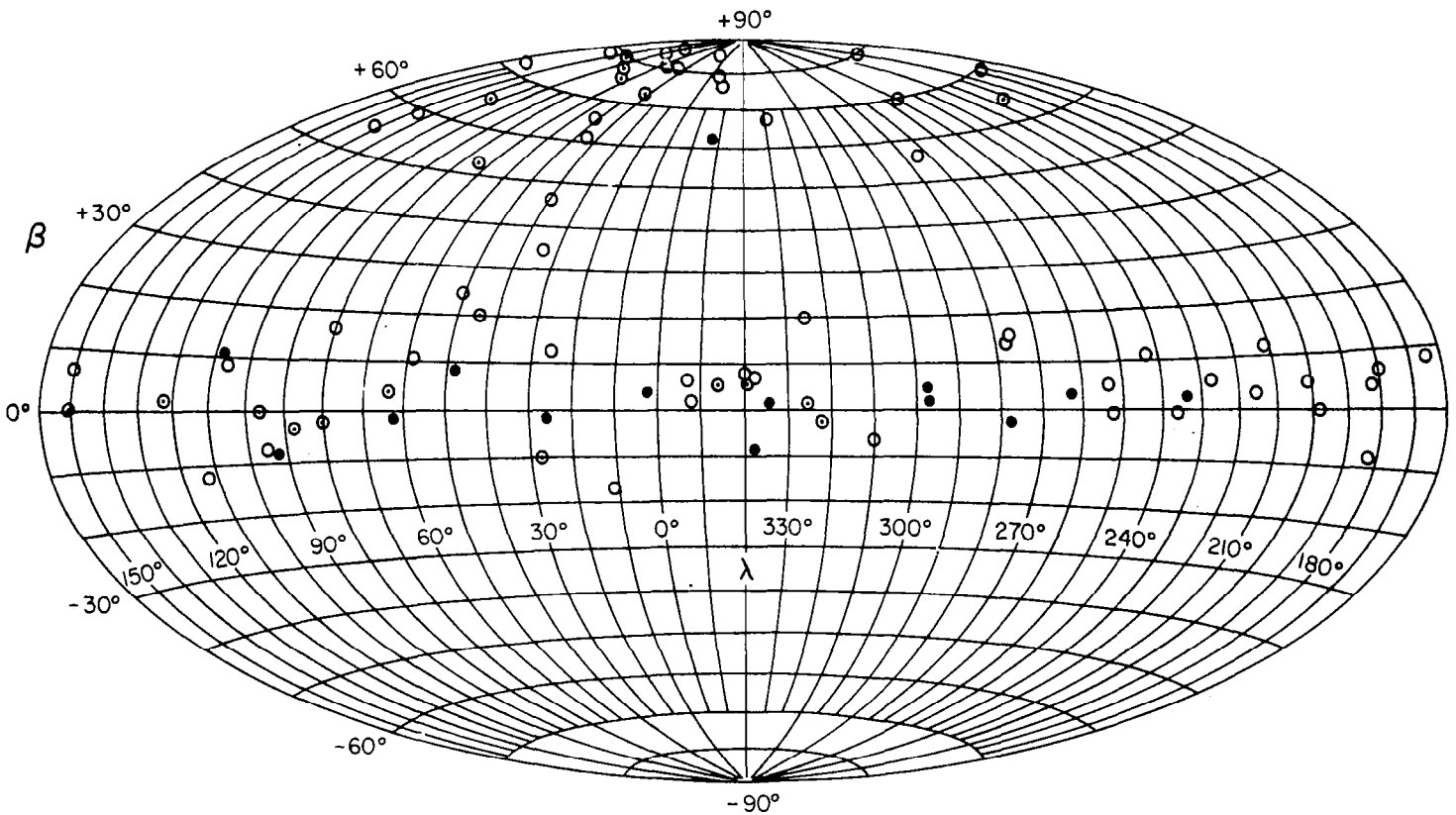

Figure 13-9. Ecliptical coordinates λ and β of the mean radiants of 83 radio streams in Hammer's equal-area projection. Solid circles stand for streams with more than 20 definite members; circled points, those with 10 to 20 members; and open circles, those with less than 10 definite members.

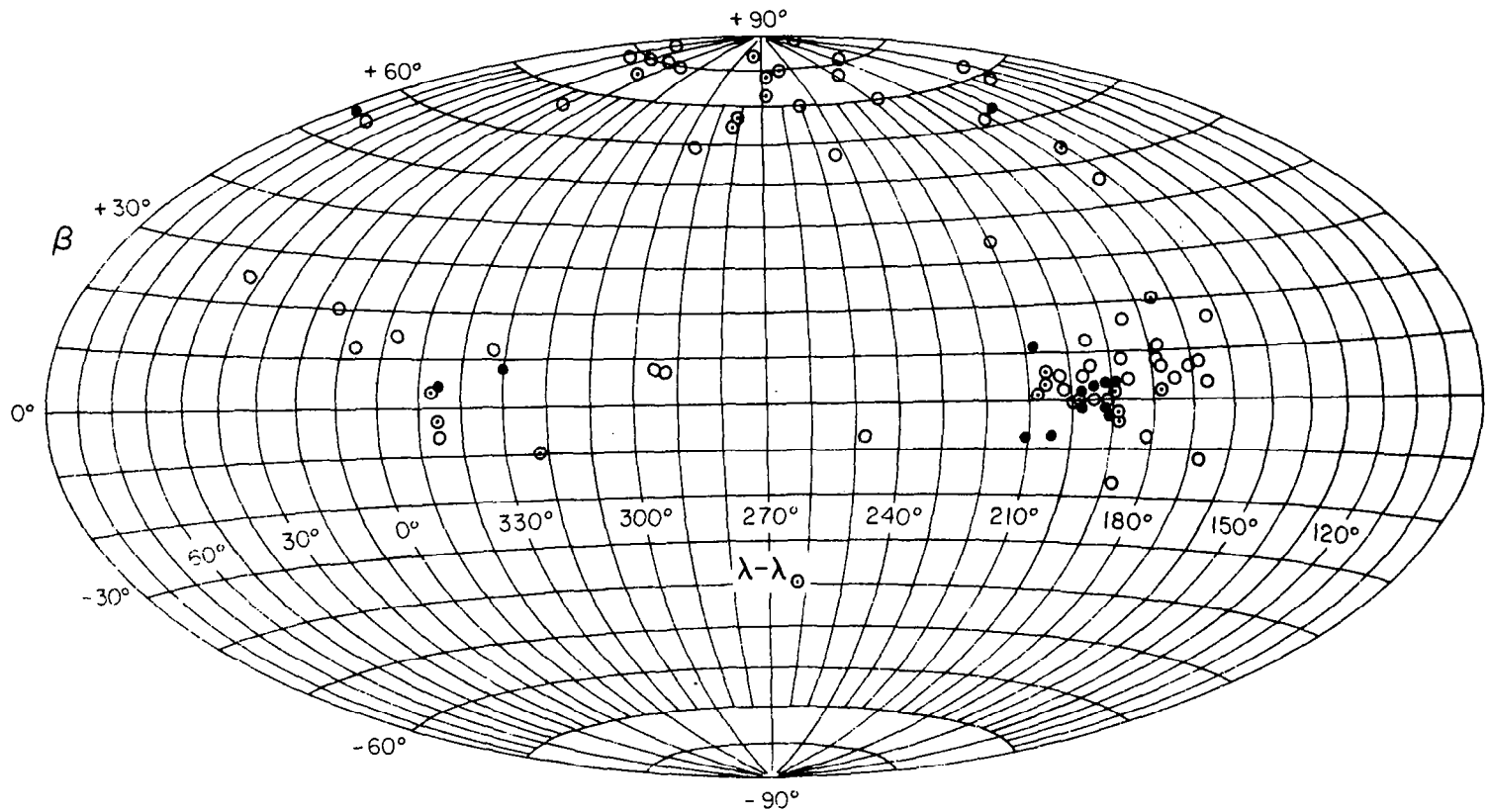

Figure 13-10. Sun-oriented ecliptical coordinates $\lambda - \lambda_{\odot}$ and β of the mean radiants of 83 radio streams in Hammer's equal-area projection. See Figure 13-9 for the symbols used for the streams.

40 photographic streams included in Jacchia and Whipple's (1961), Southworth and Hawkins's (1963), and Lindblad's (1971) lists that have not been detected among the radio meteors. The lack of fast meteors in retrograde orbits is particularly striking.

In a number of streams, dynamical differences have been found between the photographic and the radio meteors. Here we mention three of them:

A. Taurids. The gap between the Northern and Southern branches of this stream, so prominent in the photographic region, completely disappears in our radio sample (see Figure 13-11). Also, the radio Taurids appearing on the same day as the photographic Taurids have their radiants shifted eastward some 10°, on an average.

B. Southern δ Aquarids. There is a systematic difference in the no-atmosphere velocities (see Figure 13-12) between the photographic meteors of this stream (circled points, open circles) and the radio meteors (solid disks, points).

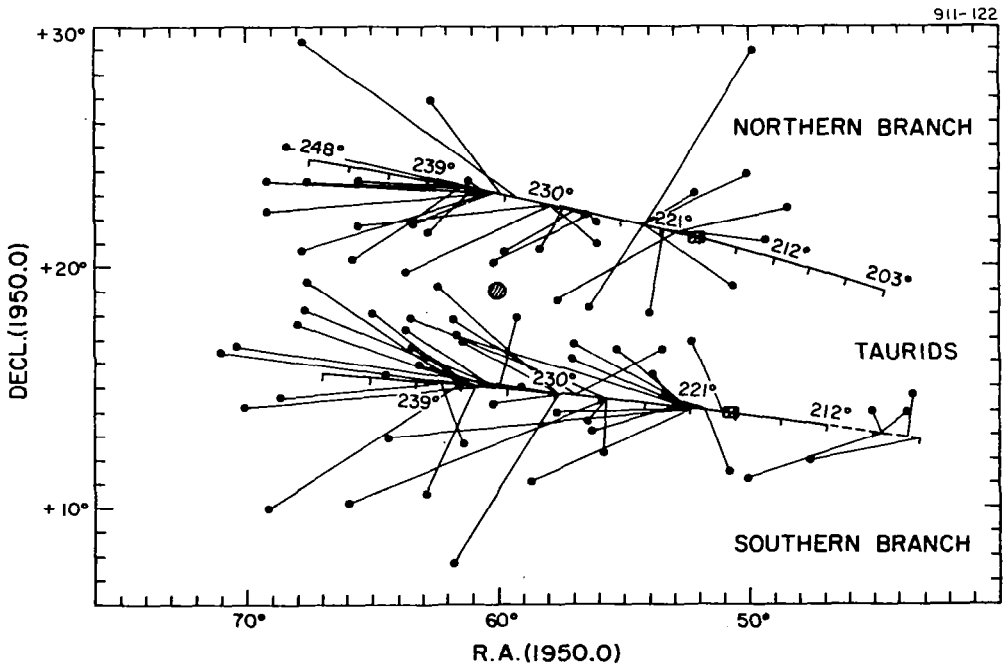

Figure 13-11. Plot of individual radiants of the Taurid radio meteors, 1961-1965 (dots). For comparison, the paths of the mean radiants of the two branches of the bright photographic Taurids are drawn after Wright and Whipple (1950).

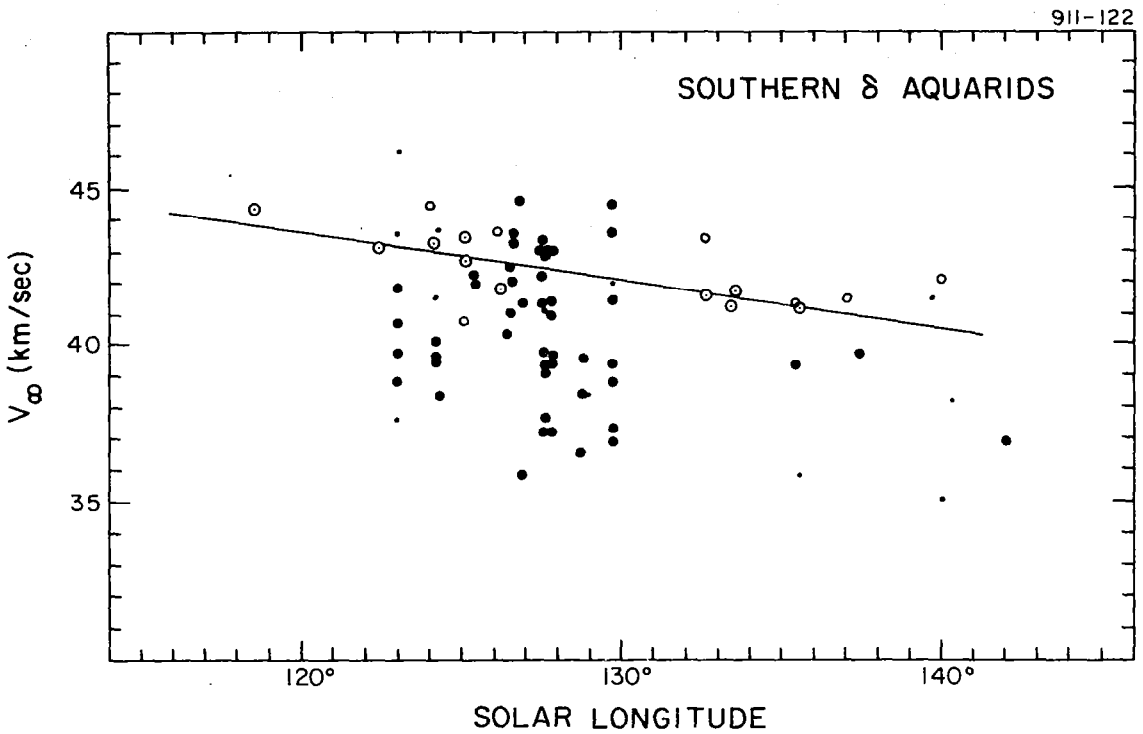

Figure 13-12. Comparison of the no-atmosphere velocities of the radio and photographic Southern δ Aquarids. The solid circles are the radio meteors of 1962-1965 with membership probability larger than 0.5; the dots, the radio meteors of 1962-1965 with membership probability between 0.1 and 0.5; the circled dots, the photographic meteors of 1952-1953 with precision orbits published by Jacchia and Whipple (1961); and the open circles, the photographic meteors of 1952-1953 with approximate orbits published by McCrosky and Posen (1961). The line is a fit of the Jacchia-Whipple data.

C. η Aquarids. Two maxima with a separation of about 2 days have been found in the η-Aquarid shower. The two radiants are very near each other, but the mean orbital elements of the two showers differ remarkably. The one passing through the node later is here called the Halleyid shower since its orbit is much closer (3 times closer, in terms of the D-criterion) to the orbit of Comet Halley (see Table 13-1).

13.5 Twin Showers

As pointed out for the first time by Whipple (1940) in the case of the Taurids, a broad meteor stream moving in a low-inclination orbit can easily meet the earth at two points, before the perihelion passage and after it, thus producing two apparently "independent," but actually closely related, showers. We will call these the twin showers.

Table 13-1. Orbits of η Aquarids, Halleyids, and P/Comet Halley (equinox 1950.0).

	η Aquarids	Halleyids	P/Halley
ω	79°.5 ± 1.6	96°.7 ± 2.2	111°.7
Ω	44°.9 ± 0.4	47°.1 ± 1.7	57°.8
i	161°.2 ± 0.9	164°.6 ± 0.8	162°.2
q (a.u.)	0.468 ± 0.010	0.587 ± 0.018	0.587
e	0.834 ± 0.014	0.894 ± 0.017	0.967
a (a.u.)	2.823	5.550	17.95
P (yr)	4.74	13.1	76.0
π	124°.4	143°.8	169°.5
$\Omega - \omega$	325°.4	310°.4	306°.1
Radiant R.A.	338°.3 ± 0.5	338°.1 ± 1.2	336°*
Radiant Decl.	-0°.3 ± 0.5	-1°.3 ± 0.8	-1°*
Date of pass through node (UT, epoch 1950)	May 5.9	May 8.2	May 8†

*Theoretical radiant.

†Date of pass through the closest point to the earth's path in 1910.

We have been investigating the possibility of the appearance of twin showers in the radio meteor sample, especially because of Hoffmeister's (1948) prediction of daytime showers associated with the Scorpiids-Sagittariids, Piscids, and Virginids (in addition to the Taurids). We have confirmed two twins already reported by Almond (1951) and have disclosed a few more. They are all listed in Table 13-2.

Table 13-2. Twin showers.

	Twin showers				Observed			Computed*		(O - C) in	
	Preperihelion	Postperihelion	D	i	$\Delta\beta$	$\Delta\lambda$	$\Delta\lambda_*$	$\Delta\lambda$	$\Delta\lambda_*$	$\Delta\lambda$	$\Delta\lambda_*$
I	Southern Arietids	ζ Perseids	0.103	3°	+ 5°.1	37°.5	147°.7	35°.2	149°.1	+ 2°.3	-1°.4
II	Orionids	Halleyids	0.113	165	+14.6	244.6	44.8	234.3	44.7	+10.3	+0.1
III	Scorpiids-Sagittariids	Capricornids-Sagittariids	0.149	5	+ 7.6	20.5	153.9	28.0	155.4	- 7.5	-1.5
IV	Taurids	β Taurids	0.175	2	- 0.4	18.4	153.6	28.4	154.6	-10.0	-1.0
V	σ Capricornids	χ Capricornids	0.187	4	- 8.1	13.7	156.2	24.2	158.0	-10.5	-1.8
VI	ζ Aurigids	March Andromedids	0.212	7	+ 9.1	330.0	242.5	327.7	233.1	+ 2.3	+9.4
VII	Triangulids	χ Piscids	0.352	10	- 8.7	341.0	191.8	347.1	194.4	- 6.1	-2.6

*For D = 0 and β = 0.

With the exception of the meteors associated with Halley's comet, the twin showers seem to have their radiants fairly near each other. We have investigated the problem generally for a meteor stream moving in an elliptic orbit coplanar with the earth's orbit. We found that the difference in the longitude of radiants between the twin showers, $\Delta\lambda = \lambda_{\text{postperihelion}} - \lambda_{\text{preperihelion}}$, is given by the relation

$$\tan\left(\frac{1}{2}\Delta\lambda\right) = \frac{(1 \mp \sqrt{p/r})\sqrt{2 - (p/r) - (r/a)}}{1 - (p/r) \pm \sqrt{p/r}[1 - (r/a)]} , \qquad (13\text{-}1)$$

where p is the stream's orbital semilatus rectum, a its semimajor axis, and r the solar distance of the encounter. The upper signs stand for the direct orbits; the lower, for the retrograde ones. Although the formula allows for the ellipticity of the earth's orbit, we have put r = 1 a.u. and plotted the curves of constant longitudinal difference $\Delta\lambda$ in Figure 13-13. The figure readily explains why twin showers typically have small $\Delta\lambda$: For direct orbits and semimajor axes over 1 a.u., the radiants must always be less than 40° apart for any q > 0.35 a.u. For retrograde orbits, on the other hand, the radiants must be more than 90° apart for any q < 0.7 a.u.

Similarly, the longitudinal difference between the radiants of the twin showers relative to the sun, $\Delta\lambda_* = (\lambda - \lambda_\odot)_{\text{postperihelion}} - (\lambda - \lambda_\odot)_{\text{preperihelion}}$, is

$$\tan\left(\frac{1}{2}\Delta\lambda_*\right) = \frac{\sqrt{2 - (p/r) - (r/a)}}{1 \mp \sqrt{p/r}} , \qquad (13\text{-}2)$$

with the symbols defined as above.

The curves of constant $\Delta\lambda_*$ are represented in Figure 13-14. For direct orbits with semimajor axes larger than 1 a.u., $\Delta\lambda_*$ approaches 180° within 45° for any q between 0.3 and 0.8 a.u. For retrograde orbits, on the other hand, $\Delta\lambda_* < 60°$ for any q > 0.4 a.u. and $\Delta\lambda_* < 75°$ for any q > 0.2 a.u. In other words, the twin showers of a stream of direct motion are typically one nighttime and one daytime, while those of a stream of retrograde motion can both be nighttime, as in the case of the showers associated with Comet Halley. The distribution of inclinations in the stream can somehow modify the numerical data mentioned, but it does not violate the basic rule. To

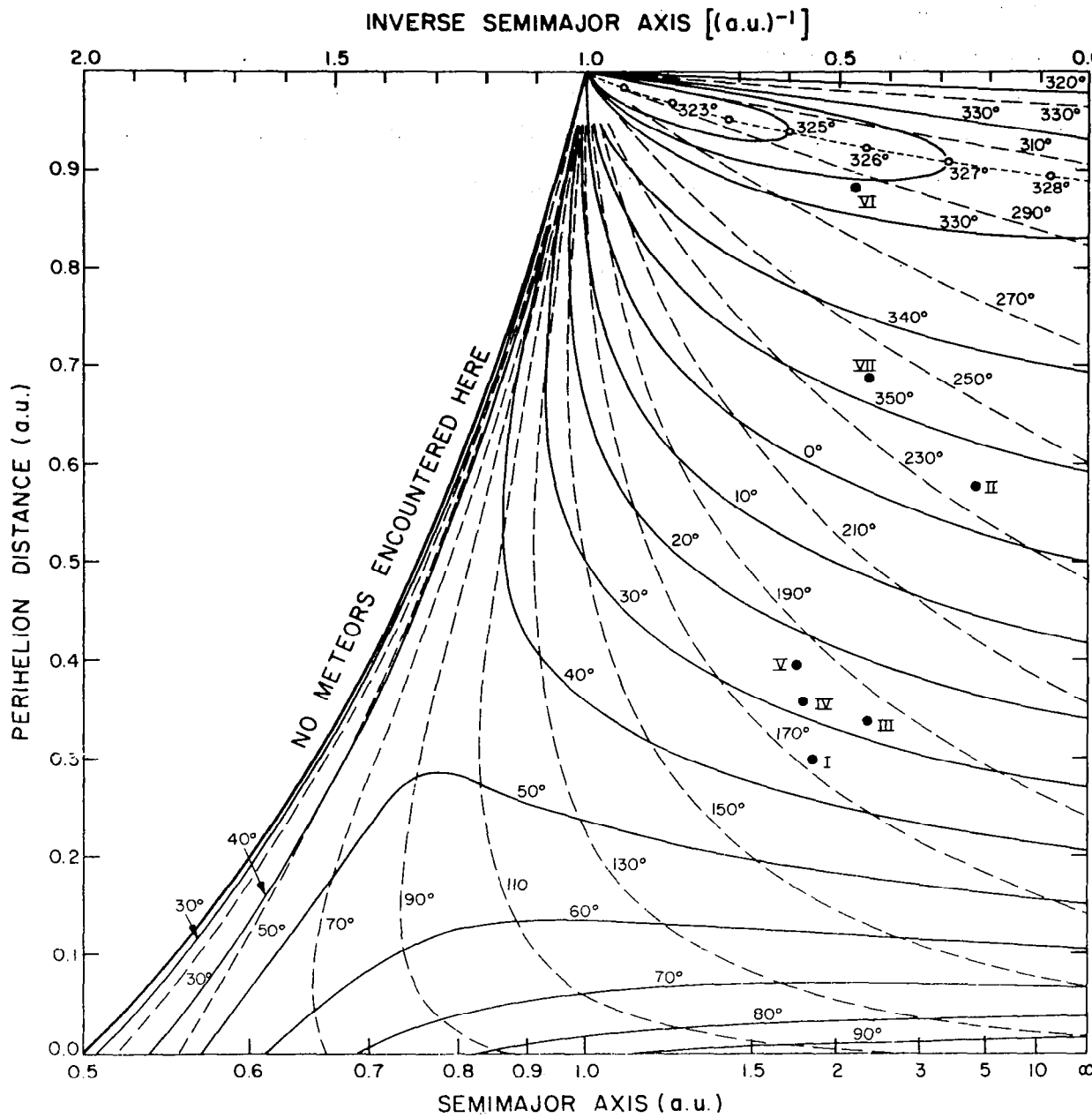

Figure 13-13. Difference $\Delta\lambda$ in the longitude of radiants between the twin showers (in the sense "postperihelion minus preperihelion") of an ecliptical stream versus the semimajor axis and the perihelion distance of the stream. Solid curves are the loci of constant $\Delta\lambda$ for streams in direct orbits; broken curves, those for streams in retrograde orbits. The dotted curve is the locus of the tips of loops, the open circles indicating $\Delta\lambda$ at 1° separation. The large solid circles represent detected twin showers (for their identification, see Table 13-2).

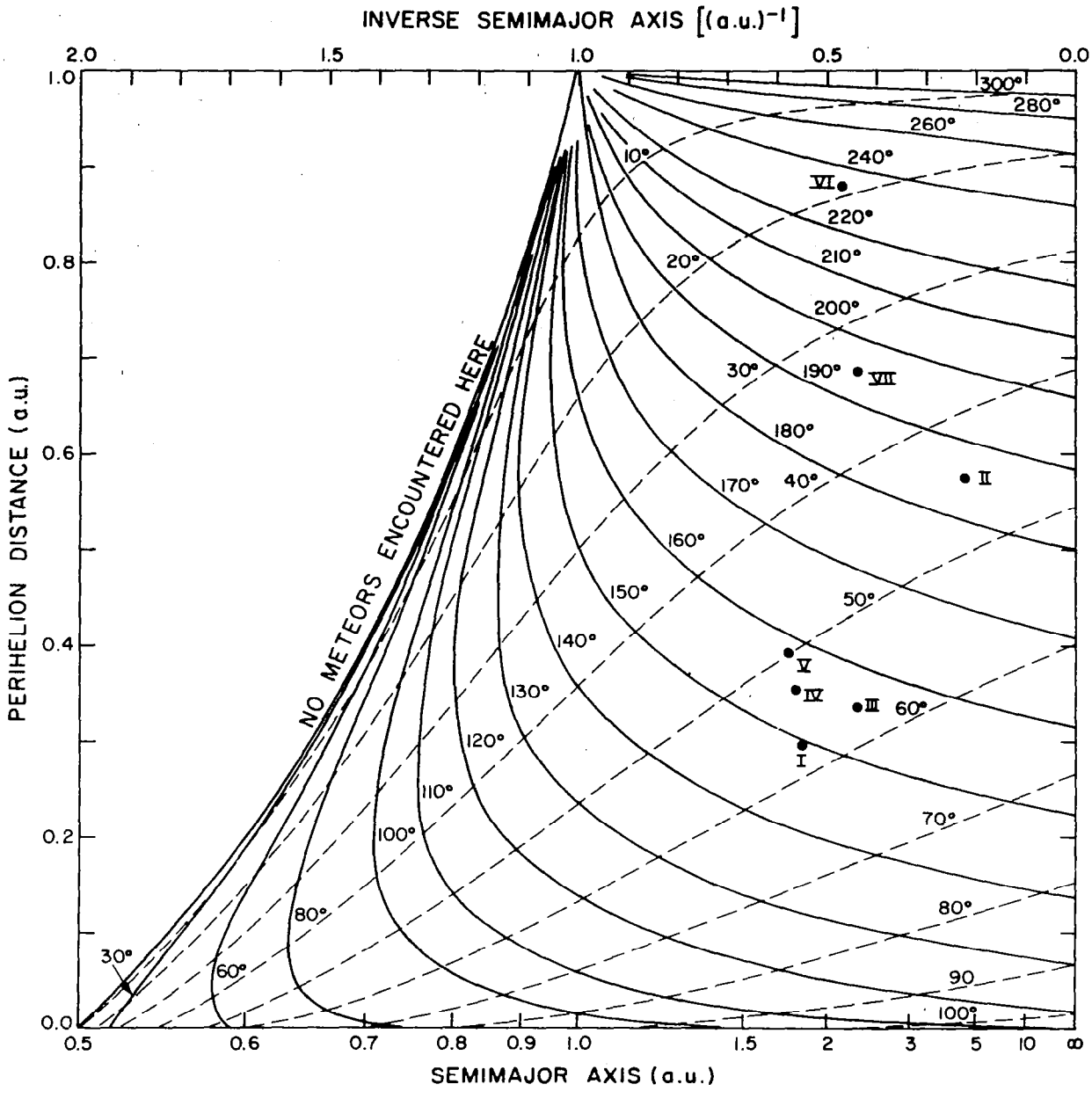

Figure 13-14. Difference $\Delta\lambda_*$ in the sun-oriented longitude of radiants between the twin showers (in the sense "postperihelion minus preperihelion") of an ecliptical stream versus the semimajor axis and the perihelion distance of the stream. Solid curves are the loci of constant $\Delta\lambda_*$ for the streams in direct orbits; broken curves, those for the streams in retrograde orbits. The large solid circles represent detected twin showers (for their identification, see Table 13-2).

prove the validity of the rule in practice, we have calculated the radiant differences for the seven pairs of twin showers detected in our sample. Table 13-2 confirms that our prediction of $\Delta\lambda$ and $\Delta\lambda_*$ is good within about 10°, the deviations being essentially due to the differences in the shapes between the orbits of the twin showers (which had to be averaged in order to apply equation (13-1)), rather than to the inclination effect.

13.6 Associations of the Radio Meteor Streams with Comets and Minor Planets

Calculations modeling random perturbations by the planets of a meteor stream suggest that the intrinsic D-distribution keeps essentially its Maxwellian character but becomes increasingly broader with time. Consequently, the dispersion σ apparently measures the degree of dissipation of the stream, and therefore indirectly its "age." The calculations also suggest that the D-value of the criterion between the stream's mean orbit and the parent object, D_p, is related, statistically, to the σ dispersion by

$$D_p \approx 3.4\,\sigma \quad . \tag{13-3}$$

Table 13-3 lists the potential parent objects for streams where an association appears possible. Investigation of the associations is put on a quantitative basis following the above suggestions. However, since the D_p^+/σ criterion is only a statistical test, a reasonably low value of this parameter by no means indicates that the association is certain. Especially for very disperse streams, the above ratio can easily come out pretty small, and indeed we have found more than one potential parent for a few streams (Piscids, Southern Arietids, and Triangulids).

Each possible association must therefore be considered in connection with other evidence available in each specific case. For example, the apparent resemblance between the orbits of the Ophiuchids and periodic Comet Lexell is likely to be quite fortuitous. Cook (1970) gave significant arguments against the existence of any stream associated with this comet.

Table 13-3. Possible comet-meteor and asteroid-meteor associations ($D_p/\sigma \leq 6$).

Potential parent object	Meteor stream	D_p	D_p/σ
P/Biela	γ Camelopardalids	0.330	3.5
	Triangulids	0.277	3.6
	Andromedids	0.188	4.6
P/Crommelin	November Cepheids	0.279	4.7
P/Encke	Taurids	0.235	2.0
	β Taurids	0.220	3.5
	Southern Arietids	0.423	3.5
P/Giacobini-Zinner	October Draconids	0.393	5.9
P/Halley	Halleyids	0.126	2.7
	Orionids	0.214	5.0
P/Honda-Mrkos-Pajdušáková	α Capricornids	0.290	3.3
	Aquarids-Capricornids	0.272	3.5
P/Lexell	Ophiuchids	0.310	2.2
	June Scutids	0.317	3.8
P/Mellish	Monocerids	0.234	2.1
P/Pons-Winnecke	July Draconids	0.213	3.4
1861 I	Lyrids	0.197	4.6
(1566) Icarus	Taurids-Perseids	0.083	1.4
	Piscids	0.462	3.3
	Southern Arietids	0.468	3.9
	Arietids	0.245	4.2
(1580) Betulia	June Draconids	0.374	4.3
1932 HA Apollo	ν Librids	0.125	2.8
	χ Scorpiids	0.162	4.9
1936 CA Adonis	σ Capricornids	0.097	0.8
	Scorpiids-Sagittariids	0.215	1.9
	Capricornids-Sagittariids	0.318	2.3
	χ Capricornids	0.185	3.4
1937 UB Hermes	χ Piscids	0.107	1.3
	Piscids	0.457	3.3
	Southern Arietids	0.430	3.6
	Triangulids	0.351	4.5
	β Cetids	0.340	5.4
1950 DA	May Ursids	0.285	3.2
	April Ursids	0.277	6.0
1968 AA	α Cygnids	0.267	2.0
	χ Draconids	0.272	2.9
	δ Cygnids	0.212	4.7
Meteorite Příbram	σ Leonids	0.352	5.9

One has to be particularly careful about interpreting the resemblance between the orbits of some of the detected radio streams and those of the minor planets of the Apollo and Albert types. If these associations were confirmed, they would represent a major argument in favor of the hypothesis, considering these minor planets to be defunct cometary nuclei. We have studied possible evolution of such objects (Sekanina, 1971a, b), assuming that they underwent a process similar to that recently experienced by periodic Comet Encke. The process is caused by accumulation of the secular effects of the nongravitational mechanism and dynamically results in a systematic reduction of the aphelion distance. The calculations show, however, that such a process is of low efficiency and that our present knowledge of the nongravitational mechanism gives no satisfactory explanation for evolutionary paths of the minor planets with aphelia nearer than 3 to 3.5 a.u. from the sun.

It is therefore imperative that each of the potential asteroid-meteor associations be checked by applying more rigorous dynamical tests. We have tested the likely evolutionary relationship between Adonis and a radio stream, using a method suggested for the Encke-Taurid association by S. E. Hamid (1970, private communication). It explains the differences between the present orbits of a meteor and the parent body by the combined effect of the conditions at the time of ejection and differential secular perturbations. We have assumed that the ejection occurred at perihelion, in the orbit plane, and with a velocity of 50 m sec^{-1}, which corresponds to an average mass of the associated meteors of the order of 10^{-4} g. We have also assumed that the motion of Adonis was affected in the past by a nongravitational acceleration, which implies that the material should have been ejected preferentially in the direction of motion. Such an impulse would suddenly increase the eccentricity of the expelled material by 0.003 relative to Adonis but keep the other elements unchanged. We have computed differential secular perturbations for various times of ejection in the past and found that the best agreement between the model and the mean orbit of the associated meteors from the sample is achieved if the ejection is assumed to have occurred about 9000 yr ago.

13.7 A Working List of Meteor Streams

A. F. Cook has prepared a list of those streams that he is convinced do exist. Most catalogs of streams, if they are large, include many that have only a certain probability of existence. An extreme case is that of the old catalogs of visual radiants. The apparent distribution of radiants of individual sporadic meteors exhibits not the true distribution of numbers larger than a chosen mass as a function of direction, but an apparent distribution greatly affected by the luminous efficiency of meteors, which emphasizes the meteors of higher velocity. This distribution has its primary maximum on the ecliptic 165° behind the sun (and another equal primary maximum only 15° behind the sun, which is only detectable among radar meteors). There is a broad secondary maximum about the meteoric apex 90° behind the sun, from which the highest velocity meteors come, and two tertiary maxima at the celestial longitude of the apex (90° behind the sun) and at celestial latitudes ±75° (and thus near the poles of the ecliptic). These combine with a natural weighting toward the zenith of an observer to give a rather nonuniform background of radiants of sporadic meteors and have caused visual radiant catalogs to cover the sky with spurious radiants.

Radar observations suffer from a similar effect, so care in identification of radar streams is required. It is now abundantly clear that similar care is required in identification of streams among photographed meteors.

Cook's list (see Attachment A) contains 57 entries. Three of these (the Daytime β Taurids, the Southern Taurids, and the Northern Taurids) are associated with P/Comet Encke. Two (the η Aquarids and the Orionids) are associated with P/Comet Halley. Two Andromedid radiants are given, one an annual moving radiant with a pronounced change in orbit as it moves, and the other the radiant of the great Andromedid showers. These are associated with P/Comet Biela. Four other pairs are not associated with a known comet. Two are pairs of a daytime with a nighttime shower (Daytime Arietids with the Southern δ Aquarids and Daytime ζ Perseids with the Northern Piscids), and two are pairs of northern and southern branches of the same streams (ι Aquarids and χ Orionids). The 57 entries thus come from 49 streams. There are two additional pairings that appear to indicate a common origin for the parent bodies of the streams. These are the Daytime Sextantids with the Geminids

and the Pegasids with the December Phoenicids. The December Phoenicids, in turn, plainly come from Comet 1819 IV Blanpain. The parent body of the Pegasids may no longer exist, but it and the comet must have separated rather a long time ago, in view of the difference in the orbital planes. The absence of a large dispersed system of meteoroids like that of P/Comet Encke is shown by the absence of continuous simultaneous activity from the Pegasids and Phoenicids throughout October, November, and December.

Cook suggests that a small comet or asteroid-like body may be found moving in the currently predicted orbit of P/Comet Biela. Comet Blanpain has not been seen since 1819, so a search for it would be pretty hopeless. Condensed streams for which comets might be sought are the Quadrantids, Librids, and Corvids, with the first offering much the best prospect. Small asteroids might be searched for along the orbits of the Geminids and the Daytime Sextantids, with the former offering the better prospect. In short, first priority for such searches should go to P/Comet Biela, the Quadrantids, and the Geminids.

13.8 References

Almond, M. (1951). The summer daytime meteor streams of 1949 and 1950. III. Computation of the orbits. Mon. Not. Roy. Astron. Soc., vol. 111, pp. 37-44.

Cook, A. F. (1970). Discrete levels of beginning height of meteors in streams. Smithsonian Astrophys. Obs. Spec. Rep. No. 324; also in Smithsonian Contr. Astrophys., in press.

Davies, J. G. (1957). Radio observations of meteors. In Advances in Electronics and Electron Physics, Academic Press, New York, vol. 9, pp. 95-128.

Hawkins, G. S. (1963). The Harvard Radio Meteor Project. Smithsonian Contr. Astrophys., vol. 7, pp. 53-62.

Hoffmeister, C. (1948). Meteorströme. Werden & Wirken, Weimar.

Jacchia, L. G., and Whipple, F. L. (1961). Precision orbits of 413 photographic meteors. Smithsonian Contr. Astrophys., vol. 4, pp. 97-129.

Lindblad, B.-A. (1971). A computerized stream search among 2401 photographic meteor orbits. Smithsonian Contr. Astrophys., no. 12, pp. 14-24.

McCrosky, R. E., and Posen, A. (1961). Orbital elements of photographic meteors. Smithsonian Contr. Astrophys., vol. 4, pp. 15-84.

Sekanina, Z. (1971a). Dynamical evolution of extinct comets (abstract). Bull. Amer. Astron. Soc., vol. 3, p. 271.

Sekanina, Z. (1971b). A core-mantle model for cometary nuclei and asteroids of possible cometary origin. In Physical Studies of Minor Planets, I.A.U. Colloquium No. 12, in press.

Southworth, R. B., and Hawkins, G. S. (1963). Statistics of meteor streams. Smithsonian Contr. Astrophys., vol. 7, pp. 261-285.

Wright, F. W., and Whipple, F. L. (1950). The photographic Taurid meteors. Harvard Reprint Ser. II, No. 35, pp. 1-44.

Whipple, F. L. (1940). Photographic meteor studies. III. The Taurid meteor shower. Proc. Amer. Phil. Soc., vol. 83, pp. 711-745.

14. PERSONNEL OF THE RADIO METEOR PROJECT: 1966 to 1971

The Radio Meteor Project has been under the direction of Dr. Whipple since its inception in 1955. It was transferred from HCO to SAO in January 1966, from which time Drs. R. B. Southworth and R. E. McCrosky have been Principal Investigators. From 1966 to 1969, Dr. G. S. Hawkins coordinated the project. Mr. Dorik Mechau was Administrator in 1966, followed by Mr. C. Hagge, from 1966 to 1970. Mr. P. Sozanski then served as interim Administrator until Mr. H. E. Rosenthal was appointed Administrative Officer in 1970.

The members of the SAO headquarters staff have been as follows (listed according to their starting dates):

Mathematicians: Mr. R. Lacy, 1966-1969; Mrs. S. Rosenthal, 1966-present; Mrs. A. Posen, 1966-present; Mr. D. Wilson, 1967.

Astronomers: Dr. G. S. Hawkins, 1966-1969; Dr. G. Forti, 1966-1971; Dr. A. F. Cook, 1966-present.

Physicists: Mrs. G. Southworth, 1966-1969; Dr. M. R. Flannery, 1968-1970; Dr. H. Levy II, 1968-1970; Dr. Z. Sekanina, 1969-present. Dr. A. Dalgarno acted as advisor to Drs. Flannery and Levy.

Astrophysicist: Dr. C. S. Nilsson, 1966-1969.

Engineering Support: Dr. M. R. Schaffner, 1966-1970; Mr. J. Maxwell, 1967. Dr. W. W. Salisbury, Mr. A. Goldstein, Dr. M. D. Grossi, and Mr. W. M. Grim also assisted with the engineering support.

Electronic Technicians: Mr. F. Licata, 1966; Mr. P. Ouellette, 1969-1970.

Secretarial Support: Mrs. S. Bull, 1966-1969; Miss E. Smith, 1969-present.

Members of the Radio Meteor Project field team were as follows:

Havana

Station Manager: Mr. J. Simms, 1966-1971.

Technical Aide: Mrs. B. Daniel, 1966-1970.

Electronic Technicians: Mr. R. Stockus, 1966; Mr. D. Summers, 1966-1967; Mr. C. Ewan, 1966-1967; Mr. P. Woulfe, 1966-1969; Mr. K. Rhinehart, 1966-1969; Mr. J. Kopico, 1967-1969; Mr. D. Hallenbeck, 1967-1971.

Physical Science Aides: Mrs. J. Summers, 1967; Mrs. P. Layton, 1967-1969; Mr. D. Shaw, 1970. Dr. A. Cook and Mr. J. Shao also assisted in the field.

Urbana

Station Manager: Mr. J. T. Williams, 1967-present.

Physical Science Aides: Mr. L. Alexander, 1969-1970; Mr. D. Hutchins, 1970-1971.

Dr. Z. Ceplecha and Dr. B.-A. Lindblad were visiting scientists during the course of the Radio Meteor Project.

Various people from NASA assisted throughout the years, including A. Wineman, Mr. K. Baker, and Mr. T. D. Bess.

Mr. M. Malec, of the SAO Business Office, and Dr. C. A. Lundquist, of the Director's Office, contributed much contractual and scientific assistance.

15. BIBLIOGRAPHY OF THE RADIO METEOR PROJECT: 1966 to 1972

AYERS, W. G., McCROSKY, R. E., and SHAO, C.-Y.

1970. Photographic observations of 10 artificial meteors. Smithsonian Astrophys. Obs. Spec. Rep. No. 317, 44 pp.

BAKER, K., and FORTI, G.

1966. Preliminary study of meteor streams at faint radio magnitude. Harvard-Smithsonian Radio Meteor Res. Rep. No. 14, 15 pp.

CEPLECHA, Z.

1968. Discrete levels of meteor beginning height. Smithsonian Astrophys. Obs. Spec. Rep. No. 279, 54 pp.

COOK, A. F.

1968. The physical theory of meteors. In Physics and Dynamics of Meteors, IAU Symp. No. 33, ed. by L. Kresák and P. M. Millman, D. Reidel Publ. Co., Dordrecht-Holland, pp. 149-160.

1970. Discrete levels of beginning height of meteors in streams. Smithsonian Astrophys. Obs. Spec. Rep. No. 324, 22 pp.; also in Smithsonian Contr. Astrophys., in press.

1972. A working list of meteor streams. In Proc. IAU Colloq. No. 13, ed. by A. F. Cook, C. L. Hemenway, and P. M. Millman, NASA, Washington, in press.

COOK, A. F., FORTI, G., McCROSKY, R. E., POSEN, A., SOUTHWORTH, R. B., and WILLIAMS, J. T.

1972. Combined observations of meteors by image-orthicon television camera and multistation radar. In Proc. IAU Colloq. No. 13, ed. by A. F. Cook, C. L. Hemenway, and P. M. Millman, NASA, Washington, in press.

COOK, A. F., LINDBLAD, B.-A., MARSDEN, B. G., McCROSKY, R. E., and POSEN, A.

1972. Yet another stream search among 2401 photographic meteors. Smithsonian Contr. Astrophys., in press.

FLANNERY, M. R.

1968. Theoretical and experimental three-body ionic recombination coefficients. Phys. Rev. Lett., vol. 21, pp. 1729-1730.

1969a. Impact-parameter treatment of hydrogen-hydrogen excitation collisions. I. Two-state approximation. Phys. Rev., vol. 183, pp. 231-240.

1969b. Impact-parameter treatment of hydrogen-hydrogen excitation collisions. II. Four-state approximation. Phys. Rev., vol. 183, pp. 241-244.

1969c. Approximations to the two-state impact parameter treatment of heavy particle collisions. Journ. Phys. B (Atom. Molec. Phys.), vol. 2, pp. 909-912.

1969d. Multi-state impact parameter treatment of hydrogen-helium excitation collisions. Journ. Phys. B (Atom. Molec. Phys.), vol. 2, pp. 913-922.

1969e. The 2s and 2p excitations of hydrogen by proton and helium-ion impact. Journ. Phys. B (Atom. Molec. Phys.), vol. 2, pp. 1044-1054.

1970a. Impact parameter and wave equations for direct excitation and electron capture processes. Journ. Phys. B (Atom. Molec. Phys.), vol. 3, pp. 21-28.

1970b. Semi-quantal theory of heavy-particle excitation, deexcitation, and ionization by neutral atoms. I. Slow and intermediate energy collisions. Smithsonian Astrophys. Obs. Spec. Rep. No. 322, 43 pp.; also in Ann. Phys., vol. 61, pp. 465-487.

1970c. The $2\,^1S$ and $2\,^1P$ excitations of helium by proton and electron impact. Journ. Phys. B (Atom. Molec. Phys.), vol. 3, pp. 306-314.

1970d. Inclusion of higher state couplings in a multistate impact-parameter treatment of heavy-particle collisions. Journ. Phys. B (Atom. Molec. Phys.), vol. 3, pp. 798-803.

1970e. The $n \rightarrow n + 1$ transition of atomic hydrogen induced by hydrogen-atom impact. Astrophys. Journ., vol. 161, pp. L41-L42.

1970f. Excitation and ionization of hydrogen by hydrogen-atom impact. Journ. Phys. B (Atom. Molec. Phys.), vol. 3, pp. L97-L100.

1970g. Long-range effects in the 2s and 2p excitations of hydrogen by proton and helium ion impact. Journ. Phys. B (Atom. Molec. Phys.), vol. 3, pp. 1083-1089.

FLANNERY, M. R.

1970h. Semi-quantal theory of heavy-particle excitation by neutral atoms. I. Low and intermediate energies. Ann. Phys. (N.Y.), vol. 61, pp. 465-487.

1970i. The excitation of atomic hydrogen from n to n + 1 by electron impact. Astrophys. Lett., vol. 6, pp. 85-88.

1970j. Classical theory of excitation, de-excitation and ionization of atoms by charged particles. Journ. Phys. B (Atom. Molec. Phys.), vol. 3, pp. 1610-1619.

1970k. Impact parameter treatment of hydrogen-hydrogen excitation collisions. III. Electron-exchange and nuclear symmetry effects. Journ. Phys. B (Atom. Molec. Phys.), vol. 3, pp. 1600-1609.

1970*l*. Collisional quenching of metastable hydrogen by ground-state hydrogen atoms. Physica, vol. 53, pp. 28-31.

FLANNERY, M. R., and LEVY II, H.

1969a. H-H interaction potentials. Journ. Phys. B (Atom. Molec. Phys.), vol. 2, pp. 314-321.

1969b. Simple analytic expression for general two-center Coulomb integrals. Journ. Chem. Phys., vol. 50, pp. 2938-2940.

1970. Single and double excitations in hydrogen-hydrogen collisions. Journ. Phys. B (Atom. Molec. Phys.), vol. 3, pp. L21-L23.

FORTI, G.

1972. A determination of meteor mass distribution from meteor echoes. In Proc. IAU Colloq. No. 13, ed. by A. F. Cook, C. L. Hemenway, and P. M. Millman, NASA, Washington, in press.

HAWKINS, G. S., and BROWN, J. C.

1967. A comprehensive study of the characteristics of meteor echoes - I. Smithsonian Astrophys. Obs. Spec. Rep. No. 254, 30 pp.

LACY, R. G.

1966. A tabulation of meteor-echo rates, July 1965–June 1966. Harvard-Smithsonian Radio Meteor Project Res. Rep. No. 13, 23 pp.

LEVY II, H.

1969a. Impact-parameter calculation of hydrogen-hydrogen double-excitation collisions. Phys. Rev., vol. 184, pp. 97-101.

LEVY II, H.

1969b. Born wave calculation of atom-atom inelastic cross sections: Description of target atom by elastic and inelastic X-ray form factors. Phys. Rev., vol. 185, pp. 7-15.

1969c. Born-wave calculation of atom-atom inelastic cross sections: Excitation of He(1^1S) to He(N^1L) by hydrogen atoms. Phys. Rev., vol. 187, pp. 130-135.

1969d. Multistate impact-parameter calculation of atom-atom excitation cross sections: Excitation of H(1s) by He(1^1S). Phys. Rev., vol. 187, pp. 136-142.

1970a. Multistate impact-parameter calculations of atom-atom excitation cross sections: Excitation of H(1s) by neon, argon, and krypton. Phys. Rev. A, vol. 1, pp. 750-754.

1970b. Born wave cross-section calculations for the excitation of He(1^1S) to He(N^1L) by helium, neon, argon, and krypton. Journ. Phys. B (Atom. Molec. Phys.), vol. 3, pp. 1501-1509.

1971. Born wave cross-section calculations for collisional quenching of metastable H(2s) by helium, neon, argon, and krypton. Phys. Rev. A, vol. 3, pp. 1987-1991.

McCROSKY, R. E.

1968. Meteors without sodium. Smithsonian Astrophys. Obs. Spec. Rep. No. 270, 13 pp.

NILSSON, C. S.

1967. Orbital distribution of meteors of limiting magnitude +6 observed from the southern hemisphere. In The Zodiacal Light and the Interplanetary Medium, ed. by J. L. Weinberg, NASA SP-150, pp. 201-211; also in Smithsonian Astrophys. Obs. Spec. Rep. No. 239, pp. 99-121.

NILSSON, C. S., and SOUTHWORTH, R. B.

1967. The flux of meteors and meteoroids in the neighborhood of the earth. Smithsonian Astrophys. Obs. Spec. Rep. No. 263, 13 pp; also in Physics and Dynamics of Meteors, IAU Symp. No. 33, ed. by L. Kresák and P. M. Millman, D. Reidel Publ. Co., Dordrecht-Holland, pp. 280-286, 1968.

SCHAFFNER, M. R.

1966. The circulating page loose system, a new solution for data processing. Harvard-Smithsonian Radio Meteor Project Res. Rep. No. 15, 129 pp.

SEKANINA, Z.

1970a. Statistical model of meteor streams. I. Analysis of the model. Icarus, vol. 13, pp. 459-474.

1970b. Statistical model of meteor streams. II. Major showers. Icarus, vol. 13, pp. 475-493.

1970c. A new model for meteor streams. Presented at 14th IAU General Assembly, Commission 22, Brighton, England, August.

1970d. Dynamics of meteor streams and new asteroid-meteor and comet-meteor associations (abstract). Bull. Amer. Astron. Soc., vol. 2, pp. 217-218.

1971. On the age of a radio meteor stream associated with minor planet Adonis (abstract). Bull. Amer. Astron. Soc., vol. 3, p. 271.

1972. Statistical model of meteor streams. III. Stream search among 19303 radio meteors. Submitted to Icarus.

SOUTHWORTH, R. B.

1967a. Space density of radio meteors. In The Zodiacal Light and the Interplanetary Medium, ed. by J. L. Weinberg, NASA SP-150, pp. 179-188; also in Smithsonian Astrophys. Obs. Spec. Rep. No. 239, pp. 75-97.

1967b. Phase function of the zodiacal cloud. In The Zodiacal Light and the Interplanetary Medium, ed. by J. L. Weinberg, NASA SP-150, pp. 257-270; also in Smithsonian Astrophys. Obs. Spec. Rep. No. 239, pp. 47-74.

1968. Discrimination of stream and sporadic meteors (abstract). In Physics and Dynamics of Meteors, IAU Symp. No. 33, ed. by L. Kresák and P. M. Millman, D. Reidel Publ. Co., Dordrecht-Holland, p. 404.

1972. Recombination in radar meteors. In Proc. IAU Colloq. No. 13, ed. by A. F. Cook, C. L. Hemenway, and P. M. Millman, NASA, Washington, in press.

VERNIANI, F.

1966a. Physical characteristics of 320 faint radio meteors. Journ. Geophys. Res., vol. 71, pp. 2749-2761.

1966b. Meteor masses and luminosity. Smithsonian Astrophys. Obs. Spec. Rep. No. 219, 46 pp.

WHIPPLE, F. L.

1967. On maintaining the meteoritic complex. In The Zodiacal Light and the Interplanetary Medium, ed. by J. L. Weinberg, NASA SP-150, pp. 409-426; also in Smithsonian Astrophys. Obs. Spec. Rep. No. 239, pp. 1-46.

During the period 1966 to 1970, Semiannual Technical Reports on the Meteor Research Program were issued. These reports contained scientific results and discussions that were not published elsewhere or were published in a different form. Such contributions follow:

Semiannual Technical Report No. 1, January 1 to June 30, 1966

Echo analyzer data 1965-1966, by R. G. Lacy.
Artificial meteor data, by R. E. McCrosky.

Semiannual Technical Report No. 2, July 1 to December 31, 1966

Reliability of diffusion heights, by R. B. Southworth.
Radio meteor influx, by R. B. Southworth.
Artificial meteor data, by R. E. McCrosky.
Super-Schmidt reductions, by R. E. McCrosky.
Feasibility of image-orthicon use, by R. E. McCrosky.

Semiannual Technical Report No. 3, January 1 to June 30, 1967

Artificial meteor data, by R. E. McCrosky.
Super-Schmidt reductions, by R. E. McCrosky and C.-Y. Shao.
Radio meteor influx, by C. S. Nilsson and R. B. Southworth.

Semiannual Technical Report No. 4, July 1 to December 31, 1967

Super-Schmidt reductions, by R. E. McCrosky and C.-Y. Shao.
On the width of the Geminid shower at faint radio magnitude, by G. Forti.
Parameters of concern in coincident observation of meteors by radar and image-orthicon techniques, by R. E. McCrosky.

Semiannual Technical Report No. 5, January 1 to June 30, 1968

Annual review of Smithsonian studies of the meteor environment in space, by R. B. Southworth.

Photographic observations of nine artificial meteors, by R. E. McCrosky and and C.-Y. Shao.

Semiannual Technical Report No. 6, July 1 to December 31, 1968

Super-Schmidt reductions, by R. E. McCrosky and C.-Y. Shao.

Semiannual Technical Report No. 7, January 1 to June 30, 1969

Results from Fresnel pattern analyses and diffusion heights, by R. B. Southworth.

Super-Schmidt reductions, by R. E. McCrosky and C.-Y. Shao.

Annual review of Smithsonian studies of the meteor environment in space, by R. B. Southworth.

Semiannual Technical Report No. 8, July 1 to December 31, 1969

Review of meteor research for the past decade, by R. E. McCrosky and R. B. Southworth.

ATTACHMENT A

A WORKING LIST OF METEOR STREAMS

Allan F. Cook, II

This working list has been compiled from the following sources:

A. A selection by myself (Cook, 1970) from a list by Lindblad (1971a), which he found from a computer search among 2401 orbits of meteors photographed by the Harvard Super-Schmidt cameras in New Mexico.

B. Five additional radiants found by McCrosky and Posen (1959) by a visual search among the radiants and velocities of the same 2401 meteors.

C. A further visual search among these radiants and velocities by Cook, Lindblad, Marsden, McCrosky, and Posen (1972).

D. A computer search by Lindblad (1971b) among 1827 precisely reduced photographed meteors from all available sources.

E. Visual radiants reported by Hoffmeister (1948).

F. A report on the Phoenicid shower of December 5, 1956, by Ridley (1962).

G. A list of visual radiants by McIntosh (1935).

H. A report on the June Lyrids by Hindley (1969).

I. Two papers on radar radiants in the southern sky by Weiss (1960a, b).

J. A paper on radar radiants in the southern hemisphere by Nilsson (1964).

K. Several compilations of visual, photographic, and radar radiants by Whipple and Hawkins (1959), McKinley (1961), Millman and McKinley (1963), and Jacchia (1963).

This list is restricted to streams that the author is convinced do exist. It is perhaps still too comprehensive in that there are six streams with activity near the

threshold of detection by photography not related to any known comet and not shown to be active for as long as a decade. Unless activity can be confirmed in earlier or later years or unless an associated comet appears, these streams should probably be dropped from a later version of this list. The author will be much more receptive to suggestions for deletions from this list than he will be to suggestions for additions to it. Clear evidence that the threshold for visual detection of a stream has been passed (as in the case of the June Lyrids) should qualify it for permanent inclusion.

A comment on the matching sets of orbits is in order. It is the directions of perihelion that should match, a condition clearly met in most cases:

A. April Lyrids and Comet 1861 I Thatcher.

B. η Aquarids, Orionids, and P/Comet Halley.

C. τ Herculids and Comet 1930 VI Schwassmann-Wachmann 3.

D. Daytime β Taurids, Southern Taurids, Northern Taurids, and P/Comet Encke.

E. June Boötids and P/Comet Pons-Winnecke 1915 III.

F. o Draconids and Comet 1919 V Metcalf.

G. Southern and Northern ι Aquarids.

H. Perseids and Comet 1862 III Swift-Tuttle.

I. Aurigids and Comet 1911 II Kiess.

J. Daytime Sextantids and Geminids.

K. Annual Andromedids and the predicted orbit of P/Comet Biela for 1972.

L. Andromedids and P/Comet Biela 1852 III.

M. October Draconids and P/Comet Giacobini-Zinner 1946 V.

N. Leo Minorids and Comet 1739 Zanotti.

O. Pegasids, December Phoenicids, and Comet 1819 IV Blanplain.

P. Leonids and P/Comet Tempel-Tuttle 1965 IV.

Q. Monocerotids and Comet 1917 I Mellish.

R. Northern and Southern χ Orionids.

S. Ursids and P/Comet Tuttle.

In the case of the Sextantids and the Geminids, the temporary character of the Sextantids and the concentration and strength of the Geminids suggest two parent bodies for the streams. The similarities in the directions of perihelion, distances at perihelion, and semimajor axes then imply that these two parent bodies separated from a common body at an earlier time. In the case of the Pegasids, December Phoenicids, and Comet 1819 IV Blanplain, the strength, concentration, and single apparition of the December Phoenicids suggest that a small comet still exists; the presence of meteors in the orbital plane of the Pegasids suggests that another comet separated long ago from Comet 1819 IV. If we were in the presence of a broad distribution of meteoroids, there would be continuous activity from northern and southern radiants in October, November, and December.

In two cases some serious failure to match occurs. Among the Daytime Arietids, Northern δ Aquarids, and Southern δ Aquarids, it is clear that the Northern δ Aquarids do not fit and are dubious members of the system; and in the case of the Daytime ζ Perseids, Southern Piscids, and Northern Piscids, it is clear that the Southern Piscids do not fit and are dubious members of the system. The traditional association between the ∝Capricornids and P/Comet Honda-Mrkos-Pajdušáková is rejected, as the directions of perihelia diverge by nearly 30°.

Of the 57 entries in the list, two are additional radiants associated with P/Comet Encke and six more are associated with another radiant, each in the sense that they appear to come from the same parent body. One of these pairs is the η Aquarids and Orionids associated with P/Comet Halley. Another is the pair of Andromedid radiants, one that of the great showers, the other that of the current weak annual stream matching the current predicted orbit of P/Comet Biela. The remaining four pairs are not associated with a comet; two are pairs of daylight and night showers – the Daytime Arietids with the Southern δ Aquarids and the Daytime ζ Perseids with the Northern Piscids. The remaining two are merely northern and southern branches of the same streams; these two cases are the ι Aquarids and the χ Orionids. Thus, we deal here with 49 separate streams. Two additional pairings appear to be at the level of parent meteoroid-shedding bodies having separated from a larger body at an earlier time. These pairings are the Daytime Sextantids with the Geminids and the Pegasids with the December Phoenicids, which in turn apparently came from Comet 1819 IV Blanplain. It appears that 47 initial parent bodies are required to explain

the present list of streams. Some 15 of the 49 currently required parent bodies have been observed as Comets. Two are lost, and P/Comet Biela is perhaps the best target for an effort at recovery. Small asteroids might be searched for along the orbits of the Geminids and Sextantids, and comets might be searched for along the orbits of the highly concentrated Quadrantids, Librids, and Corvids. The other 29 parent objects are associated with weak or diffuse stream systems, so a search for them would be tantamount to a general search of the sky!

The author is grateful for access to B. G. Marsden's forthcoming catalog of orbits of comets in advance of publication, and also for the predicted orbit of P/Comet Biela in 1972. This work was supported in part by contract NGR 09-015-033 from the National Aeronautics and Space Administration.

Name	Dates	Max.	Longitude of Sun (1950)					Geocentric Radiant			Sun
			Beginning	Half Max.	Max.	Half Max.	End	R.A. 1950	Decl. 1950	Velocity (km sec^{-1})	
Quadrantids	Jan. 1–4	Jan. 3	280°.8	282°.5	282°.7	282°.9	283°.4	230°.1	+48°.5	41.5	282°.7
δ Cancrids	Jan. 13–21	Jan. 16	293		296		301	126	+20	28	296
Virginids	Feb. 3–Apr. 15		314				25	186	0	35	350
δ Leonids	Feb. 5–Mar. 19	Feb. 26	316		338		359	159	+19	23	338
Camelopardalids	Mar. 14–Apr. 7		353				17	118.7	+68.3	6.8	359.0
σ Leonids	Mar. 21–May 13	Apr. 17	1		27		52	195	- 5	20	28
δ Draconids	Mar. 28–Apr. 17		7				27	281	+68	26.7	14
κ Serpentids	Apr. 1–7		11				17	230	+18	45	14
μ Virginids	Apr. 1–May 12	Apr. 25	12		35		51	221	- 5	29	35
α Scorpiids	Apr. 11–May 12	May 3	21		42		51	240	-22	35	42
σ Boötids	Apr. 14–May 12	Apr. 28	24		36		51	218	+19	20	36
φ Boötids	Apr. 16–May 12	May 1	26		40		51	240	+51	12	40
April Lyrids	Apr. 20–23	Apr. 22	30.7	31.2	31.7	32.2	32.7	271.4	+33.6	47.6	31.7
η Aquarids	Apr. 21–May 12	May 3	30	39	42.4	45	51	335.6	- 1.9	65.5	42.4
τ Herculids	May 19–June 14	June 3	58		72		83	228	+39	15	72
χ Scorpiids	May 27–June 20	June 5	65		74		89	247	-13	21	74
Daytime Arietids	May 29–June 19	June 7	67	71	76	83	88	44	+23	37	77
Daytime ζ Perseids	June 1–17	June 7	70	72	76	83	86	62	+23	27	78
Librids	1937 June 8–9	June 8	77.6		78.2		78.4+	227.2	-28.3	16 ± 2	78.2
Sagittariids	1957-8 June 8–16	June 11	77		80		82	304	-35	52	80
θ Ophiuchids	June 8–16	June 13	77		82		85	267	-28	26.7	82
June Lyrids	1969 June 11–21	June 16	79	81	84.5	87.5	90	278	+35	31 ± 3	84.5
Daytime β Taurids	June 24–July 6	June 29	91	93	96	99	103	86	+19	30	96
Corvids	1937 June 25–30	June 26	94.8	94.9	95.2	97.6	97.9	191.9	-19.1	10 ± 2	95.9
June Boötids	1916 June 28	June 28	97.5		97.6		97.7	219	+49	13.9	98
July Phoenicids	July 3–18	July 14	101		112		116	31.1	-47.9	47 ± 3	109.6
o Draconids	July 7–24	July 16	104				121	271	+59	28.6	113
Northern δ Aquarids	July 14–Aug. 25	Aug. 12	111		139		152	339	- 5	42.3	139
Southern δ Aquarids	July 21–Aug. 29	July 29	118	121	125	129	155	333.1	-16.5	41.4	125.0
σ Capricornids	July 15–Aug. 10	July 30	123		126		138	307	-10	22.8	127
Southern ι Aquarids	July 15–Aug. 25	Aug. 5	112		131		151	333.3	-14.7	33.8	131.0
Northern ι Aquarids	July 15–Sept. 20	Aug. 20	112		147		177	327	- 6	31.2	147
Perseids	July 23–Aug. 23	Aug. 12	120	138	139	141	150	46.2	+57.4	59.4	139.0
κ Cygnids	Aug. 9–Oct. 6	Aug. 18	136		145		193	286	+59	24.8	145
Southern Piscids	Aug. 31–Nov. 2	Sept. 20	158		177		219	6	0	26.3	177
Northern Piscids	Sept. 25–Oct. 19	Oct. 12	182		199		206	26	+14	29	199
Aurigids	1935 Sept. 1	Sept. 1			157.9			84.6	+42.0	66.3	157.9
κ Aquarids	Sept. 11–28	Sept. 21	168		178		184	338	- 5	16.0	178
Southern Taurids	Sept. 15–Nov. 26	Nov. 3	172		220		244	50.5	+13.6	27.0	220.0
Northern Taurids	Sept. 19–Dec. 1	Nov. 13	176	206	230	240	249	58.3	+22.3	29.2	230.0
Daytime Sextantids	Sept. 24–Oct. 5	Sept. 29	179		184		190	152	0	32.2	183.6
Annual Andromedids	Sept. 25–Nov. 12	Oct. 3	182	184	190	195	230	5 20	+ 8 +34	23.2 18.2	190 228

Name	Dates	Max.	Longitude of Sun (1950)					Geocentric Radiant			Sun
			Beginning	Half Max.	Max.	Half Max.	End	R.A. 1950	Decl. 1950	Velocity (km sec^{-1})	
Andromedids	1885 Nov. 27	Nov. 27	246°.6	246°.65	246°.7	246°.75	246°.8	25°	+44°	16.5	247°
Orionids	Oct. 2–Nov. 7	Oct. 21	189	206.7	207.7	208.3	225	94.5	+15.8	66.4	208.0
October Draconids	Oct. 9	Oct. 9	196.25		196.3		196.35	262.1	+54.1	20.43	196.3
ε Geminids	Oct. 14–27	Oct. 19	201		206		214	104	+27	69.4	209
Leo Minorids	Oct. 22–24	Oct. 24	209		211		211	162	+37	61.8	211
Pegasids	Oct. 29–Nov. 12	Nov. 12	215		230		230	335	+21	11.2	230
Leonids	Nov. 14–20	Nov. 17	231	234.447	234.462	234.477	237	152.3	+22.2	70.7	234.5
Monocerotids	Nov. 27–Dec. 17	Dec. 10	245		258		265	99.8	+14.0	42.4	257.6
σ Hydrids	Dec. 3–15	Dec. 11	251		259		263	126.6	+ 1.6	58.4	259.0
Northern χ Orionids	Dec. 4–15	Dec. 10	252		258		261	84	+26	25.2	258
Southern χ Orionids	Dec. 7–14	Dec. 11	255		259		262	85	+16	25.5	259
Geminids	Dec. 4–16	Dec. 14	252	260.6	261.7	262.1	264.2	112.3	+32.5	34.4	261.0
December Phoenicids	1956 Dec. 5	Dec. 5	253.18	253.45	253.55	253.65	253.70	15	-55	12.7	253
								15	-45	11.7	254
δ Arietids	Dec. 8–14		256				262	52	+22	13.2	257.6
Coma Berenicids	Dec. 12–Jan. 23		260				303	175	+25	65	282
Ursids	Dec. 17–24	Dec. 22	265	269	270	271	272	217.06	+75.85	33.4	270.66

Name	Daily Motion of Radiant		Number in Sample of McCrosky and Posen (1961)	Maximum Visual Zenithal Rate (hr^{-1})	Maximum Radar Echo Rate (hr^{-1})
	R.A.	Decl.			
Quadrantids			17	140	
δ Cancrids			7		
Virginids	+0°.81	-0°.33	6		
δ Leonids	+0.75	-0.50	24		
Camelopardalids	+1.35	+0.51	4		
σ Leonids	+0.44	+0.11	19		
δ Draconids			4		
κ Serpentids			4		
μ Virginids	+0.53	-0.30	7		
∝ Scorpiids	+0.50	-0.19	5		
∝ Boötids	+0.7	+0.2	8		
ϕ Boötids			6		
April Lyrids	+1.1	0.0	5	12 96 (1922)	
η Aquarids	+0.9	+0.4	7	30	
τ Herculids	-0.1	+0.9	14		
χ Scorpiids	+0.9	+0.5	11		
Daytime Arietids	+0.7	+0.6			60
Daytime ζ Perseids	+1.1	+0.4			40
Librids				10 (1937)	
Sagittariids					30
θ Ophiuchids			4	2	
June Lyrids				9	
Daytime β Taurids	+0.8	+0.4			30
Corvids				13 (1937)	
June Boötids				100 (1916)	
July Phoenicids	+1.04	+0.53			30
o Draconids			3		
Northern δ Aquarids	+1.0	+0.2	9	20	
Southern δ Aquarids	+0.80	+0.18	13	30	
∝ Capricornids	+0.9	+0.3	21	30	

Name	Daily Motion of Radiant		Number in Sample of McCrosky and Posen (1961)	Maximum Visual Zenithal Rate (hr^{-1})	Maximum Radar Echo Rate (hr^{-1})
	R.A.	Decl.			
Southern ι Aquarids	+1°.07	+0°.18	12	15	
Northern ι Aquarids	+1.03	+0.13	3	15	
Perseids	+1.35	+0.12	45	70	
κ Cygnids	0.0	0.0	8	5	
Southern Piscids			14		
Northern Piscids			9		
Aurigids				30	
κ Aquarids			5		
Southern Taurids	+0.79	+0.15	46	7	
Northern Taurids	+0.76	+0.10	45	<7	
Daytime Sextantids					30
Annual Andromedids	+0.38	+0.66	23		
Andromedids				13, 000(1885)	
Orionids	+1.23	+0.13	49	30	
October Draconids			2	30, 000(1933)	
ε Geminids	+0.7	0.0	7		
Leo Minorids			3		
Pegasids			6		
Leonids	+0.70	-0.42	5	14, 000(1833)	
Monocerotids			3		
σ Hydrids	+0.7	-0.2	8		
Northern χ Orionids			4		
Southern χ Orionids			8		
Geminids	+1.02	-0.07	77	70	
December Phoenicids				100	20
δ Arietids			7		
Coma Berenicids	+0.88	-0.45	11		
Ursids				20 110(1945)	

Name	Orbital Elements						
	a	e	q	ω	Ω	ι	π
Quadrantids	3.08	0.683	0.977	170°.0	282°.7	72°.5	92°.8
δ Cancrids	2.3	0.80	0.45	283	296	0	219
Virginids	2.63	0.90	0.26	304	350	3	294
δ Leonids	2.62	0.75	0.64	259	338	6	237
Camelopardalids	1.534	0.352	0.974	185.0	359.0	8.2	184.0
σ Leonids	2.35	0.66	0.75	248	28	1	276
δ Draconids	2.770	0.640	0.996	171.1	13.7	37.5	184.8
κ Serpentids	∞	1.00	0.45	275	14	64	289
μ Virginids	3.12	0.83	0.48	280	35	10	315
σ Scorpiids	2.15	0.90	0.21	134	222	3	356
π Boötids	2.65	0.71	0.75	247	36	18	283
φ Boötids	1.25	0.24	0.95	226	40	19	266
April Lyrids	28	0.968	0.919	214.3	31.7	79.0	246.0
Comet 1861 I	55.7	0.983	0.921	213.4	31.2	79.8	244.6
η Aquarids	13	0.958	0.560	95.2	42.4	163.5	137.6
Orionids	15.1	0.962	0.571	82.5	28.0	163.9	110.5
P/Comet Halley 1835 III	18.0	0.967	0.587	110.6	56.8	162.2	167.4
τ Herculids	2.70	0.63	0.97	204	72	19	276
Comet 1930 VI	3.09	0.672	1.011	192.3	76.8	17.4	269.1
χ Scorpiids	3.11	0.77	0.68	257	74	6	331
Daytime Arietids	1.6	0.94	0.09	29	77	21	106
Northern δ Aquarids	2.62	0.97	0.07	332	139	20	111
Southern δ Aquarids	2.86	0.976	0.069	152.8	305.0	27.2	97.8
Daytime ζ Perseids	1.6	0.79	0.34	59	78	0	137
Southern Piscids	2.33	0.82	0.42	107	357	2	104
Northern Piscids	2.06	0.80	0.40	291	199	3	130
Librids	2.5/10	0.65/0.92	0.88/0.85	46/49	258.2	4/5	305/308
Sagittariids	∞	1.00	0.10	142	260	99	42
θ Ophiuchids	2.90	0.84	0.46	101	262	4	4
June Lyrids	2.5/10	0.67/0.92	0.83/0.84	237/231	84.5	44/50	321/315
Daytime β Taurids	2.2	0.85	0.34	246	276.4	6	162
Southern Taurids	1.93	0.806	0.375	113.2	40.0	5.2	153.2
Northern Taurids	2.59	0.861	0.359	292.3	230.0	2.4	162.3
P/Comet Encke 1970ℓ	2.217	0.847	0.339	185.9	334.2	12.0	160.1
Corvids	2.5/10	0.60/0.90	1.013/1.012	7.6/7.9	274.9	3/4	282.5/282.8
June Boötids	3.27	0.69	1.02	180	98	18	278
P/Comet Pons-Winnecke 1915 III	3.261	0.702	0.971	172.4	99.8	18.3	272.2
July Phoenicids	2.5/∞	0.62/1.00	0.96/0.97	31/24	289.6	82/87	321/313

Name	Orbital Elements						
	a	e	q	ω	Ω	ι	π
o Draconids	∞	1.00	1.01	190°	113°	43°	303°
Comet 1919 V	∞	1.000	1.115	185.7	121.4	46.4	306.9
α Capricornids	2.53	0.77	0.59	269	127	7	36
Southern ι Aquarids	2.36	0.912	0.208	131.8	311.0	6.9	82.8
Northern ι Aquarids	1.75	0.84	0.26	308	147	5	95
Perseids	28	0.965	0.953	151.5	139.0	113.8	290.5
Comet 1862 III	24.3	0.960	0.963	152.8	138.7	113.6	291.5
κ Cygnids	3.09	0.68	0.99	194	145	38	339
Aurigids	∞	1.000	0.802	121.5	157.9	146.4	279.4
Comet 1911 II	153	0.996	0.684	110.3	158.0	148.4	268.3
κ Aquarids	3.20	0.74	0.81	236	178	2	54
Daytime Sextantids	1.25	0.87	0.16	213	3.6	22	217
Geminids	1.36	0.896	0.142	324.3	261.0	23.6	225.3
Annual Andromedids	3.22	0.82	0.58	267	190	4	97
	3.29	0.76	0.79	238	228	12	106
P/Comet Biela (1972)	3.54	0.77	0.82	255	213	8	108
Andromedids	3.53	0.76	0.86	222	247	13	109
P/Comet Biela 1852 III	3.53	0.756	0.861	223.3	247.2	12.6	110.5
October Draconids	3.51	0.717	0.996	171.8	196.3	30.7	8.1
P/Comet Giacobini-Zinner 1946 V	3.51	0.717	0.996	171.8	196.3	30.7	8.1
ε Geminids	26.77	0.97	0.77	237	209	173	86
Leo Minorids	58.6	0.99	0.65	106	211	124	317
Comet 1739	∞	1.00	0.674	104.8	210.3	124.3	315.1
Pegasids	3.86	0.75	0.97	196	230	8	65
December Phoenicids	2.96	0.68	0.98	0	73	16	74
	2.96	0.67	0.99	359	74	13	72
Comet 1819 IV	2.96	0.699	0.892	350.2	79.2	9.1	69.4
Leonids	11.5	0.915	0.985	172.5	234.5	162.6	47.0
P/Comet Tempel-Tuttle 1965 IV	10.27	0.904	0.982	172.6	232.4	162.7	45.0
Monocerotids	42	0.997	0.14	135.8	77.6	24.8	213.4
Comet 1917 I	27.64	0.993	0.190	121.3	87.5	32.7	208.8
σ Hydrids	30.0	0.992	0.244	120.7	79.0	125.5	199.8
Northern χ Orionids	2.22	0.79	0.47	281	258	2	179
Southern χ Orionids	2.18	0.78	0.47	101	79	7	180
δ Arietids	2.13	0.605	0.838	232.8	257.6	1.8	130.4
Coma Berenicids	∞	1.00	0.58	258	282	134	180
Ursids	5.70	0.85	0.9389	205.85	270.66	53.6	116.51
P/Comet Tuttle 1939 X	5.70	0.821	1.022	207.0	269.8	54.7	116.8

Notes on Individual Streams:

Virginids, σ Leonids, and μ Virginids	These streams are contributors to Hoffmeister's (1948) visual Virginids.
∝ Scorpiids	This stream is a contributor to Hoffmeister's (1948) Scorpius-Sagittarius system.
April Lyrids	This stream is a weak annual one at the threshold of detection for visual observers but has given stronger displays in 1884 (22 hr^{-1}), 1922 (96 hr^{-1}), and 1948 (20 hr^{-1}).
η Aquarids and Orionids	At this inclination, Ω-ω should be compared between orbits, not π. The three values are 307°.4, 305°.5, and 306°.2 for the η Aquarids, the Orionids, and P/Comet Halley, respectively.
τ Herculids	Some evidence exists that this stream was detected visually, its radiant being regarded as early activity of the June Boötids (Olivier, 1916; Smith, 1932).
χ Scorpiids	This stream is a contributor to Hoffmeister's (1948) Scorpius-Sagittarius system.
Librids	This shower was observed only in 1937. Two sets of elements are given to present likely extremes.
Sagittariids	This shower was observed only by radar and only in 1958. It was absent in the years 1952 to 1956.
θ Ophiuchids	This stream is the maximum of Hoffmeister's (1948) Scorpius-Sagittarius system.
June Lyrids	This weak visual stream has appeared only from 1966 onward (Hindley, 1969). Two sets of elements are given to present likely extremes.
Corvids	This shower was observed only in 1937. Two sets of elements are given to present likely extremes. Hoffmeister's Orbit I (1948, p. 122) for a = 2.5 is incorrect.
June Boötids	This shower was strong only in 1916 (100 hr^{-1}) and showed 6 hr^{-1} in 1921 (Hoffmeister, 1921).
July Phoenicids	This shower was observed only by radar from 1953 through 1958. It does not appear in visual lists, although it should if it is not a recent arrival at the earth's orbit. Two sets of elements are given to present likely extremes.
∝ Capricornids	These are Weiss' (1960b) Capricornids. They are not resolvable visually from the Southern δ Aquarids.
Southern ι Aquarids	These are Weiss' (1960b) Piscis Austrinids. They are not resolvable visually from the Southern δ Aquarids.

Northern ι Aquarids	Early on, this shower is not resolvable visually from the Southern δ Aquarids, and in its feeble late stages, it contributes to Hoffmeister's (1948) visual Piscids.
Southern Piscids and Northern Piscids	These streams contribute to Hoffmeister's (1948) visual Piscids.
Aurigids	This shower was strong for 1 hr before morning twilight on one night only.
Southern Taurids and Northern Taurids	These streams cannot be resolved from one another visually.
Annual Andromedids	This stream begins its activity by contributing to Hoffmeister's (1948) visual Piscids and then moves northward toward the radiant of the famous Andromedid showers. Two radiants and sets of elements are given to display the changes during the earth's passage through the stream.
Andromedids	Strong showers occurred on December 5, 1741; December 7, 1798 ($\sim$ 400 hr^{-1}); December 7, 1830; December 6, 1838 ($\sim$ 100 hr^{-1}); December 6, 1847 ($\sim$ 150 hr^{-1}); November 30, 1867; November 27, 1872; November 27, 1885 ($\sim$ 13,000 hr^{-1}); November 23, 1892 ($\sim$ 300 hr^{-1}); November 24, 1899 ($\sim$ 100 hr^{-1}); November 21, 1904 ($\sim$ 20 hr^{-1}); and November 15, 1940 ($\sim$ 30 hr^{-1}).
October Draconids	Strong showers occurred in 1927 (17 hr^{-1}), 1933 (30,000 hr^{-1}), 1946 (10,000 hr^{-1}), and 1952 (200 hr^{-1}).
Leonids	Strong showers occurred in 1799, 1832, 1833, 1834, 1839, 1866, 1867, 1868, 1898, 1901, 1903, 1961, 1965, 1966, and 1969. In other years, activity was very feeble.
December Phoenicids	This shower appeared only in 1965. The northern radiant is visual; the southern is from radar observations.
Coma Berenicids	The December portion of this stream is called the December Leo Minorids by Cook et al. (1972), but Lindblad (1971b) found bridging meteors that connect the December Leo Minorids to the Coma Berenicids in January.

REFERENCES

Cook, A. F. (1970). Discrete levels of beginning height of meteors in streams. Smithsonian Astrophys. Obs. Spec. Rep. No. 324; also in Smithsonian Contr. Astrophys., in press.

Cook, A. F., Lindblad, B.-A., Marsden, B. G., McCrosky, R. E., and Posen, A. (1972). Yet another stream search among 2401 photographic meteors. Smithsonian Contr. Astrophys., in press.

Hindley, K. B. (1969). The June Lyrid meteor stream in 1969. Journ. Brit. Astron. Assoc., vol. 79, pp. 480-484.

Hoffmeister, C. (1921). Die Beobachtung von Meteoren des Winneckeschen Kometen. Astron. Nachr., vol. 215, pp. 455-466.

Hoffmeister, C. (1948). Meteorströme. Johann Ambrosius Barth, Leipzig, 286 pp.

Jacchia, L. G. (1963). Meteors, meteorites, and comets: Interrelations. In The Moon, Meteorites and Comets, ed. by B. M. Middlehurst and G. P. Kuiper, Univ. of Chicago Press, Chicago, pp. 774-798.

Lindblad, B.-A. (1971a). A computerized stream search among 2401 photographic meteor orbits. Smithsonian Contr. Astrophys., no. 12, pp. 14-24.

Lindblad, B.-A. (1971b). Meteor streams. In Space Research XI, Akademie-Verlag, Berlin, in press.

McCrosky, R. E., and Posen, A. (1959). New photographic meteor showers. Astron. Journ., vol. 64, pp. 25-27.

McCrosky, R. E., and Posen, A. (1961). Orbital elements of photographic meteors. Smithsonian Contr. Astrophys., vol. 4, pp. 15-84.

McIntosh, R. A. (1935). An index to southern meteor showers. Mon. Not. Roy. Astron. Soc., vol. 95, pp. 709-718.

McKinley, D. W. R. (1961). Meteor Science and Engineering. McGraw-Hill Book Co., New York, pp. 145-157.

Millman, P. M., and McKinley, D. W. R. (1963). Meteors. In The Moon, Meteorites and Comets, ed. by B. M. Middlehurst and G. P. Kuiper, Univ. of Chicago Press, Chicago, pp. 674-773.

Nilsson, C. (1964). A southern hemisphere radio survey of meteor streams. Australian Journ. Phys., vol. 17, pp. 205-256.

Olivier, C. P. (1916). The meteor system of Pons-Winnecke's Comet. Mon. Not. Roy. Astron. Soc., vol. 77, pp. 71-75.

Ridley, H. B. (1962). The Phoenicid meteor shower of 1956 December 5. Journ. Brit. Astron. Assoc., vol. 72, pp. 266-272.

Smith, F. W. (1932). A discussion of meteor orbits connecting with the Pons-Winnecke Comet. Mon. Not. Roy. Astron. Soc., vol. 93, p. 156.

Weiss, A. A. (1960a). Radio-echo observations of southern hemisphere meteor shower activity from 1956 December to 1958 August. Mon. Not. Roy. Astron. Soc., vol. 120, pp. 387-403.

Weiss, A. A. (1960b). Southern hemisphere meteor activity in July and August. Australian Journ. Phys., vol. 13, pp. 522-531.

Whipple, F. L., and Hawkins, G. S. (1959). Meteors. Handbuch der Physik, vol. 52, pp. 519-564.